DEVELOPMENT OF NONLINEAR CONTROL SCHEMES FOR ELECTRIC POWER SYSTEM STABILIZATION

BY

AYOKUNLE AJIBOLA AWELEWA, B.Eng., M.Eng.

(CUGP040058)

A THESIS SUBMITTED TO THE SCHOOL OF POSTGRADUATE STUDIES IN PARTIAL FULFILMENT OF THE REQUIREMENTS FOR THE AWARD OF THE DOCTOR OF PHILOSOPHY DEGREE (ELECTRICAL POWER & MACHINES)

SUPERVISOR:

PROFESSOR CLAUDIUS O.A. AWOSOPE

CO-SUPERVISOR:

DR. CHARLES NDUJIUBA

MARCH 2016

DECLARATION

I hereby declare that I carried out the work reported in this Thesis in the Department of Electrical & Information Engineering, Covenant University, under the supervision of Professor Claudius O.A. Awosope and Dr. Charles Ndujiuba. I also solemnly declare that to the best of my knowledge, no part of this Thesis has been submitted here or elsewhere in a previous application for the award of a degree. All sources of knowledge used have been duly acknowledged.

AYOKUNLE AJIBOLA AWELEWA

(CUGP040058)

CERTIFICATION

This is to certify that the Thesis titled ‘‘Development of Nonlinear Control Schemes for Electric Power System Stabilization’’ by Awelewa Ayokunle Ajibola meets the requirements and regulations governing the award of the Doctor of Philosophy degree of Covenant University and is approved for its contribution to knowledge and literary presentation.

Supervisor:	Prof. Claudius O.A. Awosope	----------	----------
		Date	**Signature**
Co-supervisor:	Dr. Charles U. Ndujiuba	----------	----------
		Date	**Signature**
Head of Department:	Dr. Francis E. Idachaba	----------	----------
		Date	**Signature**

DEDICATION

This work is dedicated to Professor James Katende who showed me the real path to the forest of control systems theory and helped demystify and navigate its tortuous loops.

ACKNOWLEGEMENTS

There is some order in the world. If you push long enough and do not give up, you are ultimately going to break through. Thus, thanks be to God always who unceasingly afforded me His Holy Spirit for inner tenacity and outer strength to subdue every hurdle in the wilderness of nonlinear control research—even though the wilderness appeared to be infinitely bounded and every effort to traverse its complicated circuits seemed barely fruitful, the Great Counselor and Guide was always there with me each step of the way, and I can now indeed profess that the Lord is my Shepherd. Amen.

Oh, how can I express my profound appreciation to my supervisor, Professor Claudius Ojo Aremu Awosope, whom we fondly call Baba Awos? He has been there for, and with, me since I 'debut' as an academic, and I can attest that Baba Awos is a superfine and meticulous teacher who always wants to help define and ascertain every bit of detail. Thank you, sir, for constantly being there.

I also thank my co-supervisor, Dr. Charles Uzoanya Ndujiuba, who is very compassionate and obliging in every way. He and Professor Samuel Ndueso John, a wonderful brother that has been of immense help to me within and outside academic formality, never stopped giving me right-on-time advice and assistance which really stood me in good stead.

I am grateful to the entire faculty and staff of the Department of Electrical and Information Engineering (EIE) for their prayers and moral support. They are too many to be included here, but I'd never forget the invaluable help of my astute and highly visionary head of the Department, Dr. Francis Idachaba (Associate Professor), who orchestrated my 3-month visiting scholarship at the University of Strathclyde, Glasgow,

UK. Sir, I am highly obliged for the time, energy, and other resources you expended on my behalf to make the visit a reality. I acknowledge also Professor A.A.A Atayero, Dr. V.O. Mathews, Dr. Monday Eyinagho, Dr. Oboyerulu Edevbie Agboje, Dr. Anthony Adoghe (Associate Professor), Engr. Ademola Abdulkareem, and, of course, my very good friends and colleagues: Engr. Isaac Adekunle Samuel, Dr. Emmanuel Adetiba, and Dr. (Mrs.) Joke Atinuke Badejo.

In addition, I acknowledge the financial support (throughout my stay at the University of Strathclyde) of the management of Covenant University under the leadership of our congenial and erudite Vice Chancellor, Professor Charles Korede Ayo. I feel greatly privileged to be so sponsored.

Further, my deep appreciation goes to Professor Ojo Olorunfemi, from the Tennessee Technological University, US, and Dr. Adam Grain, from the University of Strathclyde. Professor Ojo helped me secure the visiting scholarship and also monitored my progress, while Dr. Adam immensely guided me in completing my Thesis—he painstakingly taught me many unfamiliar concepts, including very useful MATLAB tricks and dynamic simulation of synchronous machine models. (I recall the many productive and instrumental discussions we had together during the tea breaks.) Sir, I am wholeheartedly grateful to you.

In conclusion, I am proud of my family members for their unwavering understanding, patience, and love: my wife and gem, Ibiolatiwa Awe; my daughter and little friend, Jesu-Fifunmi Omo-Oluwa Awe; and my siblings, especially Pastor Ropo Awe, Engr. Olanike Arokoyo (nee Awe), Olajide Awe, and Olanrewaju Awe.

ABSTRACT

Power system stabilizers and other controllers are employed to damp oscillations in power systems, thereby guaranteeing satisfactory dynamic performance following major network disturbances. However, the parameters of these controllers are often tuned based on the power system linearized model which generally is a function of the system operating point or state. These controllers suffer from poor performance when the system state changes. The aim of the research work reported in this Thesis is to develop nonlinear synchronous generator excitation control schemes with control laws for providing improved transient stability when the system is subjected to wide parameter variations due to network disturbances. The study employed fourth-and third-order models of a single-machine-connected-to-an-infinite-bus system to design two nonlinear sliding mode control laws (CLs) and one finite-time homogeneous control law (CL), which were constructed based on a well-chosen output function of the system. The parameters of the control laws were properly selected and/or tuned to give desirable dynamic characteristics using well established linear control methods. Justifications for the selection of the fourth-and third-order synchronous generator models to design the aforesaid controllers are presented. Dynamic simulations of the system under the action of the control laws were carried out using MATLAB®/SIMULINK. In order to test the performance of the laws, several simulation studies were performed when the voltage magnitude (V) of the infinite bus and the transmission line reactance (X_E) of the system changed due to an applied three-phase symmetrical fault at the infinite bus and generator terminals. Results obtained from these studies show that the dynamic characteristics of the system being investigated have improved significantly, in terms of the rotor angle and rotor speed first peak, damping of low-frequency mechanical oscillations in rotor angle following fault clearance, and settling times of key stability indicators (rotor angle and rotor speed). For instance, for application of each of 5-cycle, 7-cycle, and 9-cycle fault at the infinite bus, the system rotor angle settled to its stable steady values within 1 - 2.2s with minimal control effort that varied between -5pu and 5pu before settling at the pre-fault value of 1.5603pu in 4.32s (CL1), in 1.92s (CL2), and in 3.32s (CL3). Whereas, CL3, which is a contribution to the improvement of the existing general higher-order sliding mode control structure for synchronous excitation control, was able to make the system withstand greater fault duration than CL1, CL2, which has a new positive parameter (called the dilation gain) incorporated into it, furnished the system with the greatest fault-retaining capability. In practice, the implementation of the three control laws can be carried out in a static exciter configuration with a very fast response.

TABLE OF CONTENTS

LIST OF FIGURES

LIST OF TABLES

LIST OF SYMBOLS AND ABBREVIATIONS

δ: Electrical rotor angle

H: Inertia constant

t: Time

Tm: Mechanical torque

ω: Angular velocity in electrical radians per second

AVR: Automatic voltage regulator

CL1: Control law 1

CL2: Control law 2

CL3: Control law 3

FL: Feedback linearization

PSM1: Power system model 1

PSM2: Power system model 2

PSS: Power system stabilizer

SC: System condition

SMC: Sliding mode control

SMIB: Single machine infinite bus

u_i: i^{th} control signal

E_f: Excitation field signal

CHAPTER ONE: INTRODUCTION

1.0 Background of the Study

Generally, a modern power system can be defined as a collection of a large number of generating electric power sources interconnected through complex networks of transmission lines for the sole purpose of meeting the power demands of a large number of domestic and industrial loads. Because each power plant has several controllable states and state-dependent outputs, it can be defined as "a high-order multivariable system whose dynamic response is influenced by a wide array of devices with different characteristics and response rates" (Kundur *et al.*, 2004). In order to accommodate more load demands and provide a constant and reliable electric power supply, several power controllers are employed at the transmission and distribution levels to deliver electric power to the load centers efficiently. The uses of these controllers have forced power system engineers to develop many techniques and strategies to be used at planning, design and operation stages. Normally, power systems tend to suffer frequently from adverse events such as large generation and load variations, transmission line faults, etc., and these events tend to affect system signals and operational parameters. Therefore, keeping the system within its operational bounds is paramount to its safe and reliable operation.

Practically, generating unit controllers such as the prime mover and excitation systems are being employed in the power systems, besides the power and voltage controllers at transmission and distribution levels, not only to realize safe operation of an electric power system, but also to enhance system dynamic performance (Mariani & Murthy, 1997). Specifically, the generating unit excitation control system can play a pivotal role

in enhancing systems stability and dynamic response to major network disturbances. Conventionally, the combination of an automatic voltage regulator (AVR) and a power system stabilizer (PSS) are used to provide constant output voltage and damp low-frequency oscillations in power systems (Colbia-Vega *et al.*, 2008; Huerta *et al.*, 2010). But, because their structures are linear, the AVR and PSS have limited dynamic responses (Ortega *et al.*, 2005; Ping *et al.*, 2014). As a result, their parameters should be changed when the operating condition of the system changes significantly. Hence, an alternative approach such as the use of nonlinear control schemes must be adopted, and this was explored in this study. Through the use of these schemes, the power system dynamic characteristics can be improved upon, leading to better and more robust stability performance independent of system operating conditions, including the conditions during network faults.

1.1 Significance and Motivation for the Study

In a deregulated large-scale power system environment, it is paramount that the power system has the ability to meet stringent performance requirements which arise as an upshot of, among other things, stressed operating conditions and uncertain power flow paths (Chow *et al.*, 2005). Realizing the dynamic performance requirements of electric power systems is more desirable and imperative to the stable and reliable operation of the systems. However, the use of linear control design methods commonly being used for power system stability improvement is limited due to the highly nonlinear nature of the system (Chiang, 2011). This limitation has spawned extensive and focused research on alternative control strategies for better stabilization. High performance robustness against system faults, which is a significant feature any strategy must meet, has further led to

constant reassessment of well established old approaches and the development of new ones in order to, especially, keep with the ever-changing nature of the power systems. One major motivation for this study is to have better dynamic performance robustness using nonlinear algorithms. The significance of these nonlinear algorithms, as presented in this work, is that they are compact and universal, can be readily tuned to yield optimal performance, and can withstand long fault durations and remove system oscillations within the shortest possible time. The research impetus behind the design, development, investigation, and complete analysis of nonlinear control algorithms is the availability of powerful and low-cost computing resources, as is evident in many practical implementations (Nandam & Sen, 1995; Unsal & Kachroo, 1999; Yoerger *et al.*, 1986), as well as versatile and efficient software tools, such as MATLAB/SIMULINK. Moreover, it is of note that technical reports are often being written to help provide information and materials that appropriately reflect current industry needs, experiences, and understanding so that new design and operating criteria can be tailored towards meeting the constant need for satisfactory system operation (IEEE PES Working Group Report, 1995; Kundur *et al.*, 2004).

1.2 Aim and Objectives

The aim of this study is to develop nonlinear excitation controllers for improving the stability of power systems when subjected to large perturbations.

The main objectives of the study are to:

i. analyze and check for partial and exact linearization of representative power system models.

ii. derive various appropriate output signals for the power system models, and then compute the relative degrees of the models with respect to these signals.

iii. design two nonlinear sliding mode control laws and one homogeneous stabilizing control law, and represent them in nonlinear feedback schemes.

iv. examine the performance of the designed control schemes under network disturbances causing wide variations in system parameters.

v. obtain the properties of the nonlinear control laws which pertain specifically to general power system behaviors.

1.3 Problem Statement

It has been known and established that reliable and secure operation of power systems hinges on the stability of the system both under normal operation and contingency situations. Conventionally, power system stabilizers have been used to provide complementary damping of system oscillations during an upset. Although the performance of these stabilizers has been somewhat satisfactory, limitations in their use have often been encountered, especially in terms of their robustness under major disturbances, and for a wide range of operating conditions (Handschin *et al.*, 1994). Therefore, the problem of transient stability, i.e., the ability of power system to regain a state of operating equilibrium when subjected to a large fault from an initial operating point, has remained till date. Particularly, if not corrected, transient angular instability can pose a severe challenge to power systems, leading to loss of synchronism of various machines or group of machines in the systems. In addition to this loss of synchronism, irregular and aperiodic oscillations, which can destabilize the entire systems, may also arise. Several blackouts, caused by large faults in power networks, have been witnessed

across the world (Pouyan *et al.*, September/October 2006). Power system controllers that will handle this nature of disturbance must have the ability to retain fault for long duration and damp out fault-induced oscillations as quickly as possible. But only nonlinear controllers designed based on the nonlinear model of the power network will be most appropriate for this type of system operating condition (Lu *et al*., 2001).

So, the problem at hand is to develop new nonlinear excitation controller structures which are capable of providing good and robust damping of oscillations when systems are subjected to disturbances that lead to protracted large variations of parameters.

This task can be reduced mathematically to a control system stabilization problem, which can be stated as follows. Under large perturbations and wide variations of parameters, consider the nonlinear dynamic model of a power system which can be expressed as

$$\dot{x} = f(x,u,t) \tag{1.1}$$

where x is the state vector. Obtain a control law, u, that will ensure that a well-chosen output signal of the system approaches (or stays close to) zero when time, *t*, approaches an infinite value, thereby damping oscillations in the system.

1.4 Methodology

The methods employed for the work are as follows:

i. Description and mathematical analysis of two power system models, which are described by a synchronous generator connected to an infinite bus.
ii. Partial and exact feedback linearization of the power system models.
iii. Establishment of three nonlinear excitation control schemes.
iv. Simulation of the system under the influence of the designed control schemes using MATLAB/SIMULINK software package.

1.5 Scope and Limitation of the Study

This study focuses on the development of three nonlinear control schemes or systems for the improvement of rotor angle stability of a synchronous generator. Since the excitation control is most effective in improving the dynamic performance and overall stability of electric power systems (Lu *et al*., 2001), the controllers developed in this work are applicable to the synchronous generator excitation systems. Besides, effects of parameter variations due to the application of only symmetrical faults are investigated, because other faults, such as asymmetrical faults, are less severe in effect. The study is limited to power system models which are based on the structure of a single machine connected to an infinite bus (SMIB)—a case of multi-machine systems is not treated. The SMIB and multi-machine structures are similar, except that the former considers the effect of one machine at a time in relation to the rest of the other machines in the power system.

1.6 Thesis Organization

Chapter one of this thesis presents introductory information, highlighting the significance, aim and objectives, and methodology of the work. A literature review together with some theoretical concepts (background) was discussed in Chapter two. The models of the power system adopted, and the design and analysis of the nonlinear excitation controllers are detailed in Chapter three. The simulation results under various test scenarios are presented in Chapter four. Chapter five gives the conclusions, stating achievements and contributions to knowledge, and recommendations for further study. In addition, references of materials used and appendices are provided at the end of Chapter five.

CHAPTER TWO: THEORETICAL FOUNDATION AND LITERATURE REVIEW

2.0 Introduction

This chapter discusses fundamental theoretical concepts which are critical for understanding of the work carried out in this Thesis. These include power system stability; power system components modeling in short-and long-term stability studies; excitation control systems; and a number of nonlinear control methods such as sliding mode control, adaptive control, feedback linearization, etc. Also, a comprehensive review of relevant existing works that have been done by numerous researchers from literature is carried out.

2.1 Theoretical Foundation

The study of power system stability and control is an extensive field of research which requires sufficient knowledge and understanding of vital components of power systems, most especially the performance characteristics of synchronous machines and the mathematical representations that govern their dynamic behaviour, as well as control system theory and techniques. This section provides a synoptic discussion of these theoretical underpinnings.

2.1.1 Power System Stability

An interconnected power system is considered to be stable following a perturbation if it returns to its previous steady state operating point or acquires a new stable operating condition (Nargsarkar & Sukhija, 2007), with system state variables kept within their permissible operating limits (Nagrath & Kothari, 2003). Such a system must have the ability to damp the oscillations following exposure to perturbation as quickly as possible,

so that the entire system can settle to a new steady-state operating condition within practically short time (Anderson & Fouad, 2003). Whether an interconnected power system, which is subjected to a disturbance, will regain its former stable operating state or return to a new state is dependent not only on the type of the disturbance, but also on the initial condition of the system (because of its non-linear nature). The operating condition of a power system can be described in terms of its behaviour around an equilibrium set or an attractor in the phase space. There are three types of attractor: a point attractor, which represents a single point; a limit circle attractor (Ravel *et al.*, 2008), which gives a closed curve; and a chaotic (or aperiodic) attractor, which represents the divergence of the system from either a single point or a closed circle (Li & Caizares, 2009). Besides, the disturbance that may impact on power systems adversely can either be event-type or norm-type. The former category is used to describe outages of particular pieces of equipment, which may be due to a fault, or intentionally initiated by human operators, while the latter actually depicts the size of the disturbance.

The various categories as well as subcategories of power system stability are shown in Fig. 2.1. The stability delineation reflected in the figure is a standard way to portray the relevant system variable in which an observation of instability is possible after an occurrence of a disturbance. Each category is discussed briefly as follows:

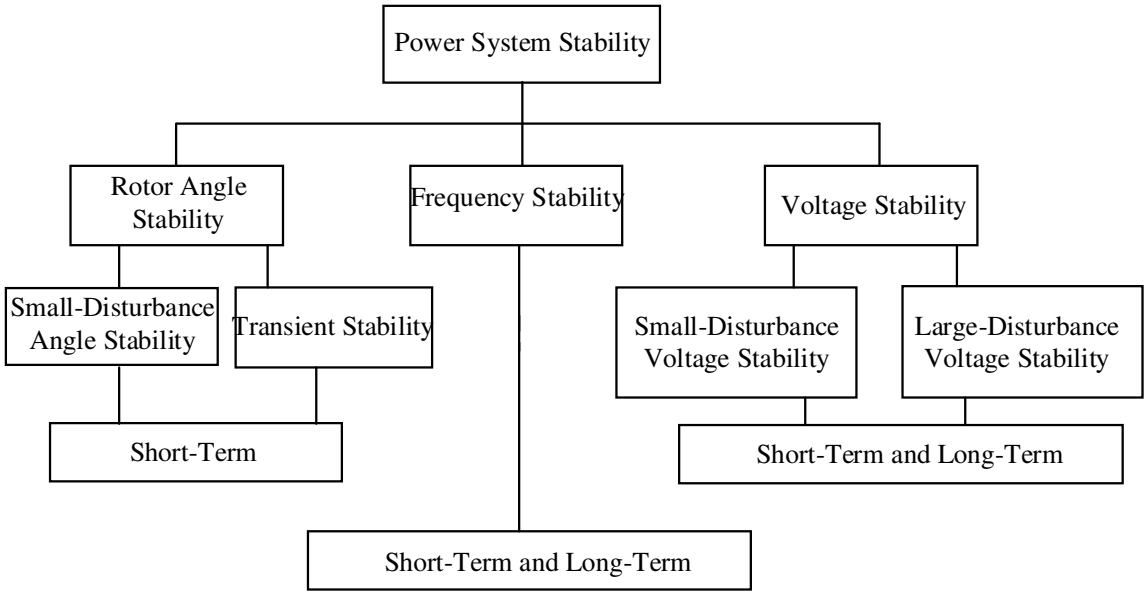

Fig. 2.1: Power System Stability Classification (Kundur *et al.*, 2004)

2.1.1.1 Rotor Angle Stability

This is classified into small-disturbance and large-disturbance (or transient) stability. It indicates the ability of an interconnected power system to stay in a state of synchronism after being perturbed, and it's usually carried out within a time frame of 10-20 seconds (Kundur *et al.*, 2004) for small-disturbance type and 3-5 seconds for large-disturbance type. Here, system synchronism implies that a state of equilibrium exists between the electromagnetic torque and the mechanical torque of each synchronous machine in the system. When a power system is subjected to a disturbance, deviations in the angular positions of the generator rotors result in two components of the electromagnetic torque, with one in phase with the rotor angle deviation (termed the synchronizing torque component) and the other in phase with the speed deviation (called the damping torque component). For the system to remain in synchronism after a perturbation, these two torque components must be sufficiently present. Lack of sufficient synchronizing torque

will lead to the so called aperiodic or non-oscillatory instability, while lack of sufficient damping torque will lead to periodic or oscillatory instability (Anderson & Fouad, 2003; Kundur, 1994).

2.1.1.2 Frequency Stability

Frequency Stability means that the system frequency remains unchanged or returns to its nominal value after a brief and small drift following disturbance. This implies that an interconnected power system is said to be frequency-stable if it retains a balance between generation and load after a system perturbation, i.e., if it results in zero accelerating power. Consequently, when system frequency abnormally deviates from the nominal value, it often results in loss of synchronism, thereby leading to loss of generations and/or loads. The duration of frequency instability generally may be short or long, depending on the response times of all the processes and devices involved. For instance, under-frequency load shedding and generation controls and protections usually respond to frequency perturbation in the order of seconds, while energy supply systems and voltage regulators do in the order of several minutes (Kundur *et al.*, 2004).

2.1.1.3 Voltage Stability

A power system is said to be voltage-stable if, after the system is subjected to a disturbance from a given initial operating condition, all system bus voltages remain steady or fixed within an acceptable range. An interconnected power system tends to experience serious voltage deviations during a system disturbance or upset when it fails to keep a reactive power balance between the load demand and supply. During voltage instability, some system bus voltages tend to increase or decrease gradually, thereby causing outages in major parts of the system. It is a general consent that voltage

instability is due to lack of sufficient provisions to meet the demand for reactive power. Conseil International des Grands Réseaux Électriques (CIGRE) Joint Task Force on Stability Terms and Definitions says that "The heart of the problem is usually the voltage drop that occurs when active power and reactive power flow through the inductive reactance associated with the transmission network" (Kundur *et al.*, 2004).

2.1.2 Power System Models

Having good models for components of electric power systems that can be used for a wide range of system studies is increasingly important, because they facilitate important studies to be carried out at the design stage and during expansion of the power systems. In addition to their use in stability study, they facilitate determination of the regions of attraction of the system's equilibrium, and are vital for the purpose of control design, which is necessary for improving the performance of the system by expanding these regions of attraction. Because electric power systems are highly nonlinear dynamic systems, their models are complicated. Therefore, careful and painstaking analysis and design tasks are geared towards enhancing and keeping their operation within a realizable region in the state space.

At present, the majority of electric energy in power systems is being sourced from synchronous generators; thus, they play a major role in the overall dynamic performance of the power systems. As a result, various representative mathematical models are developed to describe their performance characteristics, depending on the degree of detailed representation needed for a given study. Generally, synchronous generators are described by seventh-order model, but reduced-order models that can capture their

detailed behaviours are often employed for control design. These models are presented in the following sections:

2.1.2.1 Classical Model of a Synchronous Machine

The basic model used to represent a synchronous machine is that which assumes a constant voltage behind transient reactance, and it is based on the basic assumption that the flux linkage in the main field windings does not change during an occurrence of a network perturbation. This assumption, however, is valid only for a power system whose size is relatively small, and the excitation control systems are simple and slow, making the period of oscillations resulting from a network change not "much greater than one second" (Anderson & Fouad, 2003). This representation is shown in Fig. 2.2. In this figure, V is the magnitude terminal voltage, E is the magnitude of the constant voltage of the source that represents generator internal EMF (electromotive force), x_d' is the direct axis transient reactance, and δ, which together with E is derived from the initial system conditions, is the angle between the rotor position and V.

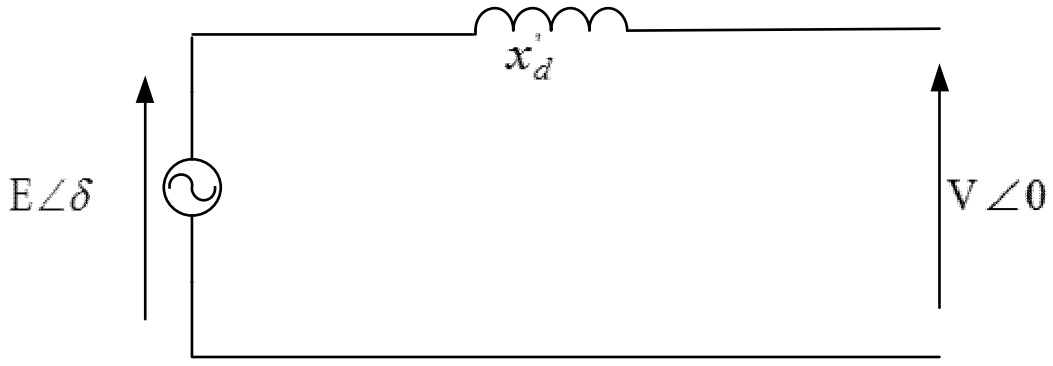

Fig. 2.2: Classical model of a synchronous machine

2.1.2.2 Classical Model of a Power System

The classical model of a power system represents synchronous machines by their classical model depicted in Fig. 2.2, and the entire power system can be collapsed and described by an equivalent single machine connected to an infinite bus (SMIB). The assumptions underlying this model are: the mechanical power input is constant during a transient; damping power is negligible; the electrical phase angle and synchronous machine load angle are equivalent; and the load fed at the terminals of the machine or infinite bus can be characterized by a constant impedance connected to ground. However, for the purpose of stability studies in wider context, this model can be extended to a system of many machines (multi-machine system) by adding an additional damping torque component to the inertia torque in the machine's equation of motion, although stability studies of multi-machine systems using this approach are restricted to short-term transient stability studies lasting for about one second (Anderson & Fouad, 2003).

Fig. 2.3 is an equivalent diagram of a single machine connected to an infinite bus through tie line, where $V_{Terminal}$ is the synchronous machine terminal voltage, Z_{Line} is the transmission network series impedance, Z_{Load} is the equivalent shunt impedance at the terminal of the machine, and other parameters in the figure are as defined in Fig. 2.2.

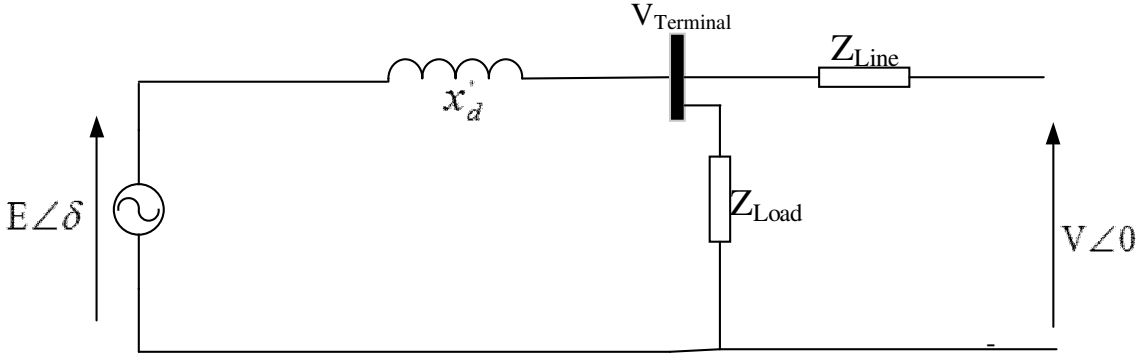

Fig. 2.3: Classical model of a power system

The state-space model that describes system dynamics in classical representation of power system is

$$\begin{aligned} \frac{d\omega}{dt} &= \frac{\omega_R}{2H}\left(P_m - E^2 Y_{11}\cos\theta_{11} - EVY_{12}\cos(\theta_{12}-\delta)\right) \\ \frac{d\delta}{dt} &= \omega - \omega_R \end{aligned} \tag{2.1}$$

where

ω = angular velocity in electrical rad/s

δ = electrical rotor angle in radians

P_m = mechanical power on per unit 3-phase base

H = inertia constant in seconds (= W_k/S_{B3}; W_k is the kinetic energy of the rotating masses in MJ and S_{B3} is the rated 3-phase MVA of the system)

ω_R = rated angular velocity in electrical rad/s

t = time in seconds

V = voltage magnitude of the infinite bus

E = voltage magnitude of the generator

Y_{11}, θ_{11} = magnitude and angle of the driving point admittance at the generator bus

Y_{12}, θ_{12} = magnitude and angle of the transfer admittance between the generator and the infinite bus

For a multi-machine system, shown in Fig. 2.4, the state-space equations that describe system dynamics increase drastically, depending on the number of machines in the system.

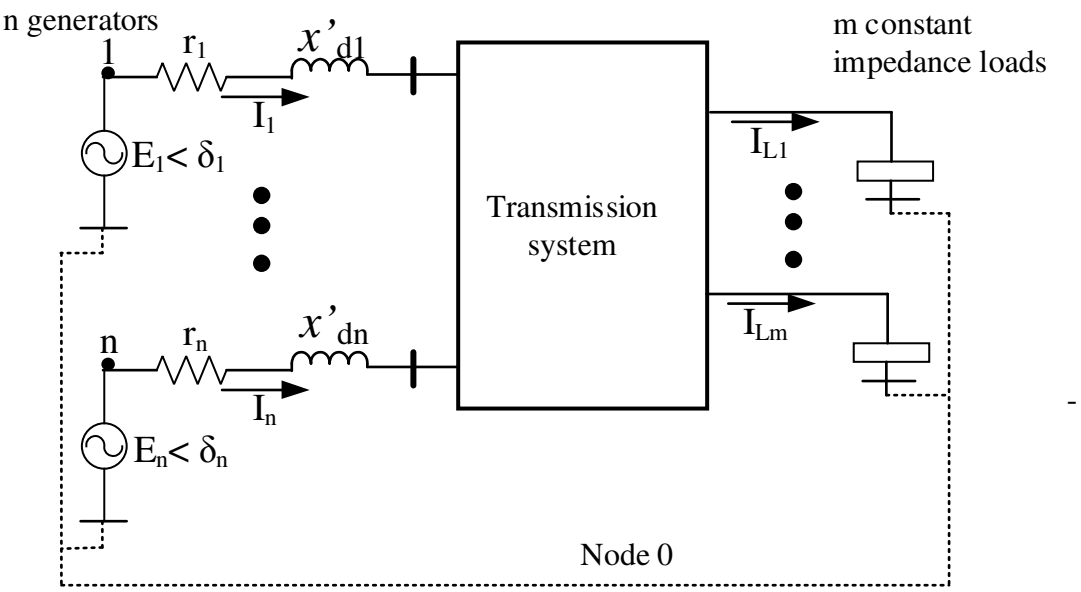

Fig. 2.4: Classical representation of a multi-machine (or n-machine) power system (Anderson & Fouad, 2003)

For example, in a two-machine system, the state-space equations are

$$\begin{aligned}
\frac{d\omega_1}{dt} &= -\frac{\omega_R D_1}{2H_1} + \frac{\omega_R}{2H_1}\left(P_{m1} - E_1{}^2 G_{11} - \sum_{j=2}^{3} E_1 E_j Y_{1j} \cos(\theta_{1j} - \delta_1 + \delta_j) \right) \\
\frac{d\delta_1}{dt} &= \omega_1 - \omega_R \\
\frac{d\omega_2}{dt} &= -\frac{\omega_R D_2}{2H_2} + \frac{\omega_R}{2H_2}\left(P_{m2} - E_2{}^2 G_{22} - \sum_{\substack{j=1 \\ j\neq 2}}^{3} E_2 E_j Y_{2j} \cos(\theta_{2j} - \delta_2 + \delta_j) \right) \\
\frac{d\delta_2}{dt} &= \omega_2 - \omega_R
\end{aligned} \tag{2.2}$$

In some occasions, equation (2.2) can be reduced to two equivalent equations if the concept of relative load angle and speed is adopted. When machine 1 is assumed as a reference, the relative load angle and speed can be described as $\delta_{21}=\delta_2-\delta_1$ and $\omega_{21}=\omega_2-\omega_1$. Thus, equation (2.2) can be reduced to:

$$\frac{d\omega_{21}}{dt} = -\frac{\omega_R}{2}\left[\frac{D_2}{H_2} - \frac{D_1}{H_1}\right] + \frac{\omega_R}{2H_2}\left[P_{m2} - E_2{}^2 G_{22} - \sum_{\substack{j=1 \\ j\neq 2}}^{3} E_2 E_j Y_{2j}\cos(\theta_{2j} - \delta_2 + \delta_j)\right]$$

$$-\frac{\omega_R}{2H_1}\left[P_{m1} - E_1{}^2 G_{11} - \sum_{j=2}^{3} E_1 E_j Y_{1j}\cos(\theta_{1j} - \delta_1 + \delta_j)\right] \quad (2.3)$$

$$\frac{d\delta_{21}}{dt} = \omega_2 - \omega_1$$

where D_i = damping coefficient of the i^{th} machine.

2.1.2.3 Detailed Synchronous Machine Model

In some situations, where system behaviors during sub-transient and transient periods are of great importance, more detailed representation of a synchronous machine that can capture more appropriately the dynamic characteristics of the machine is required. A detailed synchronous machine model takes into account three-phase stator windings, one field winding, and two amortisseur windings. Such a model gives a full description of the electromagnetic characteristics of the synchronous machine and it can be found in the open literature and widely used (Anderson & Fouad, 2003; IEEE Standard 1110, 2003; Kundur, 1994). And this detailed representation is available in two forms: the current model and the flux linkage model.

The current model, in which currents, torque angle, and rotor speed are used as state variables, is given by (Anderson & Fouad, 2003)

$$\dot{X} = FX + GU \quad (2.4)$$

where

$$X = \begin{bmatrix} i_d \\ i_F \\ i_D \\ i_q \\ i_Q \\ \hline \omega \\ \delta \end{bmatrix}$$

$$GU = \begin{bmatrix} \\ -L^{-1}v \\ \\ \hline \\ \dfrac{T_m}{\tau_j} \\ -1 \end{bmatrix}$$

$$F = \left[\begin{array}{ccccc:cc} & & -L^{-1}(R+\omega N) & & & 0 & 0 \\ & & & & & 0 & 0 \\ & & & & & 0 & 0 \\ & & & & & 0 & 0 \\ & & & & & 0 & 0 \\ \hdashline \dfrac{-L_{tl}\, i_q}{3\tau_j} & \dfrac{-kM_F\, i_q}{3\tau_j} & \dfrac{-kM_D\, i_q}{3\tau_j} & \dfrac{-L_{tq}\, i_d}{3\tau_j} & \dfrac{-kM_Q\, i_d}{3\tau_j} & \dfrac{-D}{\tau_j} & 0 \\ 0 & 0 & 0 & 0 & 0 & 1 & 0 \end{array}\right]$$

The parameters **L**, **R**, and **N** in the system function **F**, and the vector signal **v** in the input function **GU** are, respectively, given by

$$L = \left[\begin{array}{ccc|cc} L_d & kM_F & kM_D & 0 & 0 \\ kM_F & L_F & M_R & 0 & 0 \\ kM_D & M_R & L_D & 0 & 0 \\ \hline 0 & 0 & 0 & L_q & kM_Q \\ 0 & 0 & 0 & kM_Q & L_Q \end{array}\right]$$

$$R = \begin{bmatrix} r & 0 & 0 & 0 & 0 \\ 0 & r_F & 0 & 0 & 0 \\ 0 & 0 & r_D & 0 & 0 \\ 0 & 0 & 0 & r & 0 \\ 0 & 0 & 0 & 0 & r_Q \end{bmatrix}$$

$$N = \begin{bmatrix} 0 & 0 & 0 & L_q & kM_Q \\ 0 & 0 & 0 & 0 & 0 \\ 0 & 0 & 0 & 0 & 0 \\ -L_d & -kM_F & -kM_D & 0 & 0 \\ 0 & 0 & 0 & 0 & 0 \end{bmatrix}$$

$$v = \begin{bmatrix} v_d \\ -v_F \\ 0 \\ v_q \\ 0 \end{bmatrix}$$

The variables and parameters in the above model are defined as follows:

i_d, v_d = the stator d-axis current and voltage, respectively, in pu

i_F, v_F = the rotor field current and voltage, respectively, in pu

i_D = the rotor d-axis damper winding current in pu

i_q, v_q = the stator q-axis current and voltage, respectively, in pu

i_Q = the rotor q-axis damper winding current pu

ω = the rotor speed in pu

δ = the torque angle in pu

T_m = the mechanical torque in pu

D = the damping coefficient

L_d = d-axis inductance in pu

L_D = D damper circuit inductance in pu

L_q = q-axis inductance in pu

L_Q = Q damper circuit inductance in pu

M_D = mutual inductance between the stator and D damper circuits in pu

M_F = mutual inductance between the stator and field circuits in pu

M_Q = mutual inductance between the stator and Q damper circuits in pu

M_R = mutual inductance between the field and D damper circuits in pu

L_F = field winding inductance in pu

r = stator resistance in pu

r_F= field resistance in pu

r_D= D damper winding resistance in pu

r_Q= Q damper winding resistance in pu

$\tau_j = 2H\omega_B$ and $k = \sqrt{3/2}$

Similarly, the flux linkage model, in which flux linkages, torque angle, and rotor speed are used as state variables, is given by (Anderson & Fouad, 2003)

$$\dot{X} = AX + BU \tag{2.5}$$

where

$$X = \begin{bmatrix} \lambda_d \\ \lambda_F \\ \lambda_D \\ \lambda_q \\ \lambda_Q \\ \underline{\omega} \\ \delta \end{bmatrix}$$

$$BU = \begin{bmatrix} -v_d \\ v_F \\ 0 \\ -v_q \\ 0 \\ \underline{T_m} \\ \tau_j \\ -1 \end{bmatrix}$$

$$A=\left[\begin{array}{ccccc|cc}
-\frac{r}{\ell_d}\left(1-\frac{L_{MD}}{\ell_d}\right) & \frac{rL_{MD}}{\ell_d\ell_F} & \frac{rL_{MD}}{\ell_d\ell_D} & -\omega & 0 & 0 & 0 \\
\frac{r_F L_{MD}}{\ell_F\ell_d} & -\frac{r_F}{\ell_F}\left(1-\frac{L_{MD}}{\ell_F}\right) & \frac{r_F L_{MD}}{\ell_F\ell_D} & 0 & 0 & 0 & 0 \\
\frac{r_D L_{MD}}{\ell_D\ell_d} & \frac{r_D L_{MD}}{\ell_D\ell_F} & -\frac{r_D}{\ell_D}\left(1-\frac{L_{MD}}{\ell_D}\right) & 0 & 0 & 0 & 0 \\
\omega & 0 & 0 & -\frac{r}{\ell_q}\left(1-\frac{L_{MQ}}{\ell_q}\right) & \frac{rL_{MQ}}{\ell_q\ell_Q} & 0 & 0 \\
0 & 0 & 0 & \frac{r_Q L_{MQ}}{\ell_Q\ell_q} & -\frac{r_Q}{\ell_Q}\left(1-\frac{L_{MQ}}{\ell_Q}\right) & 0 & 0 \\
\hline
\frac{-L_{MD}}{3\tau_j\ell_d^2}\lambda_q & \frac{-L_{MD}}{3\tau_j\ell_d\ell_F}\lambda_q & \frac{-L_{MD}}{3\tau_j\ell_d\ell_D}\lambda_q & \frac{L_{MQ}}{3\tau_j\ell_q^2}\lambda_d & \frac{L_{MQ}}{3\tau_j\ell_q\ell_Q}\lambda_d & \frac{-D}{\tau_j} & 0 \\
0 & 0 & 0 & 0 & 0 & 1 & 0
\end{array}\right]$$

The variables and parameters in the above model are defined as follows:

λ_d= flux linkage in the d-axis in pu

λ_F= flux linkage in the field winding in pu

λ_D= flux linkage in the D circuit in pu

λ_q= flux linkage in the q-axis in pu

λ_F= flux linkage in the field winding in pu

λ_Q= flux linkage in the Q circuit in pu

ℓ_d = leakage inductance of the d-axis in pu

ℓ_q = leakage inductance of the q-axis in pu

ℓ_D = leakage inductance of the D circuit in pu

ℓ_Q = leakage inductance of the Q circuit in pu

ℓ_F = leakage inductance of the field circuit in pu

$1/L_{MD} = 1/L_{AD} + 1/\ell_d + 1/\ell_F + 1/\ell_D$ in pu

$1/L_{MQ} = 1/L_{AQ} + 1/\ell_q + 1/\ell_Q$ in pu

L_{AD} = common magnetizing inductance in the d-axis circuit in pu

L_{AQ} = common magnetizing inductance in the q-axis circuit in pu

Other variables and parameters are as previously defined.

In stability studies, simplified models are often used to ease the analysis, and the choice of model details is dependent on the purpose of the analysis and the system scenario to be investigated. In addition, for control system analysis and design, approximate system or plant models are commonly used to derive control laws for dynamic stabilization and improvement. In the following, well known simplified models of synchronous machines are briefly considered.

1) **The E'_q model**: This is a fifth-order model representation obtained from the assumption that the damper windings have negligible effects on the system transient being considered (and this is often the case for machines that are tightly interconnected). Another assumption is that, if a solid round rotor is assumed, the d-axis damper winding can be ignored because the rotor inherently acts as a damper (which represents a q-axis damping winding). The model is given in per unit as (Anderson & Fouad, 2003)

$$
\begin{aligned}
\dot{\Lambda}_d &= -(r/L'_d)\Lambda_d + (r/L'_d)E'_q - \omega\Lambda_q - V_d \\
\dot{\Lambda}_q &= -\omega\Lambda_d - (r/L_q)\Lambda_q - V_q \\
\dot{E}'_q &= -\frac{L_d}{L'_d\tau'_{do}}E'_q + \frac{L_d - L'_d}{\tau'_{do}L'_d}\Lambda_d + \frac{1}{\tau'_{do}}E_{FD} \\
\dot{\omega} &= \frac{1}{\tau_j}\left(T_m - \frac{E'_q\Lambda_q}{L'_d} + (1/L'_d - 1/L_q)\Lambda_d\Lambda_q - D\omega\right) \\
\dot{\delta} &= \omega - 1
\end{aligned}
\tag{2.6}
$$

where

Λ_d = d-axis stator equivalent flux linkage

Λ_q= q-axis stator equivalent flux linkage

V_d = d-axis stator equivalent voltage

V_q = q-axis stator equivalent voltage

E'_q = d-axis stator EMF corresponding to the field flux linkage

E_{FD} = d-axis stator EMF corresponding to the field voltage

τ'_{do}= d-axis open-circuit transient time constant

L'_d = d-axis transient inductance

2) **The E″ model**: This is also a fifth-order model, and the assumption here is that the speed voltage terms are much greater than the transformer voltage terms in the stator voltage equations. It's also assumed that the rotor speed is constant, and d-and q-axis subtransient inductances are equal. In this model, the stator EMF is produced by the subtransient flux linkage.

The equations in per unit are (Anderson & Fouad, 2003)

$$
\begin{aligned}
\dot{e}''_d &= -(1/\tau''_{qo})\, e''_d - (1/\tau''_{qo})(x_q - x''_q) i_q \\
\dot{\lambda}_D &= (1/\tau''_{do})\sqrt{3}E'_q - (1/\tau''_{do})\lambda_D + (1/\tau''_{do})(x'_d - x_\ell) i_d \\
\dot{E}'_q &= (1/\tau'_{do})\, E_{FD} + \frac{(x_d - x'_d)(x''_d - x_\ell)}{\sqrt{3}\tau'_{do}(x'_d - x_\ell)} i_d - (1/\tau'_{do})\left(1 + \frac{(x_d - x'_d)(x'_d - x''_d)}{(x'_d - x_\ell)^2}\right) E'_q \\
&\quad + \frac{(x_d - x'_d)(x'_d - x''_d)}{\sqrt{3}\tau'_{do}(x'_d - x_\ell)^2} \lambda_D \qquad (2.7) \\
\dot{\omega} &= \frac{1}{\tau_j} T_m - \frac{i_q}{3\tau_j}\left(\sqrt{3}\frac{(x''_d - x_\ell)}{(x'_d - x_\ell)}\right) E'_q - \frac{i_q}{3\tau_j}\left(1 - \frac{(x''_d - x_\ell)}{(x'_d - x_\ell)}\right)\lambda_D - \frac{1}{3\tau_j} i_d e''_d - \frac{1}{\tau_j} D\omega \\
\dot{\delta} &= \omega - 1
\end{aligned}
$$

where

e''_d = stator d-axis subtransient voltage

x_q = q-axis synchronous reactance

x''_q = q-axis subtransient reactance

x'_d = d-axis transient reactance

x''_d = d-axis subtransient reactance

x_ℓ = leakage reactance

τ''_{qo}= q-axis open-circuit subtransient time constant

τ''_{do}= d-axis open-circuit subtransient time constant

Other variables and parameters are as defined previously.

3) **The two-axis or fourth-order model**: In this model, only the transient effects, which are dominated by the rotor circuits, i.e., the field winding and one q-axis winding, are considered; the subtransient effects are assumed negligible, and the transformer voltage terms in the stator equations are assumed to be appreciably small. (This last assumption is valid for a cylindrical rotor machine.)

The model equations in per unit are (Anderson & Fouad, 2003)

$$\begin{aligned}
\dot{E}'_d &= -\frac{1}{\tau'_{qo}} E'_d - \frac{1}{\tau'_{qo}} (x_q - x'_q) I_q \\
\dot{E}'_q &= \frac{1}{\tau'_{do}} (E_{FD} - E'_d - (x'_d - x_d) I_d) \\
\dot{\omega} &= T_m - D\omega - (E'_d I_d + E'_q I_q - (L'_q - L'_d) I_d I_q) \\
\dot{\delta} &= \omega - 1
\end{aligned} \tag{2.8}$$

All the variables and parameters in this equation are defined before.

4) **The one-axis or third-order model**: Here the effects of amortisseur windings and transformer voltage terms are ignored, thereby reducing the model to (Anderson & Fouad, 2003)

$$\dot{E}'_q = \frac{1}{\tau'_{do}} E_{FD} - \frac{1}{\tau'_{do}} (E'_q - (x_d - x'_d) I_d)$$
$$\dot{\omega} = \frac{1}{\tau_j} T_m - D\omega - (E'_q I_q - (L_q - L'_d) I_d I_q) \tag{2.9}$$
$$\dot{\delta} = \omega - 1$$

The above discussions show that a number of assumptions have been made to derive different synchronous machine models presented in this chapter. However, the choice among these models is dependent on the objectives of the study to be conducted. For example, in short-term stability studies, where the system behaviors during sub-transient and transient periods are increasingly important, some of the above models in which damper windings and stator resistance are neglected may not be appropriate. Also, the type of synchronous machines must be taken into account as some of these models are valid only for round rotor machines. Generally, any of these models can be used for control system design.

2.1.3 Synchronous Generator Excitation Control System

As shown in Fig. 2.5, there are primarily three major control systems associated with synchronous generators. The firing control system ensures that the boiler produces the right amount of steam at the required pressure and temperature; the governor controls the speed of the turbine by opening and closing the steam valve (for a steam turbine) or controlling the water flow in a penstock (for a hydro-turbine); and the excitation system regulates the generator terminal voltage through the generator field winding.

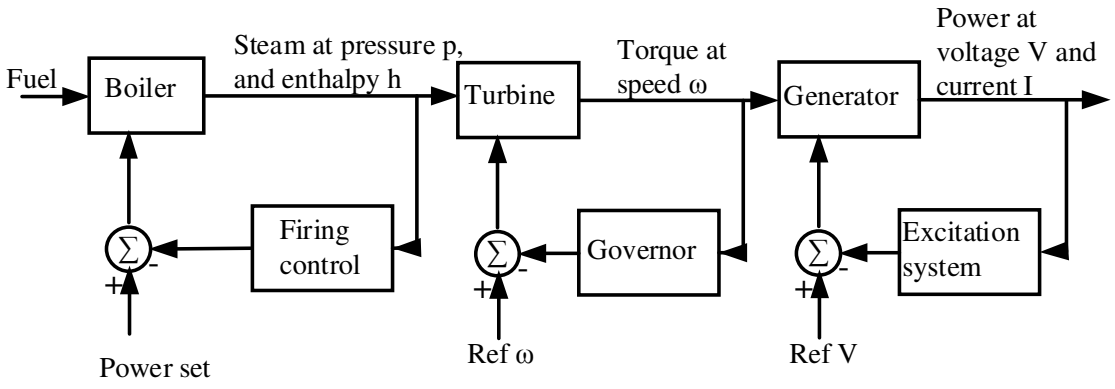

Fig. 2.5: Control systems of a synchronous generator (Anderson & Fouad, 2003)

Out of the three principal control systems of generators, it has been observed that excitation control offers the most effective means of enhancing the dynamic characteristics of power systems and stabilizing them (Lu *et al*., 2001). Early outstanding power system researchers and engineers (Concordia, 1951; Kimbark, 1956) pointed out the significance of field excitation of synchronous generators in enhancing the stability of power systems. The basic elements of an excitation control system are shown in Fig. 2.6.

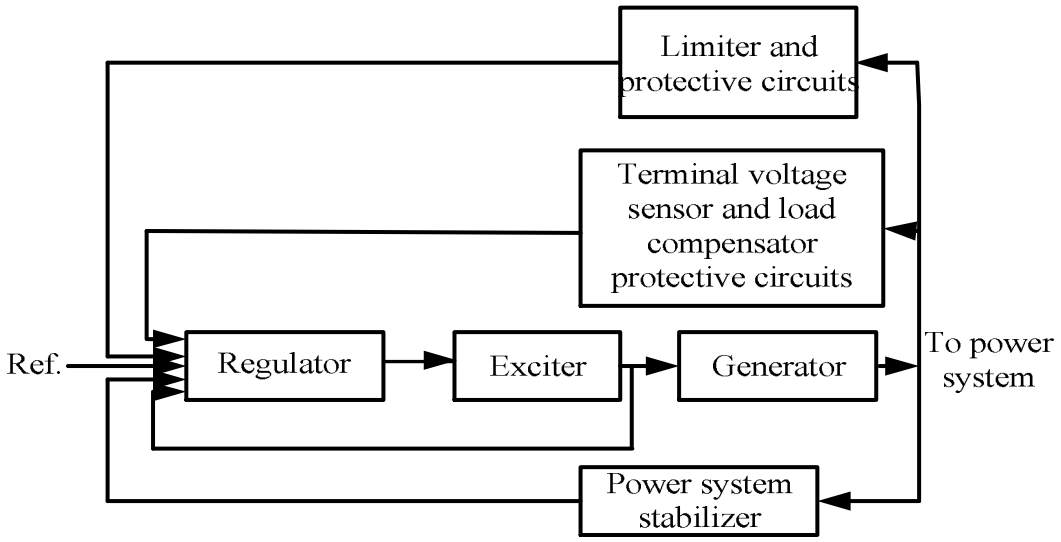

Fig. 2.6: Block diagram of a synchronous excitation control system (Kundur, 1994)

The voltage regulator in the system receives appropriate input signals and accordingly controls the output of the exciter, which supplies the required current to the field winding of the machine. To keep the terminal voltage of the generator constant after the occurrence of a fault, the regulator must be able to respond quickly and drive the field voltage to its ceiling so that the right amount of field flux can be provided. The exciter is a direct current source which is either dynamic, such as a DC generator and an AC generator coupled with a rectifying system, or static, such as a rectifier or thyristor system.

Of particular significance, because of its very high speed of response, is a static self-shunt exciter upon which better and advanced excitation control strategies can be developed (Lu *et al*., 2001). Other blocks in the excitation system perform protective and compensating functions.

During the early days of high-gain continuous-acting voltage regulators, large interconnected power systems experienced oscillations which were exacerbated by the action of the regulators. To avoid such situations, it became vital to introduce auxiliary signals for counteracting these oscillations. This led to the introduction of the power system stabilizer, which was developed by F.D. Demello and C. Concordia (Demello & Concordia, 1969), for damping oscillations in power systems. A concise excitation control system configuration with automatic voltage regulator (AVR) and power system stabilizer (PSS) is shown in Fig. 2.7. Limitations in the performance of the power system stabilizers, which have been severally modified and improved upon by a lot of researchers, led to the use of linear optimal excitation controllers (Yu *et al.*, 1970; Anderson, 1971) and more advanced excitation control methodologies (Lu *et al.*, 2000a;

Lu *et al.*, 1989b; Colbia-Vega *et al.*, 2008; Enrico *et al.*, 2008; Venkatesh & Rao, October 2012).

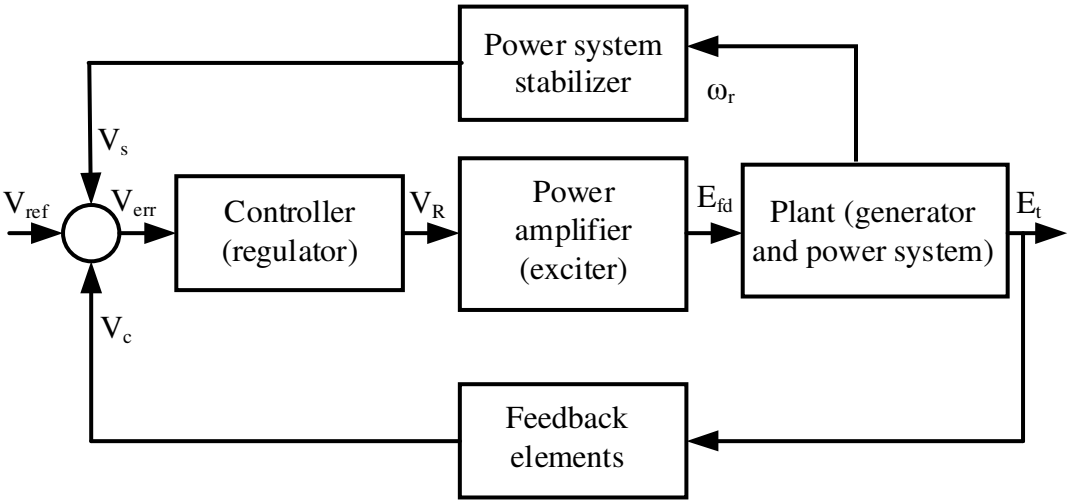

Fig. 2.7: Excitation system control with AVR and PSS

2.1.4 Nonlinear Control Systems

Most practical control systems have benefited extensively from the applications and techniques of linear control theory, though they are inherently, to some degree, nonlinear. The use of linear control strategies to solve practical control problem is pervasive, as these offer a simplified approach to analysis and design issues, and there are well established, tested and proven analytical and computer tools available in the linear control domain. The indirect method of Lyapunov (Atherton, 1981; Mohler, 1994), which states that nonlinear systems can be equivalently treated as linear systems if the operations of the nonlinear systems are restricted to small regions around their operating equilibriums, serves well to provide a theoretical validation for this so-called 'linear sense discipline'.

Moreover, nonlinear control concepts and techniques have also been developed over the years, but the available tools in this domain are still limited. Nonetheless, the ubiquity of

inexpensive, low-power, powerful and fast computing facilities has necessitated and triggered off the intensive experimental simulations of nonlinear systems, and incorporation of nonlinear control algorithms into many practical systems— a great deal of algorithms that were difficult (and some impossible) to implement before can now be efficiently implemented.

Several nonlinear control strategies have been applied to electric power systems and many other practical systems alike. These strategies are rooted in some of the well known nonlinear control paradigms and theories, which include adaptive control, feedback linearization-based control, sliding mode control, fuzzy logic, and neural networks.

2.1.4.1 Adaptive Control Systems

The structure of an adaptive control system is shown in Fig. 2.8. This system provides an on-line means of adjusting the parameters of the controller when the dynamics of the plant change due to disturbances or presence of some nonlinear actuators in the system (Nagrath & Gopal, 2007).

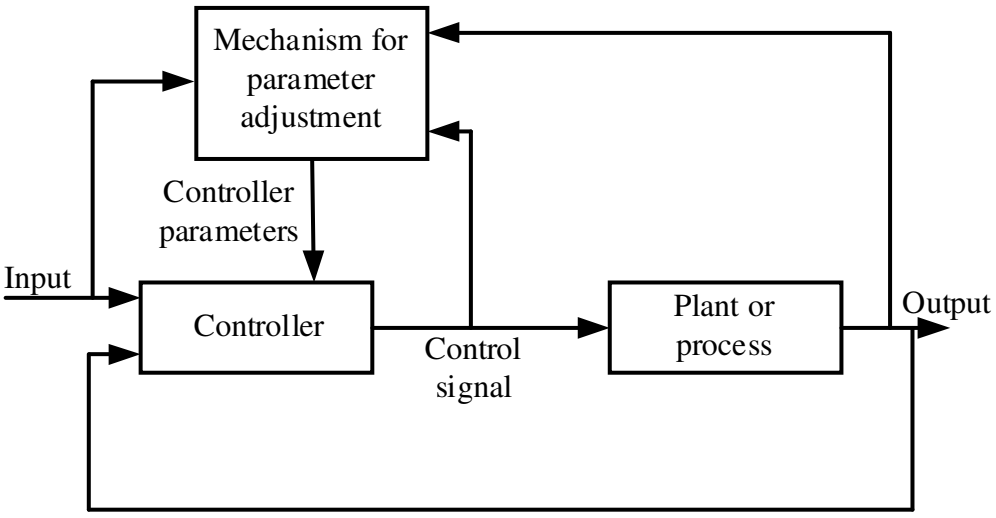

Fig. 2.8: Block diagram of an adaptive control system

There are four adaptive control schemes, viz., self-tuning regulator, model-reference adaptive control, gain scheduling and dual control. Their block diagrams are displayed in Fig. 2.9, Fig. 2.10, Fig. 2.11, and Fig. 2.12, respectively.

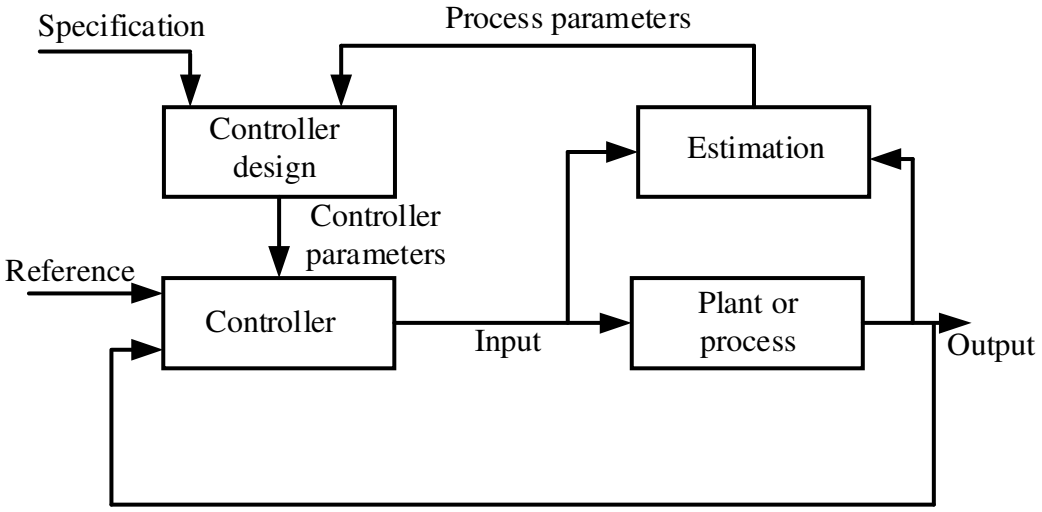

Fig. 2.9: Block diagram of a self-tuning regulator (Astrom & Wittenmark, 1995)

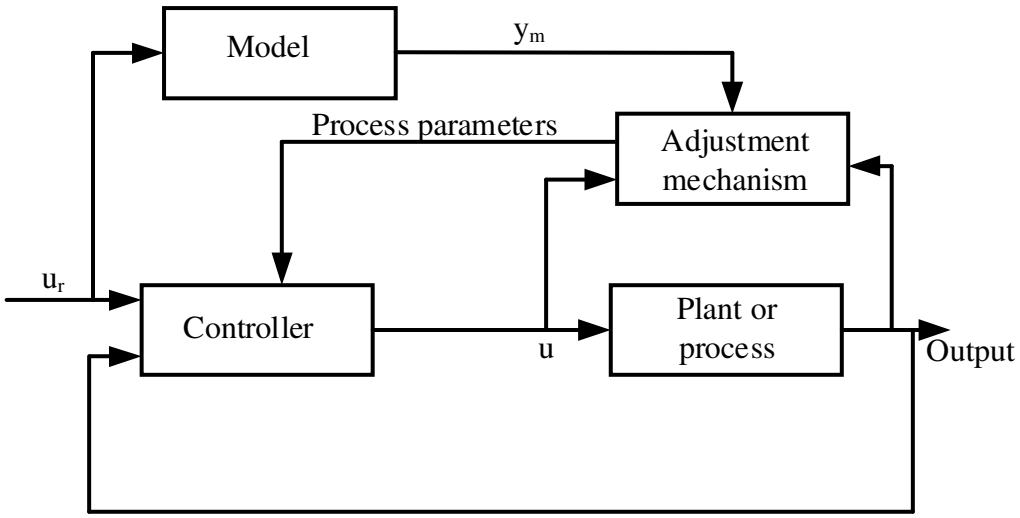

Fig. 2.10: Block diagram of a model-reference adaptive control system (Astrom & Wittenmark, 1995)

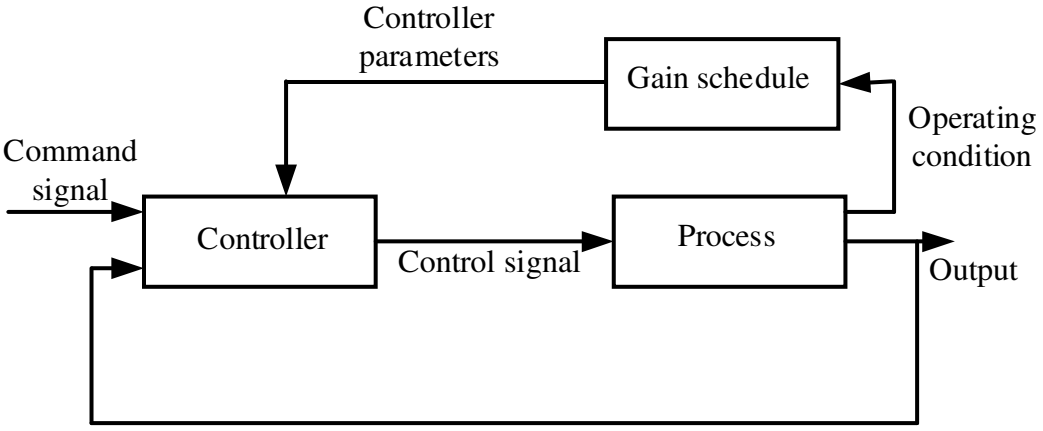

Fig. 2.11: Block diagram of a gain scheduling system (Astrom & Wittenmark, 1995)

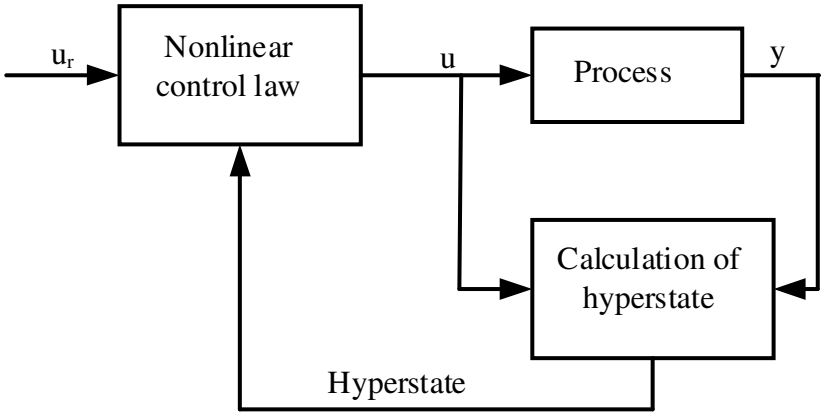

Fig. 2.12: Block diagram of a dual control system (Astrom & Wittenmark, 1995)

In the self-tuning regulators, the parameters of the controller are computed indirectly from the estimates of the parameters of the plant. Here the updates of the plant and the controller are done at each sampling time.

For the model-reference adaptive control system, the controller parameters are adjusted using the popular Massachusetts Institute of Technology (MIT) rule

$$\frac{d\theta}{dt} = -\gamma e \frac{\partial e}{\partial \theta} \tag{2.10}$$

where e is the difference between the output, y_m, of the reference model and the output, y, of the plant.

Gain scheduling is a strategy which uses a number of linear controllers, designed in correspondence with a number of small semi-operating points into which the overall system operating point is divided, to improve the performance of a plant. Each controller is scheduled for action at an appropriate semi-operating point, while controller parameters are interpolated at intervals between two semi-operating points. This is a way of mapping parameters of a process that has predictable dynamics with the parameters of the controller. In other words, the knowledge of all operating conditions is known beforehand (Albertos & Mareels, 2010). The previous adaptive control methods are based on the certainty equivalence principle in which the parameters of the plant are assumed to be correctly estimated. But in most cases, this is not usually so. The fourth adaptive control scheme, called the dual control, uses the tool of nonlinear stochastic control theory to estimate the plant parameters with accuracy.

2.1.4.2 Feedback Linearization

In the application of linear control techniques, it is always assumed that the dynamics of the system being considered are linear or can be linearized about a given operating condition using the Taylor's series method. Although this approach has been employed to solve many practical problems, it is not appropriate in problems where the system dynamics are subject to large disturbances and wide variations of parameters. One of the ways to avoid direct approximation of nonlinear system dynamics in control design is to transform the system state equations into another and equivalent state equations that are linear in form using a nonlinear state feedback control law. This results in exact or partly

exact linearization of the original nonlinear system. As long as the original states and the transformed states of the system are closely related by a coordinate transformation function called a diffeomorphism, the new state equations remain a 'true' linear representation of the original equations. Fig. 2.13 depicts a block diagram of an input-state feedback linearization technique.

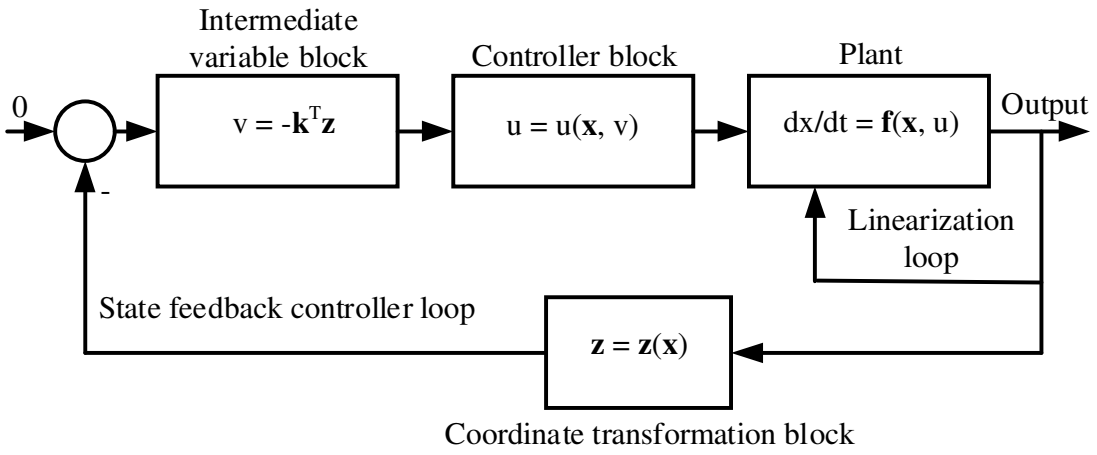

Fig. 2.13: Input-state feedback linearization control

Two highly essential differential geometric tools to all control analysis and design based on feedback linearization are the Lie derivatives and Lie brackets.

Definition 2.1 (Isidori, 1995): Consider a continuous scalar function $\beta(\mathbf{x})$, where $\mathbf{x} = [x_1\ x_2\ \ldots\ x_n]^T$, and a function vector $\mathbf{f}(\mathbf{x}) = [f_1\ f_2\ \ldots\ f_n]^T$. The Lie derivative of $\beta(\mathbf{x})$ along $\mathbf{f}(\mathbf{x})$ is given as

$$L_{\mathbf{f}}\beta(\mathbf{x}) = \frac{\partial\beta(\mathbf{x})}{\partial\mathbf{x}}\mathbf{f}(\mathbf{x}) = \sum_{i=1}^{n}\frac{\partial\beta(\mathbf{x})}{\partial\mathbf{x}_i}\mathbf{f}_i(\mathbf{x}) \tag{2.11}$$

Definition 2.2 (Isidori, 1995): Consider two function vectors $\mathbf{f}(\mathbf{x})$ and $\mathbf{g}(\mathbf{x})$. The Lie bracket of $\mathbf{g}(\mathbf{x})$ along $\mathbf{f}(\mathbf{x})$ is given as

$$\left[\mathbf{f}(\mathbf{x}),\mathbf{g}(\mathbf{x})\right] = \frac{\partial\mathbf{g}(\mathbf{x})}{\partial\mathbf{x}}\mathbf{f}(\mathbf{x}) - \frac{\partial\mathbf{f}(\mathbf{x})}{\partial\mathbf{x}}\mathbf{g}(\mathbf{x}) \tag{2.12}$$

where $\frac{\partial \mathbf{g}(\mathbf{x})}{\partial \mathbf{x}}$ and $\frac{\partial \mathbf{f}(\mathbf{x})}{\partial \mathbf{x}}$ are Jacobian matrices of functions $\mathbf{g}(\mathbf{x})$ and $\mathbf{f}(\mathbf{x})$, respectively.

The Lie derivative is useful in finding the state variables of a transformed nonlinear dynamic system from a given output function, while the Lie bracket provides a compact way of determining its involutivity, a sufficient condition for its exact linearization.

2.1.4.3 Sliding Mode Control (SMC)

SMC is a variable-structure control system methodology, which has the property of guaranteeing constant system stability and overall good performance, even when there is uncertainty in the dynamics of system (such as parametric and non-parametric uncertainty). Because of its robustness and invariance features, SMC has been severally put to use in many applications (*Hung et al.*, 1993; Nandam & Sen, 1995; Unsal & Kachroo, 1999; Yoerger *et al.*, 1986). The power of SMC is derived from the ability to change the mode (or, as it is commonly called, structure) of the control law to account for various system operating conditions. This idea is not unfamiliar in the linear control domain. It is possible to change the control structure of a linear system in order to improve its performance during operation (Itkis, 1976)—for instance, equipping a system with a flexible PID controller (in which the structure can change from a standalone P to a standalone PI or PD) can make the system perform better. The gain scheduling described earlier is an example of this.

The SMC problem can be solved using the theory of Lyapunov stability (based on the direct Lyapunov method) (Hahn, 1963; Khalil, 1996), though the analysis of the problem leads to systems with discontinuity which can be treated using the theory by Filippov

(Filippov, 1960; Utkin, 1992) for handling differential equations with a discontinuous right-hand side.

Conventionally, sliding mode controller design involves two major steps: 1) selection of a sliding surface or manifold (for a second-order system, it is a line in the state-space, while for a higher-order system, it is a hyper surface), and 2) construction of a control law to make the states of the system reach and stay on the surface while moving along it towards a desired point in a motion that is termed sliding mode. For a second-order continuous-time system, the graphical representation of the SMC strategy is shown in Fig. 2.14.

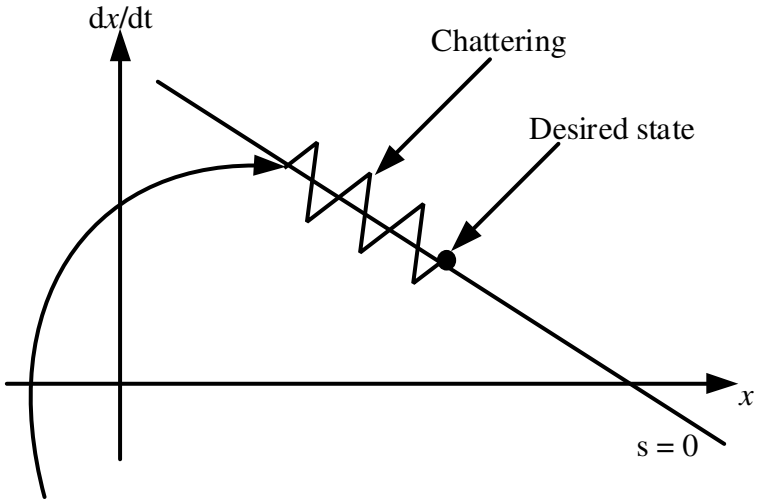

Fig. 2.14: Graphical representation of SMC for a 2nd-order system (Emel'yanov, 1959; Slotine & Li, 1991)

Generally, the surface s is selected based on the equation

$$s = \left(\frac{d}{dt} + \beta \right)^{n-1} e(t) \tag{2.13}$$

where e(t) is an error signal which is the difference between the actual system state **x** and the desired system state $\mathbf{x}_d$; constant β is strictly positive; and n is the order of the system.

For instance, when n = 2, 3, and 4, s is defined, respectively, as

$$s = \dot{e} + \beta e, \tag{2.14}$$

$$s = \ddot{e} + 2\beta\dot{e} + \beta^2 e, \tag{2.15}$$

and

$$s = \dddot{e} + 3\beta\ddot{e} + 3\beta^2\dot{e} + \beta^3. \tag{2.16}$$

Furthermore, the control law is developed such that when the states are on either side of surface of s, they are constrained to move towards it and stay on it. That is,

$$\dot{s} \leq -k \text{ if } s > 0$$

$$\dot{s} \geq k \text{ if } s < 0$$

where the number k is positive.

The control law constructed, however, requires switching from one mode to the other with an infinite speed which is not practically feasible. The delay associated with switching results in chattering, a phenomenon that may excite high-frequency unmodeled dynamics. There are methods available, such as replacement of a sliding surface with a sliding vector (Furuta & Pan, 1999), equipping the system with an asymptotic observer (Utkin, 1993), etc., to reduce this undesirable phenomenon.

2.1.4.4 Fuzzy Logic Control

All fuzzy logic systems are based on the notion that information or knowledge about the plant or process is imprecise, incomplete, or approximate (Albertos & Mareels, 2010). The underlying concept, called fuzzy set theory, of fuzzy logic was developed by Lofti Zadeh based on the principle of incompatibility, which states that "As the complexity of a system increases, our ability to make precise and yet significant statements about its behavior diminishes until a threshold is reached beyond which precision and significance

(or relevance) become almost mutually exclusive characteristics" (Zadeh, 1973). Fuzzy logic employs heuristic information, sourced from expert and experienced personnel who have complete understanding and working knowledge of the operation of the plant, to modify and improve the performance characteristics of the plant. In other words, the plant model is represented in a linguistic rule-based manner unlike conventional crisp control where the plant is described by mathematical equations.

A typical block diagram of fuzzy logic control system is shown in Fig. 2.15.

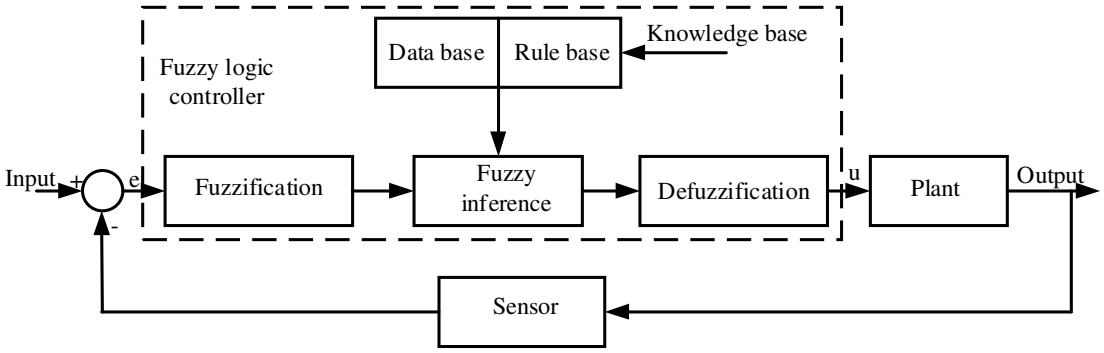

Fig. 2.15: Block diagram of a fuzzy logic control system (Ying, 2000)

As depicted in the diagram, the input (there may be more than one input, depending on the required system performance) to the fuzzy logic controller is first fuzzified, and this involves computing membership values (normally between 0 and 1) for all the fuzzy sets used to capture the universe of discourse of the input. The results of this are fuzzy input windows which go into the inference engine. The inference uses the rule base to derive corresponding output windows which are then defuzzified to obtain the input control signal. Two types of fuzzy rules are available (Takagi & Sugeno, 1985): Mamdani fuzzy rules and Takagi-Sugeno fuzzy rules.

The Mamdani rule for a fuzzy controller is stated as

$$IF\ e_1\ is\ A_1\ AND\ e_2\ is\ A_2\ \ldots\ AND\ e_n\ is\ A_n\ THEN\ u_1\ is\ B_1,\ \ldots,\ u_n\ is\ B_n \qquad (2.17)$$

where e_1, e_2, . . ., e_n are input variables; u_1, u_2, . . ., u_n are output variables; A_1, A_2, … A_n and B_1, B_2, …, B_n are fuzzy sets; and AND is a fuzzy logic AND operator.

The Takagi-Sugeno rule for a fuzzy controller is similarly defined as

$$IF\ e_1\ is\ A_1\ .\ .\ .\ AND\ e_n\ is\ A_n\ THEN\ u_1 = f(e_1, \ldots, e_n), \ldots, u_n = g(e_1, \ldots, e_n) \qquad (2.18)$$

where f(), . . ., g() are real functions.

Defuzzification is a process of generating continuous-time control signals from the output variables u_1, u_2, . . ., u_n given in equations (2.17) and (2.18). The generalized defuzzifier is given as (Ying, 2000)

$$u = \frac{\sum_{i=1}^{N} \mu_i^{\alpha} . \beta_i}{\sum_{i=1}^{N} \mu_i^{\alpha}} \qquad (2.19)$$

where u is the fuzzy controller output variable, μ_is are the output fuzzy set membership values generated by the fuzzy inference, and β_is are the nonzero values of the output fuzzy sets.

2.1.4.5 Artificial Neural Network-Based Control

Artificial neural networks were developed by McCulloch and Pitts (McCulloch & Pitts, 1943) after the pattern of the biological neural networks to equip engineered systems with some level of intelligence, i.e., ability to reason, learn, remember, and respond to unfamiliar inputs. The general model of an artificial neuron is shown in Fig. 2.16. The inputs to the neuron are x_1, x_2, . . .,x_n; b_i is a bias; f_i is the neuron's activation function; and y_i is its output. The neuron produces an output if the weighted sum of all its inputs is above a threshold value.

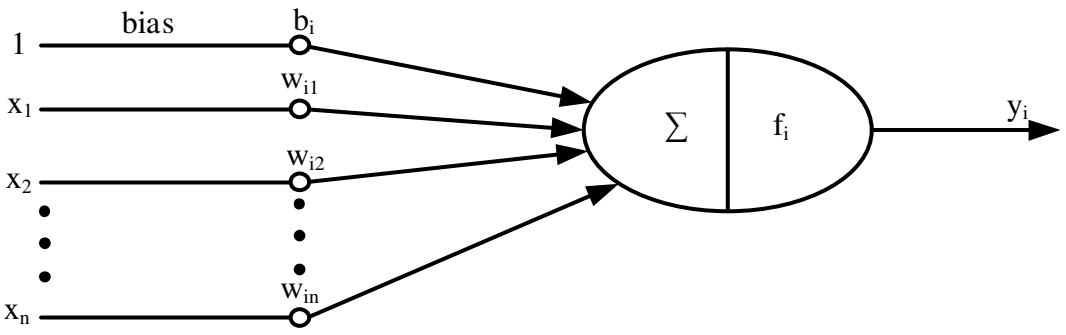

Fig. 2.16: Model of an artificial neuron

Two commonly used ANN networks are the feed forward and recurrent networks, and they can be trained in a supervised and an unsupervised manner depending on the application. Fig. 2.17 depicts how a neural network controller can be trained to emulate the behavior of an existing controller (Burns, 2001).

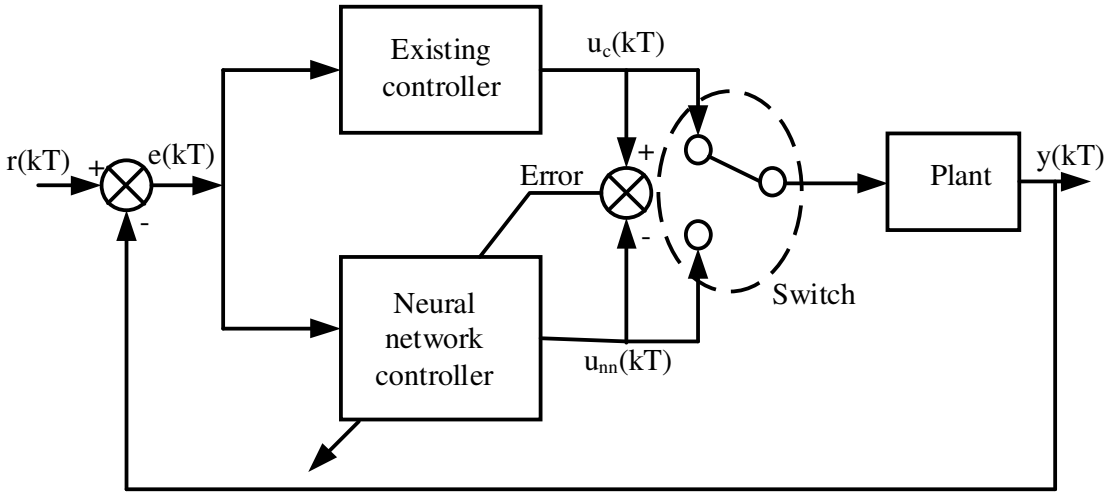

Fig. 2.17: Neural network controller training (Burns, 2001)

Nonlinear control strategies as well as techniques have continued to witness development in many fields of learning, even though "it is well known that there is no general nonlinear control or modeling theory because general nonlinear system theory has not been, and most likely will not be, established" (Ying, 2000).

Applications of some of these strategies to electric power systems are detailed in related literature, although many are based on the approximate (linearized) models of the systems. A review of the relevant literature is provided in the following subsection:

2.2 General Review of Relevant Works

Oscillations such as local plant and inter-area occur in power systems, and pose major challenges to power system control engineers. These oscillations are usually caused by lack of sufficient generator rotor damping torque (and this phenomenon characterized the earliest exciter/AVR due to the increase in bandwidth associated with the AVR loop) (Dandeno *et al.*, 1987; Hajagos, 2003). The challenges become more stringent as power systems undergo changes due to network alterations (caused by faults or switching events) and/or variations in loads.

Conventionally, power system stabilizers (PSSs), which may be single-or double-input, have been employed to handle these oscillation problems. They are complementary excitation controllers which provide positive damping torque to improve the overall generator rotor damping (Demello *et al.*, 1978; Ghandakly & Farhoud, 1992; Irvin *et al.*, 1979; Kasturi & Doraraju, 1970; Kundur *et al.*, 1989; Larsen & Swann, 1981; Lim & Elangovan, 1985; Yu & Moussa, 1972; Kumar *et al.*, 2012). To some degree, they have performed satisfactorily well, but it has been noted that in the same way that a power system stabilizer can improve stability if tuned properly, it also has the ability to destabilize a generator's operation if incorrectly tuned" (Hajagos, 2003). So, serious outstanding issues regarding the tuning of the conventional power system stabilizers and its performance for a wide range of operating conditions still remain (Huerta *et al.*, 2011). Fig. 2.18 shows a single-input PSS.

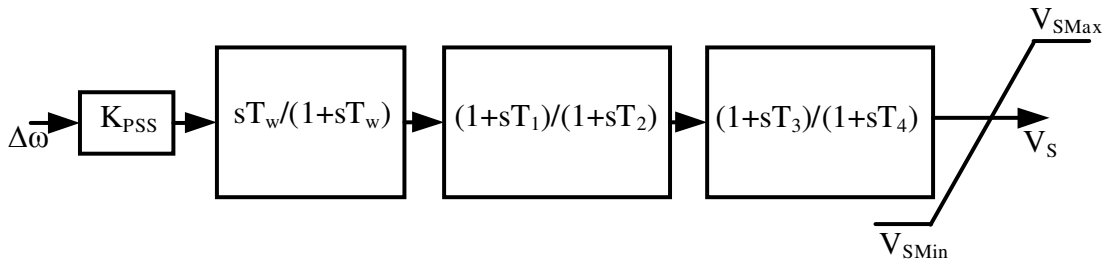

Fig. 2.18: Single-input PSS controller with a washout and two lead-lag stages(Li-Jun & Erlich, 2005)

However, many control techniques have been developed to enhance the performance of the conventional PSSs; they range from adaptive, robust, feedback linearization, to intelligent control strategies, with combinations of these strategies or their modifications having been implemented. Adaptive control strategies, such as model reference adaptive control (MRAC) and self-tuning control (STC), have been offered as solutions for providing adjustment of controller parameters as systems undergo changes due to parameter variations—they adjust their parameters on-line in response to changing operating conditions (Pierre, 1987). More commonly used is the self-tuning adaptive control, which comprises an approximator for on-line parameter identification, and a controller structure for guaranteeing good stability and dynamic response. Ghandakly & Farhoud (1992) proposed a self-tuning regulator for power system stabilizers using a recursive least squares identification technique, and a parameter optimization approach which employed a quadratic performance criterion. This regulator was shown to outperform the previously designed regulators based on minimum variance, generalized minimum variance, PID, and deadbeat control strategies (Ghandakly & Kronegger, 1987; Gu & Bollinger, 1989; Kanniah *et al.*, 1984; Wu & Hsu, 1988), but the machine

considered was represented by the classical swing-equation model with a first-order exciter, and subjected to a three-phase fault of duration not more than 0.1s. The speed response, it was shown, settled within 2-3s. Also, by employing a pole-shifting factor to make all closed-loop poles remain within the unit circle, Ghandakly & Dai (1992) demonstrated the effectiveness and robustness of a generalized multivariable self-tuning controller. The controller was shown to settle the system response in about 2s after subjecting the model power system used to a series of fault conditions.

Moreover, a set of power system stabilizer schemes, using various control strategies, was considered by Falkner & Hech (1995), and, although the authors raised some pertinent issues (i.e., limited controller sophistication; set point tracking) which suggested further investigations into the controllers discussed, it was inferred by them that linear robust and fuzzy controllers performed best in comparison to linear power system stabilizer, and nonlinear robust and sliding mode controllers. Criteria based on unmodeled dynamics, parameter variations, measurement noise, and input disturbance were used to draw the inferences.

Meanwhile, Abdel-Magid *et al*. (1999) proposed a new method of tuning the conventional power system stabilizers using the genetic algorithm (GA) approach. In the study, the problem of stabilizing a set of plants, representing various operating conditions, was converted into a GA-based optimization problem in which the considered power system stabilizer's parameters (only three of them) were optimally tuned to stabilize the set of plants. However, the objective function used was formulated based on the eigenvalues that needed to be shifted / placed, thereby making accurate tracking of eigenvalues a necessary condition for the success of the parameter tuning. Besides, the

settling time of the speed variations was as much as 2.4s in some disturbance cases considered.

Another significant area of applications of control techniques for power system stabilization is feedback linearization control (FBLC), which involves complete or partial transformation of nonlinear systems into equivalent linear ones that are amenable to linear control design techniques (Khalil, 2015; Lin, 1964). Several versions of FBLC have been applied to the design of power system excitation control (Chapman *et al*., 1993; Mielczarski & Zajaczkowjki, 1994; Nambu & Ohsawa, 1996; Sun & Lu, 1996). But Gan. et al. (2000) set out to address some major design issues associated with FBLC, such as knowledge of the equilibrium point of the power system, dependence on the topology of the power system, and lack of guarantee that terminal voltages would remain within their operating limits. The authors proposed an improved FBLC using a linear optimal state-space feedback and saturation-type nonlinear robust control strategies, although a single-axis model was employed and the rotor angle oscillations were damped out in a long duration of about 15s (after perturbing system under the action of the proposed controller). Associated with FBLC is the method of zero dynamics which allows the output function of any nonlinear system to be kept very close to zero using a nonlinear state feedback control. Mahmud *et al.* (November 2011) used this method of zero dynamics for feedback linearizing excitation control for power systems. A disturbance in form of change in the rotor angle operating point was applied, and it was observed that the speed deviation steadied to zero in 2.6s.

Other control principles and design techniques that have gained prominence in realizing control laws for power system stabilization are Lyapunov stability theory, passivity

theory, optimal control theory, and variable structure control; they have been implicitly or explicitly used in designing control systems that led to good performance and reliable system behavior (Espinosa-Perez *et al*., 1997; Falkner & Heck, 2000; Katende & Awelewa, 2007; Lu & Xu, 1996; Mukhopadhyay & Malik, 1972; Pogromsky *et al*., 1996; Roberts & Ian, 1997; Samarasinghe & Pahalawatha, 1994). Lyapunov-based control design involves searching for, or constructing, a candidate energy function that would guarantee asymptotic stability and acceptable response of a closed-loop system (Ogata, 1997). Passivity theory is a method of constructing a Lyapunov function for a combination of systems of subsystems with known individual Lyapunov functions; it provides procedures for generating physically meaningful Lyapunov functions for dynamical systems as long as certain properties are satisfied (Lin, 1964). This method of Lyapunov function was employed by Rui *et al.* (2010) to design a novel excitation controller using the adaptive backstepping technique. The controller worked well by removing oscillations within 2.5s from the system after the system was subjected to an 8-cycle fault. One general drawback with this approach is how to determine the Lyapunov function whose existence is not certain. In the case of optimal control, the thrust of the design is to maximize the performance of a dynamic system at a minimum cost; it consists of designing a control law that will give an optimal state trajectory such that a cost function, known as a performance index, is minimized. Variable structure control strategies have been known to offer robustness in the face of system uncertainty (Juan & Gerald, 2010; Huerta *et al*., 2011), and sliding mode control is highly useful in this regard. Using sliding mode control, Colbia-Vega *et al*. (2008) designed robust excitation controller for power systems. The controller caused system variables to converge to the

equilibrium point in 2.5s after the removal of a 5-cycle fault to which the system was subjected. Also, Huerta *et al*. (2010) proposed a sliding mode speed stabilizer (SMSS)-sliding mode voltage regulator (SMVR) scheme which is similar to the classical AVR-PSS scheme. Although the performance of the proposed scheme depended on the proper coordination of the SMSS and SMVR blocks, the scheme offered better damping of oscillations than the AVR-PSS scheme. In the work, oscillations caused by a three-phase symmetrical fault lasting for 8 cycles were damped out in 1.5s to 2.5s. Another application of sliding mode control to a single-machine infinite-bus power system was carried out by Atabak and Saeed (2012). Their proposed controller was shown to outperform the conventional PSS, though, it was pointed out by the authors, determining the controller gain involved a trial-and-error process. The theory of synergetic control, which is similar to sliding mode control, has also been applied to design excitation controllers—for example, Ping *et al*. (2014) proposed an improved synergetic excitation controller for improving transient stability of power systems and voltage regulation performance. This work used a synergetic control signal to move the system variables to a manifold defined as $\psi = 0$ and then cause them to remain on this manifold at all times, thereby removing oscillations due to system faults. A 6-cycle three-phase fault to which the system was subjected led to oscillations that were damped out in 2s.

Recently, there has been a resurgence of research interest in the application of fuzzy logic and neural networks, or their combinations, to damping oscillations in power systems. For instance, in (Chaturvedi & Malik, 2005), an adaptive power system stabilizer based on a generalized neuron artificial neural network (GNANN) was presented, and shown to outperform the structures put forward in (Zhang *et al*., 1995, Zhang *et al*., March 1993,

Zhang *et al*., May 1993) which have 20 input layers, 20 hidden layers, and 1 output layer; 35 input layers and 1 output layer; and 30 input layers, 10 hidden layers, and 1 output layer, respectively. In the paper, the system, whose identifier and controller were GN-based, was able to dampen out oscillations due to, among others, a three-phase fault in about 2-3s. The authors used only a single neuron to realize the system. Meanwhile, Yee & Milanovic (2008) offered a new intelligent approach, i.e., a fuzzy logic controller that uses a systematic analytical procedure in place of a priori expert knowledge/information, to stabilize both the power output and terminal voltage of a synchronous generator. But the effectiveness of the approach was demonstrated using only the swing-equation model of a synchronous generator, and hinged on the premise that the loads must be static or that their dynamic responses are negligibly small compared to that of the generator. Likewise, a fuzzy logic-based power system stabilizer (FLPSS) was developed by Venkatesh & Rao (October 2012) to replace the classical power system stabilizer for a single machine connected to an infinite bus. In the work, the FLPSS was shown to damp out system oscillations faster than the classical PSS, though for the application of a three-phase fault that lasted for 5 cycles, the FLPSS could only make system variables settle in about 20s. This settling time is clearly too long.

More recently, an alternative approach to damping rotor angle oscillations in power systems was proposed by Garima *et al.* (2014). Using high power semiconductor devices, the authors developed a hybrid power flow controller (HPFC) to be located at an appropriate point in the transmission system. The performance of the controller was tested with a three-phase fault of 0.02 (1.2cycles), 0.04 (2.4cycles), 0.1 (6 cycles), and 0.2s (12 cycles) durations. It was observed by the authors that the HPFC damped out

oscillations and ensured system stability in 3.53, 3.7, 3.6, and 2.6s, respectively, for the above-given fault durations.

It has been pointed out that the critical clearing time, which is the maximum fault cycle that a system can withstand without losing stability, is an important aspect of transient stability (Shuji *et al.*, 2014). Therefore, it is still desirable to have controllers that can furnish the system with greater ability to withstand longer fault cycles and damp out system oscillations in much shorter time. Besides, many of the available power system controllers have complicated structures which are not amenable to easy implementation. So, a more compact nonlinear controller, which is universal and can be easily tuned for excellent system dynamic performance, is highly required—this universal controller is informed by the popular universal linear PID controller structure which has become the de facto controller for many industrial control applications (Yun *et al.*, 2006). In this work, two schemes are developed to meet these aforesaid requirements.

2.3 Summary

This chapter has presented a brief review drawn from the open literature of the fundamental theory and concepts, which are relevant to the work being carried out in this Thesis. These include different synchronous machine models and control methods, which will be further explored in the next chapter, with emphasis on control design.

CHAPTER THREE: SYSTEM MODEL ANALYSIS AND CONSTRUCTION OF CONTROL LAWS

3.0 Introduction

Generally, in any control system design, the plant model to be controlled constitutes a crucial part of the overall control problem solutions. Therefore, it is important that the plant model must be able to accurately represent state variables with significant influence on the dynamic behavior of the physical system being modeled. Besides, vital plant parameters must be represented. If reduced-order models of a physical plant are able to capture their typical low-frequency behaviors accurately, then they will be sufficient to be used for the purpose of control design, especially when the task of the controller is to improve stability and overall dynamic performance in spite of the plant's model imprecision (Slotine & Li, 1991). Considering sixth-, fourth-, and third-order models of a single machine connected to an infinite bus (SMIB) system as examples, this chapter presents three nonlinear excitation control laws. While two of these are higher order sliding mode laws, the third is based on the concept of dynamic system homogeneity. The construction of these laws leads to the overall development of control schemes for stabilizing power systems. Importantly, novel MATLAB tools are developed for testing any affine nonlinear dynamic system for exact linearization. This concept is fundamental to many nonlinear control system design problems.

3.1 Research Design

The stages involved in solving the research problem are: modeling of power systems, derivation of output signals, construction of control laws, implementation of control laws,

and realization of control schemes. These coherent and logical steps are presented pictorially in Fig. 3.1.

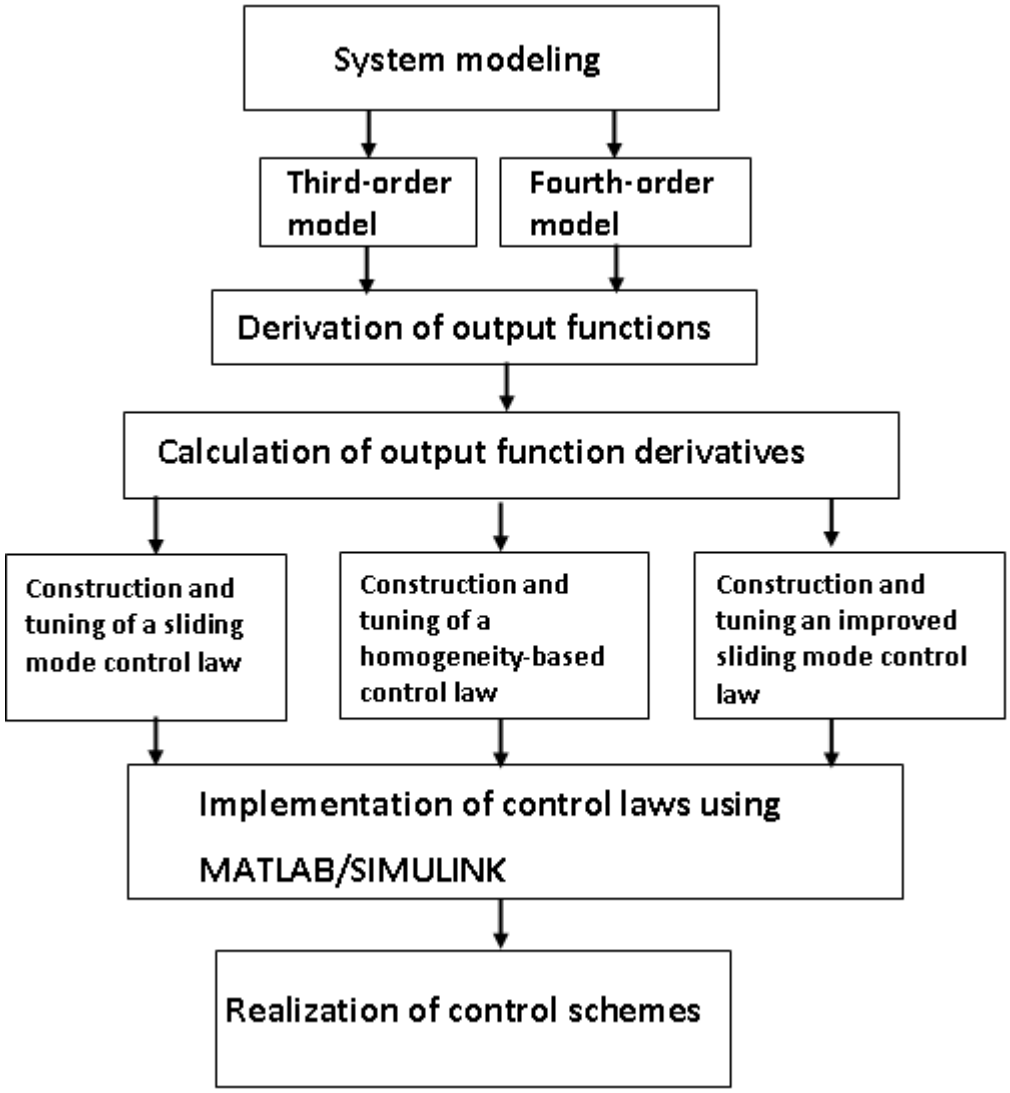

Fig. 3.1: Diagrammatical representation of the research design

As shown in the diagram, the final stage of the research is to realize control schemes that can handle large system disturbances and quickly damp out oscillations. In order to ensure that these schemes have this capability, the construction and implementation

stages are iterative. This means that the control laws are made to undergo software-based evaluation and the results of this are used to adjust the parameters of the control laws. This process of evaluation and adjustment is repeated until desirable optimal performance is obtained.

3.2 Power System Model (PSM) Description and Analysis

The general representation of a single generator connected to an infinite bus is shown in Fig. 3.2. A typical configuration is given in Fig. 3.3, with its simplified representation depicted in Fig. 3.4. Z_E in Fig. 3.3 is the equivalent impedance between the transformer terminal and the infinite bus, and is expressed as

$$Z_E = R_E + jX_E \tag{3.1}$$

where R_E and X_E are the equivalent transmission line resistance and reactance, respectively. The values of parameters R_E and X_E are lumped together with that of the generator and transformer. In other words, R_E is added to the generator armature resistance to form the overall resistance, while the sum of X_E and X_T (transformer reactance) is added to each generator reactance to get the appropriate overall reactance.

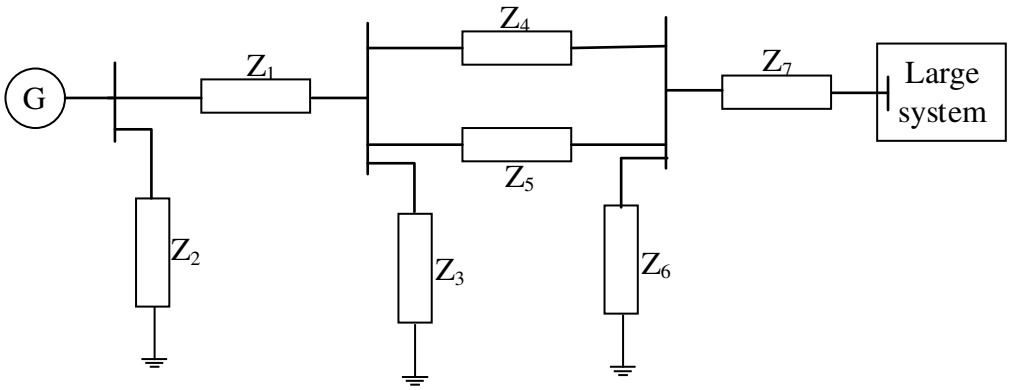

Fig. 3.2: General representation of a SMIB (Kundur, 1994)

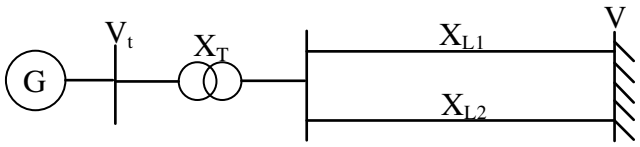

Fig. 3.3: Simplified representation of a SMIB (Mahmud *et al*., September 2011)

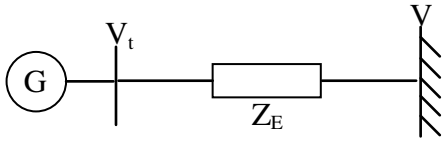

Fig. 3.4: Equivalent representation of a SMIB

Using the synchronous generator model given in the previous chapter, the dynamic equations describing this SMIB model is given in equations (3.2)-(3.7) (Anderson & Fouad, 2003; Kokotovic & Sauer, 1989) below.

$$\frac{d\delta}{dt} = \omega - \omega_s \tag{3.2}$$

$$\frac{d\omega}{dt} = \frac{T_m}{M} + \left(\frac{1}{X'_q+X_E} - \frac{1}{X'_d+X_E}\right)\frac{\psi_d\psi_q}{M} + \left(\frac{1}{X'_q+X_E}\right)\frac{\psi_d E'_d}{M} + \left(\frac{1}{X'_d+X_E}\right)\frac{\psi_q E'_q}{M} \tag{3.3}$$

$$\frac{dE'_q}{dt} = -\frac{(X_d+X_E)}{T'_{do}(X'_d+X_E)}E'_q + \frac{(X_d-X'_d)}{T'_{do}(X'_d+X_E)}\psi_d + \frac{1}{T'_{do}}E_f \tag{3.4}$$

$$\frac{d\psi_d}{dt} = -\frac{R_t\omega_s}{(X'_d+X_E)}\psi_d + \frac{R_t\omega_s}{(X'_d+X_E)}E'_q + \omega\psi_q + \omega_s V\sin\delta \tag{3.5}$$

$$\frac{d\psi_q}{dt} = -\frac{R_t\omega_s}{(X'_q+X_E)}\psi_q - \frac{R_t\omega_s}{(X'_q+X_E)}E'_d - \omega\psi_d + \omega_s V\cos\delta \tag{3.6}$$

$$T'_{qo}\frac{dE'_d}{dt} = -\frac{(X_q+X_E)}{(X'_q+X_E)}E'_d - \frac{(X_q-X'_q)}{(X'_q+X_E)}\psi_q \tag{3.7}$$

This is a sixth-order model having only one amortisseur winding in the quadrature axis. ψ_d and ψ_q are the flux linkages in the d-axis and q-axis, respectively, E'_q is the q-axis voltage which is proportional to the field winding flux linkage, E'_d is the d-axis voltage which is proportional to the amortisseur winding flux linkage, δ is the rotor or torque angle in radians, and ω is the rotor speed in radians/s. Also, T_m is the input torque, R_t is

the sum of the generator armature and transmission line resistances, V is the magnitude of the voltage of the infinite bus, ω_s is the synchronous speed of the generator, and E_f represents the excitation coil voltage. $M = 2H/\omega_s$, is the moment of inertia, where H is the generator inertia constant in seconds. All the parameters in the model, which have been defined previously, are in per unit.

In a more compact form and introducing some slight rearrangement, equations (3.2)-(3.7) can be rewritten as

$$\frac{d\delta}{dt} = \omega - \omega_s \tag{3.8}$$

$$\frac{d\omega}{dt} = A_1 + A_2\psi_d\psi_q + A_3\psi_d E'_d + A_4\psi_q E'_q \tag{3.9}$$

$$\frac{dE'_q}{dt} = -B_1 E'_q + B_2\psi_d + \frac{1}{T'_{do}} E_f \tag{3.10}$$

$$\frac{d\psi_d}{dt} = -C\psi_d + CE'_q + \omega\psi_q + V_s\sin\delta \tag{3.11}$$

$$\frac{d\psi_q}{dt} = -D\psi_q - DE'_d - \omega\psi_d + V_s\cos\delta \tag{3.12}$$

$$T'_{qo}\frac{dE'_d}{dt} = -E_1 E'_d - E_2\psi_q \tag{3.13}$$

The parameters A_1-A_4, B_1, B_2, C, D, E_1, and E_2 are defined as follows:

$$A_1 = \frac{T_m}{M}\,;\; A_2 = \left(\frac{1}{X'_q+X_E} - \frac{1}{X'_d+X_E}\right)\frac{1}{M}\,;\; A_3 = \left(\frac{1}{X'_q+X_E}\right)\frac{1}{M}\,;\; A_4 = \left(\frac{1}{X'_d+X_E}\right)\frac{1}{M}$$

$$B_1 = \frac{(X_d+X_E)}{T'_{do}(X'_d+X_E)}\,;\; B_2 = \frac{(X_d-X'_d)}{T'_{do}(X'_d+X_E)}$$

$$C = \frac{R_t\omega_s}{(X'_d+X_E)}$$

$$D = \frac{R_t\omega_s}{(X'_q+X_E)}$$

$$E_1 = \frac{(X_q+X_E)}{(X'_q+X_E)}\,;\; E_2 = \frac{(X_q-X'_q)}{(X'_q+X_E)}$$

$$V_s = \omega_s V$$

The two-axis and one-axis models can be derived from the sixth-order model described above by introducing relevant assumptions as carried out in the previous chapter. But to reveal some fundamental issues regarding these reduced-order models and gain proper mathematical insights about their structure, the concept of integral manifold is employed to derive them. Sauer, *et al*. (1988) forms the basis for this derivation, though some extensions to this are included here.

3.2.1 Two-Axis Model (PSM1)

This is a reduced-order model which assumes that the stator transients are restricted to an integral manifold in the state space. This manifold represents the solutions of the stator differential equations (3.11) and (3.12) when the resistance R_t is zero.

With these solutions given as (Sauer *et al.*, 1988)

$$\psi_d = V\cos\delta \tag{3.14}$$

$$\psi_q = -V\sin\delta, \tag{3.15}$$

the manifold facilitates the reduction of the sixth-order model described by equations (3.8)-(3.13) to the following fourth-order model (Fitzgerald *et al*., 1983; Kundur & Dandeno, 1983):

$$\frac{d\delta}{dt} = \omega - \omega_s \tag{3.16}$$

$$\frac{d\omega}{dt} = A_1 - \frac{1}{2}A_2V^2\sin2\delta + A_3VE'_d\cos\delta - A_4VE'_q\sin\delta \tag{3.17}$$

$$\frac{dE'_q}{dt} = -B_1E'_q + B_2V\cos\delta + \frac{1}{T'_{do}}E_f \tag{3.18}$$

$$T'_{qo}\frac{dE'_d}{dt} = -E_1E'_d + E_2V\sin\delta \tag{3.19}$$

when the initial conditions $\delta(0)$, $\psi_d(0)$, and $\psi_q(0)$ are on the manifold, i.e., when the initial conditions of the stator transients are on the manifold. As demonstrated in (Sauer *et al.*, 1988), this two-axis model approximates the sixth-order model very well, although, when the stator transient initial conditions are off the manifold, the model yields (Sauer *et al.*, 1988) the following:

$$\frac{d\delta}{dt} = \omega - \omega_s \tag{3.20}$$

$$\frac{d\omega}{dt} = A_1 - \frac{1}{2}A_2V^2\sin 2\delta + A_3VE'_d\cos\delta - A_4VE'_q\sin\delta + T_{st} \tag{3.21}$$

$$\frac{dE'_q}{dt} = -B_1E'_q + B_2(V\cos\delta + d_d) + \frac{1}{T'_{do}}E_f \tag{3.22}$$

$$T'_{qo}\frac{dE'_d}{dt} = -E_1E'_d + E_2(V\sin\delta - d_q) \tag{3.23}$$

where T_{st} (a component of torque associated with the initial conditions of the stator transients) is given as

$$T_{st} = \frac{1}{M}\left[A_2(d_dd_q - d_dV\sin\delta + d_qV\cos\delta) + A_3d_dE'_d + A_4d_qE'_q\right] \tag{3.24}$$

with

$$d_d = \sqrt{d_d^2(0) + d_q^2(0)}\cos\left[\omega_st + \delta - \delta(0) - \mathrm{Tan}^{-1}\left(\frac{d_q(0)}{d_d(0)}\right)\right] \tag{3.25}$$

$$d_q = \sqrt{d_d^2(0) + d_q^2(0)}\sin\left[\omega_st + \delta - \delta(0) - \mathrm{Tan}^{-1}\left(\frac{d_q(0)}{d_d(0)}\right)\right] \tag{3.26}$$

3.2.2 One-Axis Model (PSM2)

This reduced-order model is obtained by eliminating the influence of the damper winding or, in other words, assuming that T'_{qo} is a very small number α. This requires that E'_d be solved for in terms of δ, ω, and E'_q from equation (3.19) and then substituted into

equation (3.17). For better accuracy, a third-order approximation is considered here. (A case of second-order approximation is treated by Sauer *et al.* (1988))

Let the solution of E'_d be given by the function

$$E'_d = G(\delta, \omega, E'_q, \alpha). \tag{3.27}$$

Substituting this last equation into equation (3.19) yields

$$\alpha \frac{dG}{dt} = -E_1 G + E_2 V \sin\delta \tag{3.28}$$

where

$$\alpha \frac{dG}{dt} = \alpha \frac{\partial G}{\partial \delta}\frac{d\delta}{dt} + \alpha \frac{\partial G}{\partial \omega}\frac{d\omega}{dt} + \alpha \frac{\partial G}{\partial E'_q}\frac{dE'_q}{dt} \tag{3.29}$$

Since α is small, equation (3.27) can be expanded using Taylor's series to give

$$E'_d = G(\alpha) + G'(\alpha)\alpha + \frac{G''(\alpha)}{2!}\alpha^2 + \frac{G^{(3)}(\alpha)}{3!}\alpha^3 + \cdots$$

or, ignoring higher-order powers of α,

$$E'_d = G_0 + G_1\alpha + G_2\alpha^2 \tag{3.30}$$

with

$$G_0 = G(\alpha)$$

$$G_1 = G'(\alpha)$$

$$G_2 = \frac{G''(\alpha)}{2!}.$$

Again, equating equation (3.28) and equation (3.29) after the substitution of equation (3.30) gives

$$\alpha \frac{\partial(G_0+G_1\alpha+G_2\alpha^2)}{\partial \delta}\frac{d\delta}{dt} + \alpha \frac{\partial(G_0+G_1\alpha+G_2\alpha^2)}{\partial \omega}\frac{d\omega}{dt} + \alpha \frac{\partial(G_0+G_1\alpha+G_2\alpha^2)}{\partial E'_q}\frac{dE'_q}{dt}$$

$$= -E_1(G_0 + G_1\alpha + G_2\alpha^2) + E_2 V \sin\delta \tag{3.31}$$

Equation (3.31) is now manipulated by equating corresponding coefficients of various powers of α on both sides to yield G_0, G_1, and G_2.

For α^2 approximation, G_0 and G_1 form the component of E'_d, and are given as

$$G_0 = F_1 V \sin\delta \tag{3.32}$$

$$G_1 = -\frac{F_1}{E_1} V(\omega - \omega_s)\cos\delta \tag{3.33}$$

where $F_1 = \frac{E_2}{E_1}$.

Likewise, for α^3 approximation, G_0, G_1, and G_2 form the components of E'_d, with G_2 given as

$$G_2 = -\frac{F_1}{E_1^2}(\omega - \omega_s)^2 V \sin\delta + \frac{F_1}{E_1^2} V \cos\delta \left[T_1 + A_3 F_1 V^2 \sin\delta\cos\delta - A_4 V E'_q \sin\delta\right] \tag{3.34}$$

where $T_1 = (A_1 - A_2 V^2 \sin\delta\cos\delta)$.

(The full derivations of equations (3.32), (3.33), and (3.34) are provided in Appendix A.)

From equation (3.30), based on these two approximations, E'_d is given respectively in equations (3.35) and (3.36) as follows:

$$E'_d = F_1 V \sin\delta - \alpha \frac{F_1}{E_1} V(\omega - \omega_s)\cos\delta \tag{3.35}$$

$$E'_d = F_1 V \sin\delta - \alpha \frac{F_1}{E_1} V(\omega - \omega_s)\cos\delta - \alpha^2 \frac{F_1}{E_1^2}(\omega - \omega_s)^2 V \sin\delta + \alpha^2 \frac{F_1}{E_1^2} V \cos\delta \left[T_1 + A_3 F_1 V^2 \sin\delta\cos\delta - A_4 V E'_q \sin\delta\right] \tag{3.36}$$

Therefore, substituting equation (3.35) into equation (3.17) and combining the result with equations (3.16) and (3.18) yields the following third-order model

$$\frac{d\delta}{dt} = \omega - \omega_s \tag{3.37}$$

$$\frac{d\omega}{dt} = A_1 + \frac{F_2 V^2}{2}\sin 2\delta - A_4 V E'_q \sin\delta - \underbrace{T'_{q0}\frac{F_3 F_1}{M} V^2 \cos^2\delta}(\omega - \omega_S) \tag{3.38}$$

$$\frac{dE'_q}{dt} = -B_1 E'_q + B_2 V\cos\delta + \frac{1}{T'_{do}} E_f \tag{3.39}$$

with $F_2 = \left(\frac{1}{X'_d + X_E} - \frac{1}{X_q + X_E}\right)\frac{1}{M}$ and $F_3 = \left(\frac{1}{X_q + X_E}\right)$.

The last term in equation (3.38) actually denotes the torque component associated with the damper winding. The accented part of this term is often represented in the literature (Anderson & Fouad, 2003; Fusco & Russo, 2012; Arjona *et al.*, 2009) as D/M, where D is called the damping constant, and M is as defined previously. Hence, the popular flux decay model is

$$\frac{d\delta}{dt} = \omega - \omega_s \tag{3.40}$$

$$\frac{d\omega}{dt} = A_1 - \frac{D}{M}(\omega - \omega_S) + \frac{F_2 V^2}{2}\sin 2\delta - A_4 V E'_q \sin\delta \tag{3.41}$$

$$\frac{dE'_q}{dt} = -B_1 E'_q + B_2 V\cos\delta + \frac{1}{T'_{do}} E_f \tag{3.42}$$

The third-order model can be improved upon if equation (3.36) is substituted into equations (3.16)-(3.18) with one more additional term (due to the damper winding) added. This improved model is reflected in the rotor speed differential equation:

$$\frac{d\omega}{dt} = A_1 + \frac{F_2 V^2}{2}\sin 2\delta - A_4 V E'_q \sin\delta - \underbrace{T'_{q0}\frac{F_3 F_1}{M} V^2 \cos^2\delta}(\omega - \omega_S) -$$

$$\underbrace{\frac{(T'_{q0})^2 A_3 F_1}{2E_1^2} V^2 \sin 2\delta}(\omega - \omega_S)^2 \tag{3.43}$$

The complete derivation is shown in Appendix A. In a similar fashion to equations (3.40)-(3.42), the improved flux decay model is given as

$$\frac{d\delta}{dt} = \omega - \omega_s \tag{3.44}$$

$$\frac{d\omega}{dt} = A_1 - \frac{D_1(\omega-\omega_S)}{M} - \frac{D_2(\omega-\omega_S)^2}{M} + \frac{F_2V^2}{2}\sin 2\delta - A_4 V E'_q \sin\delta \quad (3.45)$$

$$\frac{dE'_q}{dt} = -B_1 E'_q + B_2 V\cos\delta + \frac{1}{T'_{do}} E_f \quad (3.46)$$

It is instructive that when T'_{qo} is significantly small, the flux decay model in equations (3.40)-(3.42) will sufficiently approximate the higher-order models. Otherwise, equations (3.44)-(3.46) are a better approximation.

To investigate the accuracy of the reduced-order models discussed so far, a disturbance, which is a short-circuit fault at the infinite bus, is applied for the duration of 0.1second (5-cycle fault), 0.14second (7-cycle fault) and 0.18second (9-cycle fault) after the system has reached a steady state. Fig. 3.5 to Fig. 3.13 show the response waveforms of the three models (equations (3.8)-(3.13), equations (3.16)-(3.19) and equations (3.37)-(3.39)) under the three different fault cycles for the initial conditions x_0 = [0.6836, 317.43, 1.1413], x_0 = [0.6836, 317.43, 0.2956], and x_0 = [0.6836, 317.43, 1.1413, 0.7874, -0.6326, 0.2956]. (These initial conditions represent small deviations of the system states from their equilibrium values as obtained in Chapter 4, Section 4.1.) The system parameters used in this study are given in Table 3.1. The main stability indicators used in this chapter to validate the 3rd- and 4th-order synchronous machine models against their 6th-order counterpart are rotor load angle, rotor speed, and quadrature-axis EMF (E'_q).

Table 3.1: Typical system parameters for a SMIB (Anderson & Fouad, 2003; Sauer *et al.*, 1988)

System Parameter	Value
Synchronous reactance	X_d = 0.9 p.u.; X_q = 0.7 p.u.
Transient reactance	X'_d= 0.2 p.u.; X'_q= 0.2 p.u.
Open-circuit transient time constant	T'_{do}= 5.00 s; T'_{qo} = 0.13 s
Inertial constant	H = 5.00 s
Input torque	T_m = 0.8413
Transmission line reactance	X_E = 0.24 p.u.
Transformer reactance	X_T = 0.13 p.u.
Infinite-bus voltage magnitude	V = 1.0 p.u.

From the simulation waveforms displayed in Fig. 3.5 to Fig. 3.13, the general observation is that as the fault duration increases, the peak overshoots of the system variables being used as main stability indicators (δ, ω and E'_q) also increase. It is seen that the fourth-order model is able to approximate or reproduce the outputs of the sixth-order model with high degree of accuracy, while the third-order model deviates slightly from that of the sixth-order model. Particularly, the rotor angle 'δ' and the Q-axis voltage 'E'_q' obtained from the third-order model show noticeable deviations from those of the sixth-order model, especially during the first peak and subsequent oscillations from the fault clearance instances. For the rotor angle, the estimated first peak (swing) error is between 5^o and 6^o as the fault clearance time is varied from 5 to 9 cycles, while the error in the Q-axis voltage is minimal and ranges from 0.005pu to 0.01pu. Also, the error in E'_q between the two models being compared steadily decreases as the system approaches the steady state. Based on this investigation, it can be concluded that the third-order model state variables correctly match their corresponding variables from the 4^{th}-and 6^{th}-order models,

with negligible error during the first peak. Hence, it can be said that the fourth-and third-order models are good representations of the sixth-order model.

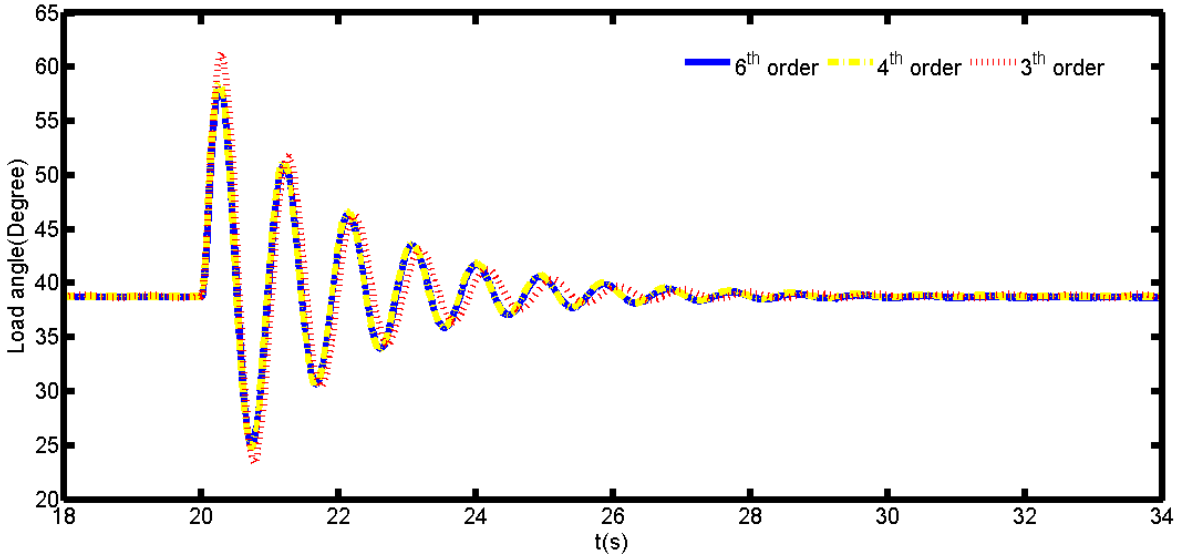

Fig. 3.5: Rotor angle waveforms for a 5-cycle fault

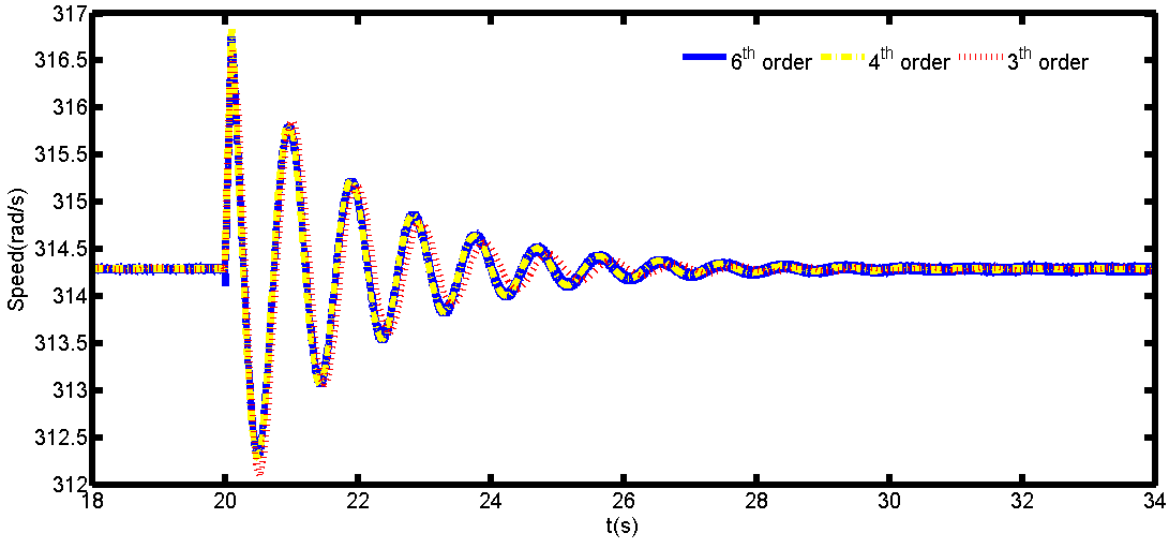

Fig. 3.6: Rotor speed waveforms for a 5-cycle fault

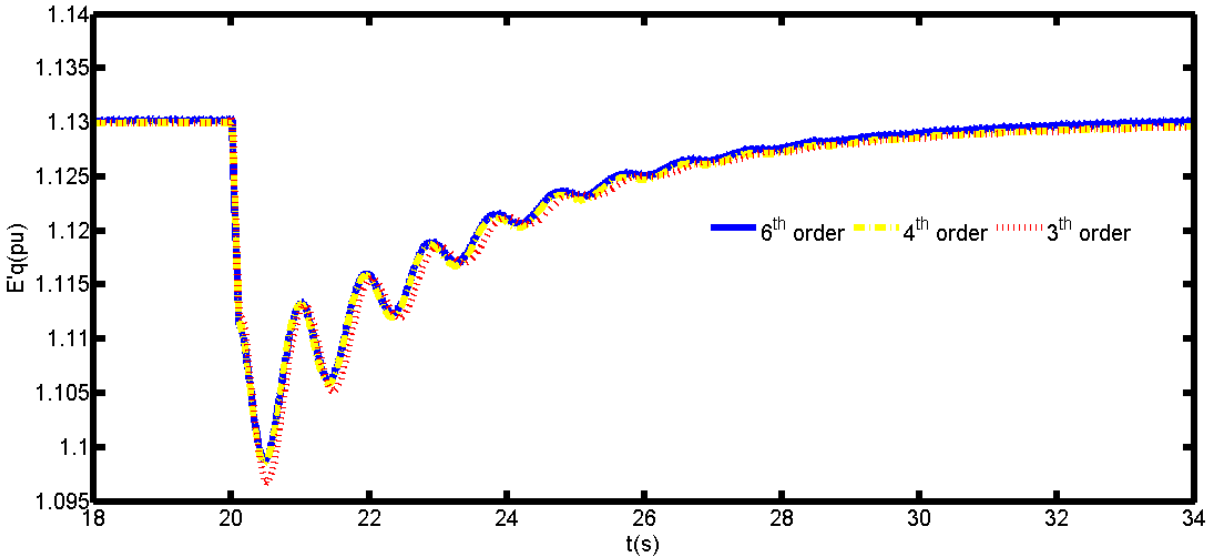

Fig. 3.7: Q-axis voltage waveforms for a 5-cycle fault

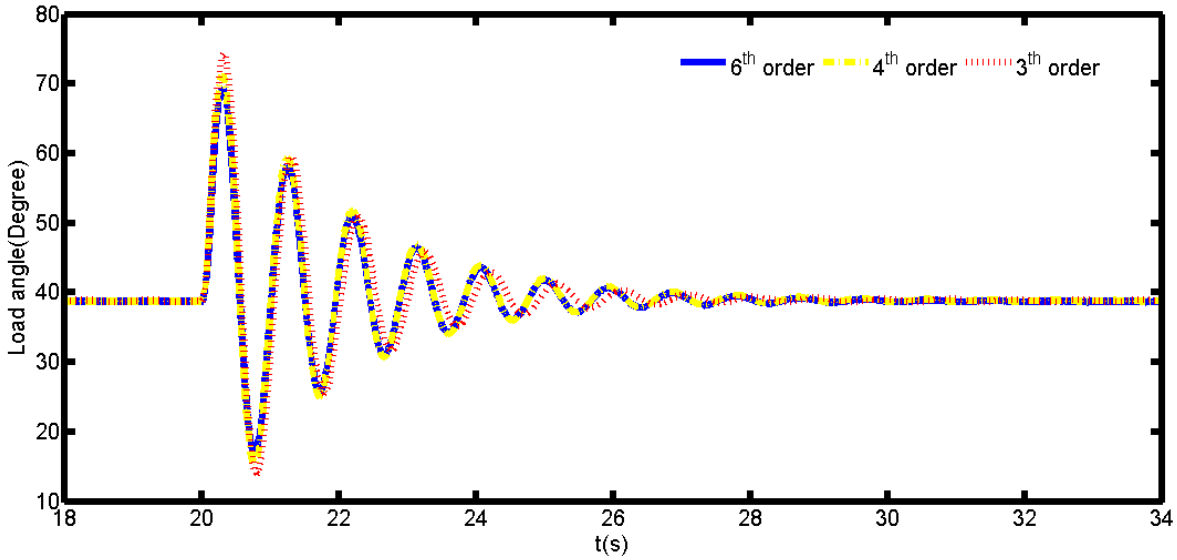

Fig. 3.8: Rotor angle waveforms for a 7-cycle fault

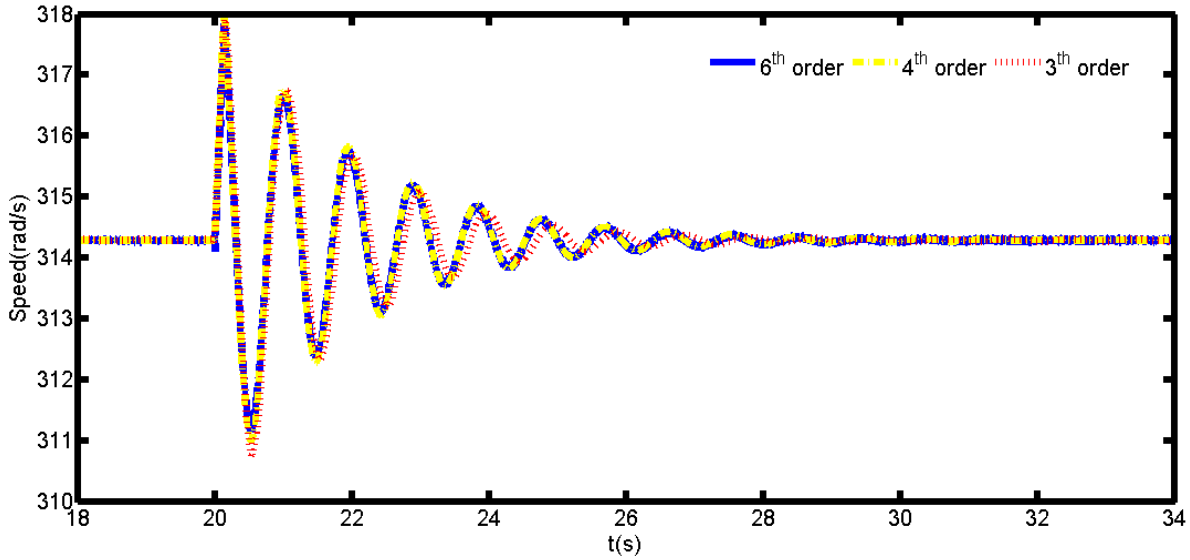

Fig. 3.9: Rotor speed waveforms for a 7-cycle fault

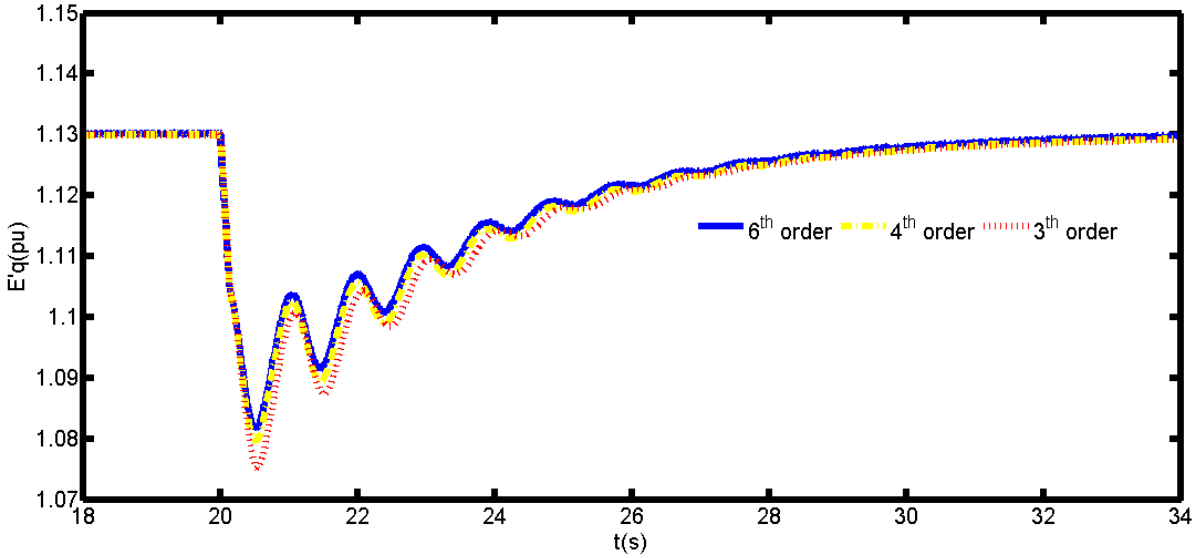

Fig. 3.10: Q-axis voltage waveforms for a 7-cycle fault

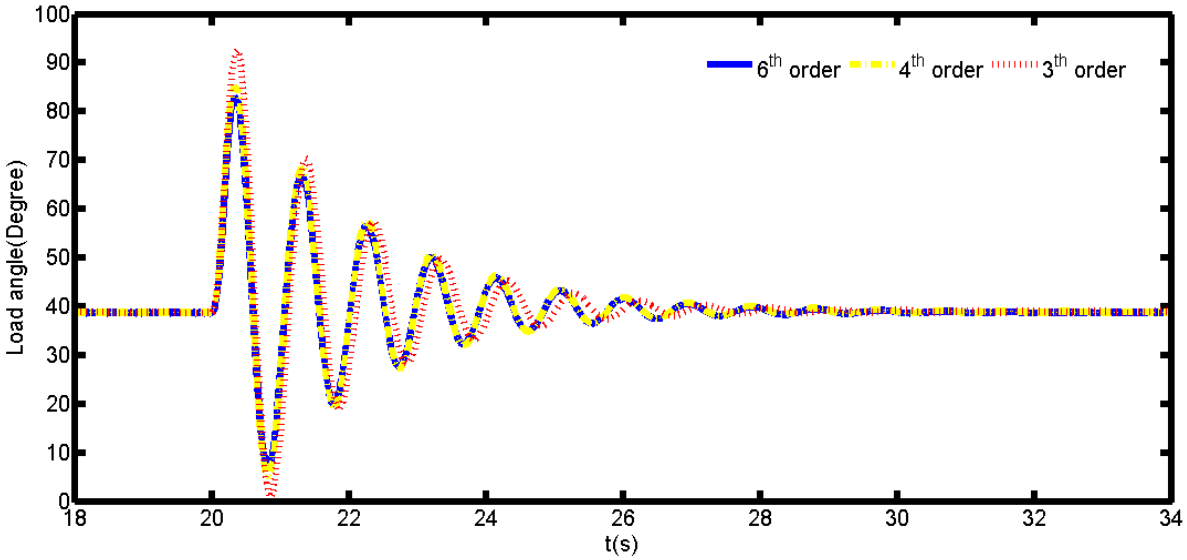

Fig. 3.11: Rotor angle waveforms for a 9-cycle fault

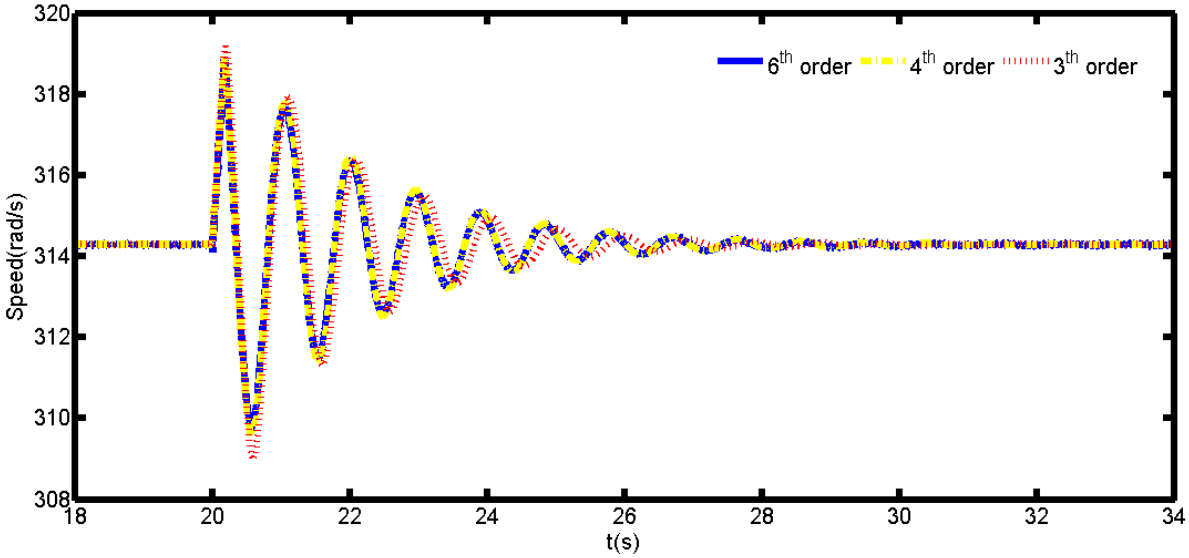

Fig. 3.12: Rotor speed waveforms for a 9-cycle fault

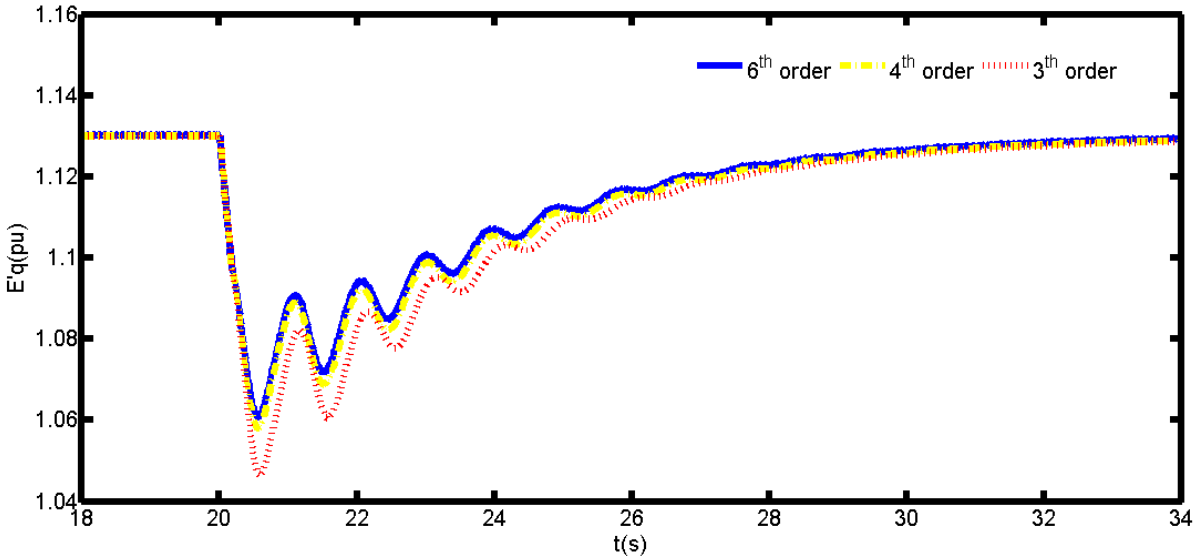

Fig. 3.13: Q-axis voltage waveforms for a 9-cycle fault

3.3 Control Law Construction

Consider an affine nonlinear power system represented by the model

$$\dot{x} = \mathrm{f}(x, \mathrm{t}) + \mathrm{g}(x)\mathrm{u} \tag{3.47}$$

where $x \in \mathbb{R}^n$is the system state vector, $\mathrm{f} \in \mathbb{R}^n$ and $\mathrm{g} \in \mathbb{R}^n$ are continuously differentiable function vectors, and u is the control signal. The control design problem involves construction of a nonlinear control law, u, that will ensure that the output signal becomes zero in finite time and remains so (with minimum control effort) thereafter, including under both normal and disturbance-induced conditions. This task requires a pre-selection or derivation of an output signal or function that naturally goes to zero when the system reaches its steady operating condition. In this regard, the relative degree of the system with respect to the chosen output is vital.

Notice that the control laws constructed in this chapter are based on the fourth-order and third-order models which were presented and validated earlier on. For the purpose of easy reference, the third-order model will be termed ‘power system model 1’ (PSM1), while

the fourth-order model will be termed 'power system model 2' (PSM2). Similarly, the control laws will be referenced accordingly—that is, 'control law 1' (CL1), 'control law 2' (CL2), etc.

3.3.1 Determination of System Outputs for Control Design

Generally, the chosen system output is such that the system relative degree (denoted as r) with respect to it is greater than or equal to the order of the system (denoted as n) i.e., $r \leq n$. In cases where $r < n$, then the system internal dynamics must be stable. In a broad term, the relative degree of any nonlinear system given by equation (3.47) is the number of times its output function will be time-differentiated to yield most immediately an expression which is a function of the control signal.

Definition 3.1: Consider the nonlinear system in equation (3.47). The relative degree, r, of the system equals the order, n, of the system if the matrix

$$\mathrm{P} = [\mathrm{g}(x) \quad \mathrm{ad_f g}(x) \quad \mathrm{ad_f^2 g}(x) \quad \cdots \quad \mathrm{ad_f^{n-1} g}(x)] \tag{3.48}$$

has rank n near the system operating point, x_0, and the matrix

$$\mathrm{D} = [\mathrm{g}(x) \quad \mathrm{ad_f g}(x) \quad \mathrm{ad_f^2 g}(x) \quad \cdots \quad \mathrm{ad_f^{n-2} g}(x)] \tag{3.49}$$

involutes at $x = x_0$. The involutivity condition is that matrix D and any of its variant

$$\mathrm{D_s} = \left[\mathrm{g}(x) \quad \mathrm{ad_f g}(x) \quad \cdots \quad \mathrm{ad_f^{n-2} g}(x) \quad \left[\mathrm{ad_f^i g}(x), \mathrm{ad_f^j g}(x)\right]\right] \tag{3.50}$$

have rank n-2, where i = 1, 2, …, n-2, j = 1, 2, …, n-2, and $i \neq j$. The symbol $\mathrm{ad_f g}(x)$ or $[f(x), g(x)]$ is called the Lie bracket of $g(x)$ along $f(x)$, and $\mathrm{ad_f^i g}(x) = \mathrm{ad_f}\left(\mathrm{ad_f^{i-1} g}(x)\right)$.

When the conditions in Definition 3.1 are satisfied, then the output function that makes r to be equal to n can be derived by either solving the system of partial differential equations

$$\frac{\partial y(x)}{\partial x}[g(x) \quad ad_f g(x) \quad \cdots \quad ad_f^{n-2} g(x)] = 0 \tag{3.51}$$

where y(x) is the unknown output function, or using the general algorithm given in Appendix B. $\frac{\partial y(x)}{\partial x}$ is the gradient of y(x) along $x = [x_1\ x_2\ x_3\ \ldots\ x_n]$. However, when the conditions in Definition 3.1 fail, it means the system relative degree is less than n, and the output function can be obtained only through equation (3.51).

Definition 3.2: Consider again the nonlinear system in equation (3.47). The relative degree of this system with respect to an intuitively pre-selected output function y(x) is the value of k such that

$$L_g y(x) = L_g L_f y(x) = L_g L_f^2 y(x) = \cdots = L_g L_f^{k-2} y(x) = 0 \tag{3.52}$$

but

$$L_g L_f^{k-1} y(x) \neq 0 \tag{3.53}$$

within a region of $x = x_0$, where $L_g L_f^i y(x)$ represents the Lie derivative of $L_f^i y(x)$ along the function g(x). Various output functions (measurable and/or convenient) can be chosen and then tested using equations (3.42) and (3.43). Two MATLAB programs—one for computing the relative degree of a nonlinear system and the other for verifying whether an output function that yields r = n exists—have been developed and are given in Appendix C. These MATLAB tools are general for any affine nonlinear system. The flowcharts for the programs are shown in Fig. 3.14 and Fig. 3.15.

Thus, for each of the models being considered, the system relative degree with respect to a number of output functions is computed using the MATLAB tools mentioned previously. Table 3.2 and Table 3.3 depict the results for the fourth-order and third-order models, respectively. The manual calculations are given in Sections 3.2.1.1 and 3.2.1.2.

Table 3.2: System relative degree for the fourth-order model

System output	Relative degree
$E'_{d\Delta}$	4
δ_{Δ}	3
ω_{Δ}	2
$E'_{q\Delta}$	1

Table 3.3: System relative degree for the third-order model

System output	Relative degree
δ_{Δ}	3
ω_{Δ}	2
$E'_{q\Delta}$	1

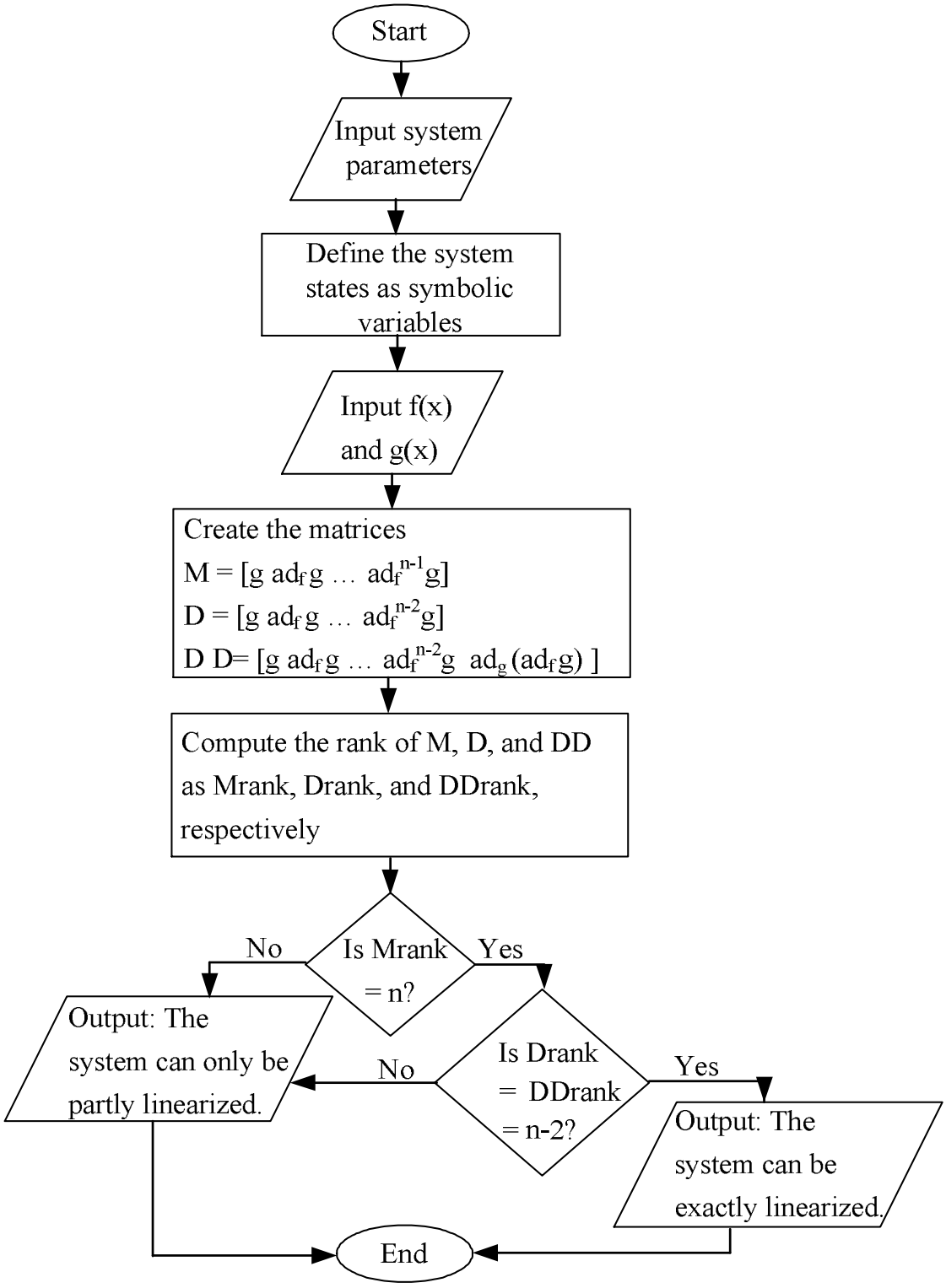

Fig. 3.14: Flowchart for testing the exact linearization condition

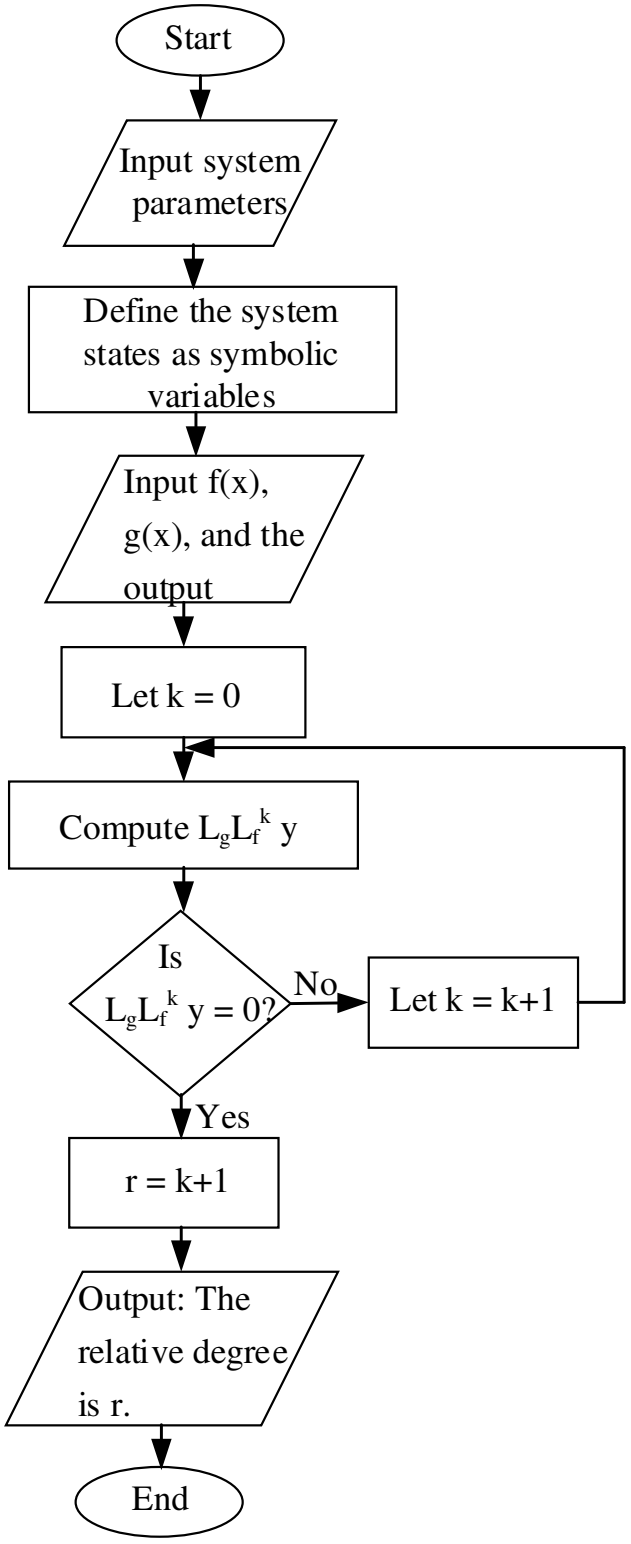

Fig. 3.15: Flowchart for computing the relative degree of a nonlinear system

3.3.1.1 Exact and Inexact Linearization of PSM1

PSM1, from equations (3.37)-(3.39), can be rewritten in a more compact form as

$$\dot{x} = \mathrm{f}(x) + \mathrm{g}(x)\mathrm{u} \tag{3.54}$$

where

$$x = \begin{pmatrix} x_1 \\ x_2 \\ x_3 \end{pmatrix} = \begin{pmatrix} \delta \\ \omega \\ \mathrm{E}'_{\mathrm{q}} \end{pmatrix},$$

$$\mathrm{f}(x) = \begin{pmatrix} \mathrm{f}_1 \\ \mathrm{f}_2 \\ \mathrm{f}_3 \end{pmatrix} = \begin{pmatrix} \omega - \omega_{\mathrm{s}} \\ \mathrm{A}_1 + \frac{\mathrm{F}_2\mathrm{V}^2}{2}\sin 2\delta - \mathrm{A}_4\mathrm{V}\mathrm{E}'_{\mathrm{q}}\sin\delta - \mathrm{T}'_{\mathrm{q}0}\frac{\mathrm{F}_3\mathrm{F}_1}{\mathrm{M}}\mathrm{V}^2\cos^2\delta(\omega - \omega_{\mathrm{S}}) \\ -\mathrm{B}_1\mathrm{E}'_{\mathrm{q}} + \mathrm{B}_2\mathrm{V}\cos\delta \end{pmatrix}$$

$$\mathrm{g}(x) = \begin{pmatrix} \mathrm{g}_1 \\ \mathrm{g}_2 \\ \mathrm{g}_3 \end{pmatrix} = \begin{pmatrix} 0 \\ 0 \\ 1/T'_{do} \end{pmatrix}, \text{ and } \mathrm{u} = \mathrm{E}_{\mathrm{f}}.$$

Linearization of PSM1 for output function $\delta_\Delta = \delta - \delta_0$

For $\delta_\Delta = \delta - \delta_0$, equations (3.42) and (3.43) give

$$\text{Term 1: } \mathrm{L}_{\mathrm{g}}\delta_\Delta = \frac{\mathrm{d}\delta_\Delta}{\mathrm{d}x}\mathrm{g}(x) = \begin{bmatrix} 1 & 0 & 0 \end{bmatrix}\begin{bmatrix} 0 \\ 0 \\ 1/T'_{do} \end{bmatrix} = 0.$$

$$\text{Term 2: } \mathrm{L}_{\mathrm{g}}\mathrm{L}_{\mathrm{f}}\delta_\Delta = \frac{\mathrm{d}(\mathrm{L}_{\mathrm{f}}\delta_\Delta)}{\mathrm{d}x}\mathrm{g}(x)$$

$$\mathrm{L}_{\mathrm{f}}\delta_\Delta = \frac{\mathrm{d}\delta_\Delta}{\mathrm{d}x}\mathrm{f}(x) = \begin{bmatrix} 1 & 0 & 0 \end{bmatrix}\begin{bmatrix} f_1 \\ f_2 \\ f_3 \end{bmatrix} = f_1 = \omega - \omega_s$$

$$\mathrm{L}_{\mathrm{g}}\mathrm{L}_{\mathrm{f}}\delta_\Delta = \frac{\mathrm{d}(\omega - \omega_s)}{\mathrm{d}x}\mathrm{g}(x) = \begin{bmatrix} 0 & 1 & 0 \end{bmatrix}\begin{bmatrix} 0 \\ 0 \\ 1/T'_{do} \end{bmatrix} = 0.$$

Term 3: $\mathrm{L_g L_f^2 \delta_\Delta} = \frac{\mathrm{d(L_f^2 \delta_\Delta)}}{\mathrm{d}x} \mathrm{g}(x)$

$$\mathrm{L_f^2 \delta_\Delta} = \frac{\mathrm{d(L_f \delta_\Delta)}}{\mathrm{d}x} \mathrm{f}(x) = [0 \quad 1 \quad 0] \begin{bmatrix} f_1 \\ f_2 \\ f_3 \end{bmatrix} = f_2$$

$$\mathrm{L_g L_f^2 \delta_\Delta} = \frac{\mathrm{d(L_f^2 \delta_\Delta)}}{\mathrm{d}x} \mathrm{g}(x) =$$

$$[\mathrm{F_2 V^2 cos2\delta - A_4 V E_q' cos\delta + T_{q0}' \frac{F_3 F_1}{M} V^2 (\omega - \omega_s) sin2\delta}$$

$$-\mathrm{T_{q0}' \frac{F_3 F_1}{M} V^2 cos^2\delta - \ A_4 V sin\delta}] \begin{bmatrix} 0 \\ 0 \\ 1/T_{do}' \end{bmatrix} = -\frac{\mathrm{A_4 V}}{T_{do}'} \mathrm{sin\delta}$$

Since the third term, i.e., $\mathrm{L_g L_f^2 \delta_\Delta}$, is not equal to zero (for $\delta \neq 0$ or $\pm m\pi$, where m is a positive integer), then the relative degree of PSM1 with respect to δ_Δ is 3. This also implies that PSM1 can be exactly linearized in the Bruvnosky normal form as follows:

$$\frac{\mathrm{dz_1}}{\mathrm{dt}} = \mathrm{z_2} \tag{3.55}$$

$$\frac{\mathrm{dz_2}}{\mathrm{dt}} = \mathrm{z_3} \tag{3.56}$$

$$\frac{\mathrm{dz_3}}{\mathrm{dt}} = \mathrm{v} \tag{3.57}$$

where $\mathrm{z_1} = \delta_\Delta$, $\mathrm{z_2} = \mathrm{L_f \delta_\Delta}$, $z_3 = \mathrm{L_f^2 \delta_\Delta}$, and $\mathrm{v} = \mathrm{L_f^3 \delta_\Delta} + \mathrm{L_g L_f^2 \delta_\Delta} u$.

Linearization of PSM1 for output function $\omega_\Delta = \omega - \omega_0$

Similarly, for $\omega_\Delta = \omega - \omega_0$, equations (3.42) and (3.43) give

$$\text{Term 1: } \mathrm{L_g \omega_\Delta} = \frac{\mathrm{d\omega_\Delta}}{\mathrm{d}x} \mathrm{g}(x) = [0 \quad 1 \quad 0] \begin{bmatrix} 0 \\ 0 \\ 1/T_{do}' \end{bmatrix} = 0.$$

Term 2: $\mathrm{L_g L_f \omega_\Delta} = \frac{\mathrm{d(L_f \omega_\Delta)}}{\mathrm{d}x} \mathrm{g}(x)$

$$L_f\omega_\Delta = \frac{d\omega_\Delta}{dx} f(x) = [0 \quad 1 \quad 0] \begin{bmatrix} f_1 \\ f_2 \\ f_3 \end{bmatrix} = f_2$$

$L_g L_f \omega_\Delta = \frac{df_2}{dx} g(x) = -\frac{A_4 V}{T'_{do}} \sin\delta.$

Here $L_g L_f \omega_\Delta$ is not equal to zero, and therefore, the relative degree of PSM1 with respect to ω_Δ is 2. This system can be partly linearized as follows:

$$\frac{dz_1}{dt} = z_2 \tag{3.58}$$

$$\frac{dz_2}{dt} = v \tag{3.59}$$

$$\frac{dz_3}{dt} = L_f\theta \tag{3.60}$$

such that $L_g\theta = 0$, where $z_1 = \omega_\Delta$, $z_2 = L_f\omega_\Delta$, $z_3 = \theta$, and $v = L_f^2\omega_\Delta + L_g L_f \omega_\Delta u$.

Equations (3.58)-(3.60) indicate that at a steady operating condition, the external dynamics, i.e., equations (3.58) and (3.59), vanish, while the internal dynamics, called zero dynamics, determine the state (and therefore, stability) of the system.

By solving

$$L_g\theta = 0,$$

it can be deduced that

$$\theta = x_1 = \delta.$$

Therefore, the internal dynamics

$$\frac{dz_3}{dt} = L_f\theta = \frac{d\theta}{dx} f(x) = \omega_\Delta$$

also vanish, keeping the system stable.

Linearization of PSM1 for output function $E'_{q\Delta} = E'_q - E'_{q0}$

For this output function, the first term in equation (3.42) is not zero. That is,

$$\text{Term 1: } L_g E'_{q\Delta} = \frac{dE'_{q\Delta}}{dx} g(x) = [0 \quad 0 \quad B_1] \begin{bmatrix} 0 \\ 0 \\ 1/T'_{do} \end{bmatrix} = \frac{B_1}{T'_{do}}.$$

So, the relative degree is 1. And the system is partly linearized thus:

$$\frac{dz_1}{dt} = v \tag{3.61}$$

$$\frac{dz_2}{dt} = L_f \theta_2 \tag{3.62}$$

$$\frac{dz_3}{dt} = L_f \theta_3 \tag{3.63}$$

with $L_g \theta_2 = 0$ and $L_g \theta_3 = 0$, where $z_1 = E'_{q\Delta}$, $z_2 = \theta_2$, $z_3 = \theta_3$, and $v = L_f E'_{q\Delta} + L_g E'_{q\Delta} u$. Since $\theta_2 = \delta$, and $\theta_3 = \omega$, the internal dynamics of this system become

$$\frac{dz_2}{dt} = z_3 - \omega_s$$

$$\frac{dz_3}{dt} = A_1 + \frac{F_2 V^2}{2} \sin 2z_2 - A_4 V E'_{q0} \sin z_2 - T'_{q0} \frac{F_3 F_1}{M} V^2 \cos^2 z_2 (z_3 - \omega_s)$$

These internal dynamic equations are very interesting and significant, as they represent the system swing equations. The import of this in terms of system dynamic performance is that any controller that drives $E'_{q\Delta}$ to zero and stabilizes the system will implicitly have stabilized its electromechanical dynamics.

3.3.1.2 Exact and Inexact Linearization of PSM2

Again, with PSM2, equations (3.16)-(3.19), expressed in the general form of equation (3.54), *x*, f(*x*), and g(*x*) are defined as follows:

$$x = \begin{pmatrix} x_1 \\ x_2 \\ x_3 \\ x_4 \end{pmatrix} = \begin{pmatrix} \delta \\ \omega \\ E'_q \\ E'_d \end{pmatrix};$$

$$f(x) = \begin{pmatrix} f_1 \\ f_2 \\ f_3 \\ f_4 \end{pmatrix} = \begin{pmatrix} \omega - \omega_s \\ A_1 - \frac{1}{2}A_2V^2\sin 2\delta - A_4VE'_q\sin\delta + A_3VE'_d\cos\delta \\ -B_1E'_q + B_2V\cos\delta \\ -\frac{E_1}{T'_{qo}}E'_d + \frac{E_2}{T'_{qo}}V\sin\delta \end{pmatrix};$$

$$g(x) = \begin{pmatrix} g_1 \\ g_2 \\ g_3 \\ g_4 \end{pmatrix} = \begin{pmatrix} 0 \\ 0 \\ 1/T'_{do} \\ 0 \end{pmatrix}; u = E_f.$$

Linearization of PSM2 for output function $E'_{d\Delta} = E'_d - E'_{d0}$

Employing equations (3.42) and (3.43) to find the relative degree with respect to this output gives

$$\text{Term 1: } L_gE'_{d\Delta} = \frac{dE'_{d\Delta}}{dx}g(x) = [0 \quad 0 \quad 0 \quad 1]\begin{bmatrix} 0 \\ 0 \\ 1/T'_{do} \\ 0 \end{bmatrix} = 0.$$

$$\text{Term 2: } L_gL_fE'_{d\Delta} = \frac{d(L_fE'_{d\Delta})}{dx}g(x)$$

$$L_fE'_{d\Delta} = \frac{dE'_{d\Delta}}{dx}f(x) = [0 \quad 0 \quad 0 \quad 1]\begin{bmatrix} f_1 \\ f_2 \\ f_3 \\ f_4 \end{bmatrix}$$

$$= f_4$$

$$L_gL_fE'_{d\Delta} = \begin{bmatrix} \frac{\partial(L_fE'_{d\Delta})}{\partial x_1} & \frac{\partial(L_fE'_{d\Delta})}{\partial x_2} & \frac{\partial(L_fE'_{d\Delta})}{\partial x_3} & \frac{\partial(L_fE'_{d\Delta})}{\partial x_4} \end{bmatrix}\begin{bmatrix} 0 \\ 0 \\ 1/T'_{do} \\ 0 \end{bmatrix}$$

$$= \frac{1}{T'_{do}}\frac{\partial(L_fE'_{d\Delta})}{\partial x_3} = \frac{1}{T'_{do}}.0 = 0.$$

$$\text{Term 3: } L_gL_f^2E'_{d\Delta} = \frac{d(L_f^2E'_{d\Delta})}{dx}g(x)$$

$$L_f^2 E'_{d\Delta} = \begin{bmatrix} \frac{\partial(L_f E'_{d\Delta})}{\partial x_1} & \frac{\partial(L_f E'_{d\Delta})}{\partial x_2} & \frac{\partial(L_f E'_{d\Delta})}{\partial x_3} & \frac{\partial(L_f E'_{d\Delta})}{\partial x_4} \end{bmatrix} \begin{bmatrix} f_1 \\ f_2 \\ f_3 \\ f_4 \end{bmatrix}$$

$$= f_1 \frac{\partial(L_f E'_{d\Delta})}{\partial x_1} + f_4 \frac{\partial(L_f E'_{d\Delta})}{\partial x_4}$$

$$= V \frac{E_2}{T'_{q0}}(\omega - \omega_s)\cos\delta - \frac{E_1}{T'_{q0}}\left(-\frac{E_1}{T'_{q0}} E'_d + \frac{E_2}{T'_{q0}} V\sin\delta\right)$$

$$L_g L_f^2 E'_{d\Delta} = \begin{bmatrix} \frac{\partial(L_f^2 E'_{d\Delta})}{\partial x_1} & \frac{\partial(L_f^2 E'_{d\Delta})}{\partial x_2} & \frac{\partial(L_f^2 E'_{d\Delta})}{\partial x_3} & \frac{\partial(L_f^2 E'_{d\Delta})}{\partial x_4} \end{bmatrix} \begin{bmatrix} 0 \\ 0 \\ 1/T'_{do} \\ 0 \end{bmatrix}$$

$$= \frac{1}{T'_{do}} \frac{\partial(L_f^2 E'_{d\Delta})}{\partial x_3} = \frac{1}{T'_{do}} . 0 = 0.$$

Term 4: $L_g L_f^3 E'_{d\Delta} = \frac{d(L_f^3 E'_{d\Delta})}{dx} g(x)$

$$L_f^3 E'_{d\Delta} = \begin{bmatrix} \frac{\partial\left(L_f^2 E'_{d\Delta}\right)}{\partial x_1} & \frac{\partial\left(L_f^2 E'_{d\Delta}\right)}{\partial x_2} & \frac{\partial\left(L_f^2 E'_{d\Delta}\right)}{\partial x_3} & \frac{\partial\left(L_f^2 E'_{d\Delta}\right)}{\partial x_4} \end{bmatrix} \begin{bmatrix} f_1 \\ f_2 \\ f_3 \\ f_4 \end{bmatrix}$$

$$= f_1 \left(-\frac{E_2 E_1}{T'^2_{qo}} V\cos\delta - \frac{E_2}{T'_{q0}} V(\omega - \omega_s)\sin\delta\right) +$$

$$f_2\left(\frac{VE_2}{T'_{q0}}\cos\delta\right) + f_4\left(\frac{E_1^2}{T'^2_{q0}}\right)$$

$$L_g L_f^3 E'_{d\Delta} = \begin{bmatrix} \frac{\partial\left(L_f^3 E'_{d\Delta}\right)}{\partial x_1} & \frac{\partial\left(L_f^3 E'_{d\Delta}\right)}{\partial x_2} & \frac{\partial\left(L_f^3 E'_{d\Delta}\right)}{\partial x_3} & \frac{\partial\left(L_f^3 E'_{d\Delta}\right)}{\partial x_4} \end{bmatrix} \begin{bmatrix} 0 \\ 0 \\ 1/T'_{do} \\ 0 \end{bmatrix}$$

$$= \frac{1}{T'_{do}} \frac{\partial(L_f^3 E'_{d\Delta})}{\partial x_3}$$

$$= \frac{1}{T'_{do}}\left[-\frac{E_2}{T'_{q0}} A_4 V^2 \sin\delta\cos\delta\right] = -\frac{E_2}{2T'_{do}T'_{q0}} A_4 V^2 \sin 2\delta \neq 0.$$

The last term holds true for $\delta \neq 0$ or $\pm 0.5m\pi$, where m is a positive integer. Thus, this translates to a relative degree of 4.

Therefore, the system can be exactly linearized as given by

$$\frac{dz_1}{dt} = z_2 \tag{3.64}$$

$$\frac{dz_2}{dt} = z_3 \tag{3.65}$$

$$\frac{dz_3}{dt} = z_4 \tag{3.66}$$

$$\frac{dz_4}{dt} = v \tag{3.67}$$

where $z_1 = E'_{d\Delta}$, $z_2 = L_f E'_{d\Delta}$, $z_3 = L_f^2 E'_{d\Delta}$, $z_4 = L_f^3 E'_{d\Delta}$, and $v = L_f^4 \delta_\Delta + L_g L_f^3 \delta_\Delta u$.

Linearization of PSM2 for output function $\delta_\Delta = \delta - \delta_0$

The relative degree with respect to this output is determined as follows:

$$\text{Term 1: } L_g \delta_\Delta = \frac{d\delta_\Delta}{dx} g(x) = \begin{bmatrix} 1 & 0 & 0 & 0 \end{bmatrix} \begin{bmatrix} 0 \\ 0 \\ 1/T'_{do} \\ 0 \end{bmatrix} = 0.$$

$$\text{Term 2: } L_g L_f \delta_\Delta = \frac{d(L_f \delta_\Delta)}{dx} g(x)$$

$$L_f \delta_\Delta = \frac{d\delta_\Delta}{dx} f(x) = \begin{bmatrix} 1 & 0 & 0 & 0 \end{bmatrix} \begin{bmatrix} f_1 \\ f_2 \\ f_3 \\ f_4 \end{bmatrix} = f_1$$

$$L_g L_f \delta_\Delta = \begin{bmatrix} \frac{\partial(L_f \delta_\Delta)}{\partial x_1} & \frac{\partial(L_f \delta_\Delta)}{\partial x_2} & \frac{\partial(L_f \delta_\Delta)}{\partial x_3} & \frac{\partial(L_f \delta_\Delta)}{\partial x_4} \end{bmatrix} \begin{bmatrix} 0 \\ 0 \\ 1/T'_{do} \\ 0 \end{bmatrix}$$

$$= \frac{1}{T'_{do}} \frac{\partial(L_f \delta_\Delta)}{\partial x_3} = \frac{1}{T'_{do}} . 0 = 0.$$

$$\text{Term 3: } L_g L_f^2 \delta_\Delta = \frac{d(L_f^2 \delta_\Delta)}{dx} g(x)$$

$$L_f^2\delta_\Delta = \begin{bmatrix} \frac{\partial(L_f\delta_\Delta)}{\partial x_1} & \frac{\partial(L_f\delta_\Delta)}{\partial x_2} & \frac{\partial(L_f\delta_\Delta)}{\partial x_3} & \frac{\partial(L_f\delta_\Delta)}{\partial x_4} \end{bmatrix} \begin{bmatrix} f_1 \\ f_2 \\ f_3 \\ f_4 \end{bmatrix} = f_2$$

$$L_g L_f^2\delta_\Delta = \begin{bmatrix} \frac{\partial(L_f^2\delta_\Delta)}{\partial x_1} & \frac{\partial(L_f^2\delta_\Delta)}{\partial x_2} & \frac{\partial(L_f^2\delta_\Delta)}{\partial x_3} & \frac{\partial(L_f^2\delta_\Delta)}{\partial x_4} \end{bmatrix} \begin{bmatrix} 0 \\ 0 \\ 1/T_{do}^{'} \\ 0 \end{bmatrix}$$

$$= \frac{1}{T_{do}^{'}} \frac{\partial(L_f^2\delta_\Delta)}{\partial x_3} = -\frac{A_4 V}{T_{do}^{'}} \sin\delta \neq 0.$$

The relative degree is 3. And the linearization of the system is as follows:

$$\frac{dz_1}{dt} = z_2 \tag{3.68}$$

$$\frac{dz_2}{dt} = z_3 \tag{3.69}$$

$$\frac{dz_3}{dt} = v \tag{3.70}$$

$$\frac{dz_4}{dt} = L_f\theta \tag{3.71}$$

where $L_g\theta = 0$, $z_1 = \delta_\Delta$, $z_2 = L_f\delta_\Delta$, $z_3 = L_f^2\delta_\Delta$, $z_4 = \theta$, and $v = L_f^3\delta_\Delta + L_g L_f^2\delta_\Delta u$.

From

$$L_g\theta = 0,$$

it can be suitably deduced that $\theta = x_4 = E_d'$. Hence, the internal dynamics of the system become

$$\frac{dz_4}{dt} = -\frac{E_1}{T_{qo}'} z_4 + \frac{E_2}{T_{qo}'} V\sin\delta_0.$$

It is obvious that this dynamic equation is stable.

Linearization of PSM2 for output function $\omega_\Delta = \omega - \omega_0$

For this output, the following holds:

Term 1: $\mathrm{L_g}\omega_\Delta = \frac{\mathrm{d}\omega_\Delta}{\mathrm{d}x}\mathrm{g}(x) = [0 \quad 1 \quad 0 \quad 0]\begin{bmatrix} 0 \\ 0 \\ 1/T'_{do} \\ 0 \end{bmatrix} = 0.$

Term 2: $\mathrm{L_g L_f}\omega_\Delta = \frac{\mathrm{d}(\mathrm{L_f}\omega_\Delta)}{\mathrm{d}x}\mathrm{g}(x)$

$$\mathrm{L_f}\omega_\Delta = \frac{\mathrm{d}\omega_\Delta}{\mathrm{d}x}\mathrm{f}(x) = [0 \quad 1 \quad 0 \quad 0]\begin{bmatrix} \mathrm{f}_1 \\ \mathrm{f}_2 \\ \mathrm{f}_3 \\ \mathrm{f}_4 \end{bmatrix} = \mathrm{f}_2$$

$$\mathrm{L_g L_f}\omega_\Delta = \begin{bmatrix} \frac{\partial(\mathrm{L_f}\omega_\Delta)}{\partial x_1} & \frac{\partial(\mathrm{L_f}\omega_\Delta)}{\partial x_2} & \frac{\partial(\mathrm{L_f}\omega_\Delta)}{\partial x_3} & \frac{\partial(\mathrm{L_f}\omega_\Delta)}{\partial x_4} \end{bmatrix}\begin{bmatrix} 0 \\ 0 \\ 1/T'_{do} \\ 0 \end{bmatrix}$$

$= \frac{1}{T'_{do}}\frac{\partial(\mathrm{L_f}\omega_\Delta)}{\partial x_3} = -\frac{\mathrm{A_4 V}}{T'_{do}}\sin\delta \neq 0.$

Here the relative degree is 2, and the system transformation becomes:

$$\frac{\mathrm{dz_1}}{\mathrm{dt}} = \mathrm{z_2} \tag{3.72}$$

$$\frac{\mathrm{dz_2}}{\mathrm{dt}} = \mathrm{v} \tag{3.73}$$

$$\frac{\mathrm{dz_3}}{\mathrm{dt}} = \mathrm{L_f}\theta_3 \tag{3.74}$$

$$\frac{\mathrm{dz_4}}{\mathrm{dt}} = \mathrm{L_f}\theta_4 \tag{3.75}$$

where $\mathrm{L_g}\theta_3 = 0,\ \mathrm{L_g}\theta_4 = 0,\ \mathrm{z_1} = \omega_\Delta,\ \mathrm{z_2} = \mathrm{L_f}\omega_\Delta,\ z_3 = \theta_3,\ \mathrm{z_4} = \theta_4,$ and $\mathrm{v} = \mathrm{L_f^2}\omega_\Delta + \mathrm{L_g L_f}\omega_\Delta u.$

After solving

$\mathrm{L_g}\theta_3 = 0$, and $\mathrm{L_g}\theta_4 = 0$

to give suitably $\theta_3 = x_1$, and $\theta_4 = x_4$, the internal dynamics reduce to

$$\frac{\mathrm{dz_4}}{\mathrm{dt}} = -\frac{\mathrm{E_1}}{\mathrm{T'_{qo}}}\mathrm{z_4}.$$

This dynamic equation is stable.

Linearization of PSM2 for output function $\mathbf{E'_{q\Delta} = E'_q - E'_{q0}}$

Similarly, the relative degree here is 1, because

$$\text{Term 1: } L_g E'_{q\Delta} = \frac{dE'_{q\Delta}}{dx} g(x) = [0 \quad 0 \quad 1 \quad 0] \begin{bmatrix} 0 \\ 0 \\ 1/T'_{do} \\ 0 \end{bmatrix} \neq 0.$$

And the internal dynamic equations, which are also stable, are

$$\frac{dz_2}{dt} = z_3 - \omega_s$$

$$\frac{dz_3}{dt} = B_2 V \cos z_2 - B_1 E'_{q0}$$

$$\frac{dz_4}{dt} = -\frac{E_1}{T'_{qo}} z_4 + \frac{E_2}{T'_{qo}} V \sin z_2,$$

resulting from transforming the system to

$$\frac{dz_1}{dt} = L_f E'_{q\Delta} + L_g E'_{q\Delta} \tag{3.76}$$

$$\frac{dz_2}{dt} = L_f \theta_2 \tag{3.77}$$

$$\frac{dz_3}{dt} = L_f \theta_3 \tag{3.78}$$

$$\frac{dz_4}{dt} = L_f \theta_4 \tag{3.79}$$

such that $L_g \theta_2 = 0$, $L_g \theta_3 = 0$, and $L_g \theta_4 = 0$.

3.3.2 Control Law 1

This section presents a control law which is derived from the general higher-order SMC structure that can be tuned to achieve a desirable dynamic performance. Enjoying the feature of a variable structure control system such as insensitivity to model inaccuracy and robustness against system disturbances, it can guarantee finite-time stabilization of

uncertain differentiable dynamic systems by ensuring that a set of system output-based constraints is met.

Given the potential uncertainty in the nonlinear system in (3.47), the thrust of the control design involves subjecting system states to the following r constraints:

$$\mathrm{h}(x) = 0,$$

$$\dot{\mathrm{h}}(x) = 0,$$

$$\ddot{\mathrm{h}}(x) = 0,$$

$$\vdots$$

$$\mathrm{h}^{(\mathrm{r}-1)}(x) = 0,$$

A discontinuous feedback law is employed in order to keep the system dynamic performance intact, where r is the relative degree (which is also called the sliding order) and h(x) is the output of the system. This means that the convergence of these constraints in finite time translates to stabilizing the states of the system. The only requirements are that the relative degree must be known, the zero dynamics must be stable, and the control signal must be finite and bounded.

The structure of the universal controller is given by (Levant, 2001, 2005)

$$\mathrm{u} = -\mathrm{K}\varphi_{\mathrm{r}-1,\mathrm{r}}\left(\mathrm{h}, \dot{\mathrm{h}}, \ddot{\mathrm{h}}, \dots, \mathrm{h}^{(\mathrm{r}-1)}\right), \tag{3.80}$$

where

$$\varphi_{\mathrm{j,r}} = \mathrm{sat}\left(\frac{\mathrm{h}^{(\mathrm{j})} + \alpha_{\mathrm{j}}\mathrm{M}_{\mathrm{j,r}}\varphi_{\mathrm{j}-1,\mathrm{r}}}{\mathrm{M}_{\mathrm{r}}}, \varepsilon_{\mathrm{j}}\right),$$

$$\varphi_{0,\mathrm{r}} = \mathrm{sat}\left(\frac{\mathrm{h}}{|\mathrm{h}|}, \varepsilon_0\right),$$

and

$$\mathrm{M}_{\mathrm{j,r}} = \left(|\mathrm{h}|^{\frac{\mathrm{q}}{\mathrm{r}}} + \left|\dot{\mathrm{h}}\right|^{\frac{\mathrm{q}}{(\mathrm{r}-1)}} + \cdots + \left|\mathrm{h}^{(\mathrm{j}-1)}\right|^{\frac{\mathrm{q}}{(\mathrm{r}-\mathrm{j}+1)}}\right)^{\frac{(\mathrm{r}-\mathrm{j})}{\mathrm{q}}},$$

$$M_r = \left(|h|^{\frac{q}{r}} + \left|\dot{h}\right|^{\frac{q}{(r-1)}} + \cdots + \left|h^{(r-1)}\right|^{q}\right)^{\frac{1}{q}},$$

for j = 1, 2, …, r-1, $\varepsilon_j > 0$, and q = r!. K and α_j are the parameters of the controller.

3.3.3 Control Law 2

The second control law is designed based on the concept of geometric homogeneity. Homogeneity is the feature of functions and vector fields associated with dynamic systems, which guarantees their transformation (dilation) from one point to another in the state space (Bhat & Bernstein, 2005).

Generally, system dilation is in the form

$$\Delta_v(z) = (v^{m_1} z_1, v^{m_2} z_2, \cdots, v^{m_n} z_n), \tag{3.81}$$

which is an extension of the standard dilation

$$\Delta_v(z) = (vz_1, vz_2, \cdots, vz_n). \tag{3.82}$$

If a nonlinear dynamic system can be represented as a set of integrator chains (exact linearization into the Bruvnosky normal form)

$$\frac{dz_1}{dt} = z_2 \tag{3.83}$$

$$\frac{dz_2}{dt} = z_3 \tag{3.84}$$

$$\vdots$$

$$\frac{dz_n}{dt} = L_f^r h + \left(L_g L_f^{r-1} h\right) u = u_{eq} \tag{3.85}$$

with u_{eq} given by

$$u_{eq} = f(z),$$

then it can be dilated to result in u_{eq} given by

$$u_{eq} = f(v^m z) \text{ or } u_{eq} = f(vz). \tag{3.86}$$

This concept is employed to upgrade the finite-time stabilizing feedback controller presented in (Bhat & Bernstein, 2005) (Proposition 8.1), and given as follows: Consider the system defined in equations (3.37)-(3.39). There exists a feedback control law

$$u_{eq}(z) = -k_1 \text{sign}(z_1)|z_1|^{v_1} - \cdots - k_r \text{sign}(z_r)|z_r|^{v_r}$$

which ensures that the origin is globally finite-stable. The positive numbers k_1, k_2,. . ., k_r are appropriately selected such that the polynomial

$$p^r + k_r p^{r-1} + k_{r-1} p^{r-2} + k_1$$

is Hurwitz.

v_1, v_2, …,v_r are found from

$$v_{i-1} = \frac{v_i v_{i+1}}{2v_{i+1} - v_i}, \qquad i = 2, 3, \cdots r$$

with

$$v_{r+1} = 1;\ v_r \in (1-\varepsilon, 1); \varepsilon \in (0,1).$$

The overall control law u is now given by

$$u = \frac{u_{eq} - L_f^r h}{L_g L_f^{r-1}}. \tag{3.87}$$

3.3.4 Control Law 3

Using a saturation function for the switching in equation (3.80), this law is a modified form of CL1, and is adopted to reduce the severity of switching in u. It is given by

$$u = -K\text{sat}\left(\Gamma_{r-1,r}\left(h, \dot{h}, \ddot{h}, \ldots, h^{(r-1)}\right), \varepsilon\right), \tag{3.88}$$

where

$$\Gamma_{j,r} = h^{(j)} + \alpha_j M_{j,r} \text{sat}\left(\left(\Gamma_{j-1,r}\right), \varepsilon\right),$$

$$\Gamma_{1,r} = \dot{h} + \alpha_1 M_{1,r} \text{sign}\left(\Gamma_{0,r}\right)$$

$$\Gamma_{0,r} = h,$$

and

$$M_{j,r} = \left(|h|^{\frac{q}{r}} + \left|\dot{h}\right|^{\frac{q}{(r-1)}} + \cdots + \left|h^{(j-1)}\right|^{\frac{q}{(r-j+1)}}\right)^{\frac{(r-j)}{q}},$$

for j = 1, 2, …, r-1, ε > 0, and q = r!. K, α_j are the parameters of the controller.

It is noted that "sign" (shown in Fig. 3.16) is the *signum* function, while "sat" (shown in Fig. 3.17) represents the saturation function.

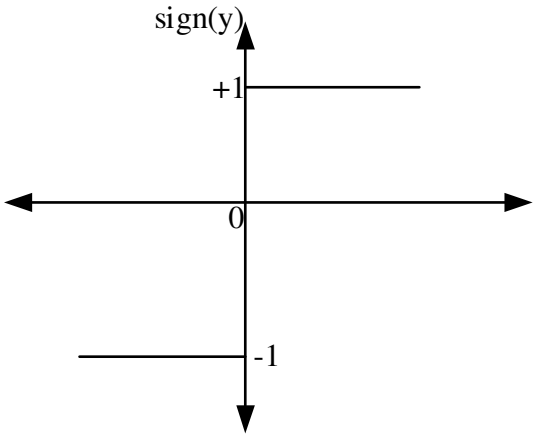

sign(y) = +1(if y > 0) or -1(if y < 0)

Fig. 3.16: Representation of sign(y)

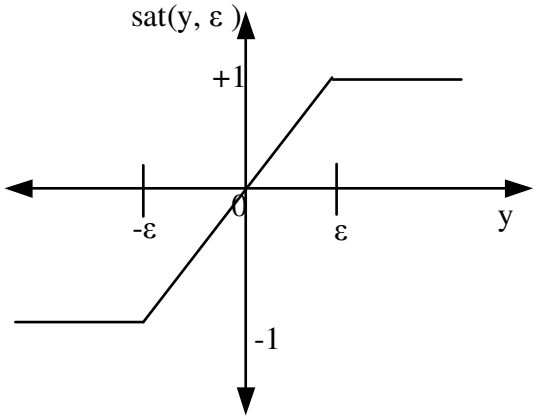

sat(y, ε) = min(1, max(-1, y/ε))

Fig. 3.17: Representation of sat(y, ε)

3.4 Control Signals and Schemes for PSM1

With h_1 representing the output function, the following equations are the respective control signals for PSM1:

$$\blacksquare h_1 = \delta_\Delta : r = n = 3.$$

$$u_1 = -K\varphi_{2,3}\left(h_1, \dot{h}_1, \ddot{h}_1\right)$$

$$= -K\text{sat}\left(\frac{\ddot{h}_1 + \alpha_2 M_{2,3}\varphi_{1,3}}{M_3}, \varepsilon_2\right) \tag{3.89}$$

$$\varphi_{1,3} = \text{sat}\left(\frac{\dot{h}_1 + \alpha_1 M_{1,3}\varphi_{0,3}}{M_3}, \varepsilon_1\right)$$

$$\varphi_{0,3} = \mathrm{sat}\left(\frac{h_1}{|h_1|}, \varepsilon_0\right)$$

$$M_{2,3} = \left(|h_1|^2 + \left|\dot{h}_1\right|^3\right)^{1/6}$$

$$M_{1,3} = (|h_1|^2)^{1/3}$$

$$M_3 = \left(|h_1|^2 + \left|\dot{h}_1\right|^3 + \left|\ddot{h}_1\right|^6\right)^{1/6}$$

$$u_2 = \frac{u_{eq} - L_f^r h}{L_g L_f^{r-1}} \tag{3.90}$$

$$u_{eq} = -k_1 \mathrm{sign}(vz_1)|vz_1|^{v_1} - k_2 \mathrm{sign}(vz_2)|vz_2|^{v_2} - k_3 \mathrm{sign}(vz_3)|vz_3|^{v_3}$$

$$= -k_1 \mathrm{sign}(z_1)|vz_1|^{v_1} - k_2 \mathrm{sign}(z_2)|vz_2|^{v_2} - k_3 \mathrm{sign}(z_3)|vz_3|^{v_3}$$

$$p^3 + k_3 p^2 + k_2 p + k_1 = (p + a_1)(p + a_2)(p + a_3) = 0$$

$$z_1 = h_1;\ z_2 = L_f h_1;\ z_3 = L_f^2 h_1$$

$$u_3 = -K\mathrm{sat}\left(\left(\Gamma_{2,3}\left(h_1, \dot{h}_1, \ddot{h}_1\right)\right), \mathrm{epsi}\right)$$

$$= -K\mathrm{sat}\left(\left(\ddot{h}_1 + \alpha_2 M_{2,3}\mathrm{sat}\left(\Gamma_{1,3}, \mathrm{epsi}\right)\right), \mathrm{epsi}\right) \tag{3.91}$$

$$\Gamma_{1,3} = \dot{h}_1 + \alpha_1 M_{1,3}\mathrm{sign}\left(\Gamma_{0,3}\right)$$

$$\Gamma_{0,3} = h_1$$

For each of the control signals u_1 and u_3, the controller gain K and parameters α_i are properly tuned to give satisfactory system performance. For control signal u_2, parameters k_i are preselected based on the placement of a_i in the complex frequency plane, and $v > 0$ is the dilation gain.

Thus, the resulting control scheme for PSM1 is shown in Fig. 3.18.

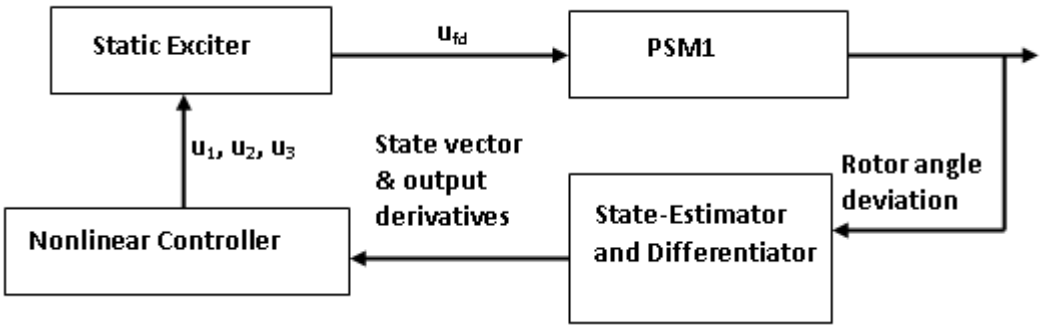

Fig. 3.18: Control scheme for PSM1

3.5 Control Signals and Schemes for PSM2

The control signals here are similar to the ones derived for PSM1. This is a good way to evaluate the above control signals under the influence of unmodeled dynamics—the design intent is to assess the performance of the three control laws when the dynamics of the system changes. The system output function is h_2, and the control signals are u_4, u_5, and u_6.

$$\blacksquare h_2 = \delta_\Delta : r = n - 1 = 3.$$

$$u_4 = -K\varphi_{2,3}\left(h_2, \dot{h}_2, \ddot{h}_2\right)$$

$$= -K\text{sat}\left(\frac{\ddot{h}_2 + \alpha_2 M_{2,3}\varphi_{1,3}}{M_3}, \varepsilon_2\right) \qquad (3.92)$$

$$\varphi_{1,3} = \text{sat}\left(\frac{\dot{h}_2 + \alpha_1 M_{1,3}\varphi_{0,3}}{M_3}, \varepsilon_1\right)$$

$$\varphi_{0,3} = \text{sat}\left(\frac{h_2}{|h_2|}, \varepsilon_0\right)$$

$$M_{2,3} = \left(|h_2|^2 + \left|\dot{h}_2\right|^3\right)^{1/6}$$

$$M_{1,3} = \left(|h_2|^2\right)^{1/3}$$

$$M_3 = \left(|h_2|^2 + \left|\dot{h}_2\right|^3 + \left|\ddot{h}_2\right|^6\right)^{1/6}$$

$$u_5 = \frac{u_{eq} - L_f^r h}{L_g L_f^{r-1}} \tag{3.93}$$

$$u_{eq} = -k_1 \text{sign}(vz_1)|vz_1|^{v_1} - k_2 \text{sign}(vz_2)|vz_2|^{v_2} - k_3 \text{sign}(vz_3)|vz_3|^{v_3}$$

$$= -k_1 \text{sign}(z_1)|vz_1|^{v_1} - k_2 \text{sign}(z_2)|vz_2|^{v_2} - k_3 \text{sign}(z_3)|vz_3|^{v_3}$$

$$p^3 + k_3 p^2 + k_2 p + k_1 = (p + a_1)(p + a_2)(p + a_3) = 0$$

$$z_1 = h_2;\ z_2 = L_f h_2;\ z_3 = L_f^2 h_2$$

$$u_6 = -\text{Ksat}\left(\left(\Gamma_{2,3}\left(h_2, \dot{h}_2, \ddot{h}_2\right)\right), \text{epsi}\right)$$

$$= -\text{Ksat}\left(\left(\ddot{h}_2 + \alpha_2 M_{2,3} \text{sat}\left(\Gamma_{1,3}, \text{epsi}\right)\right), \text{epsi}\right) \tag{3.94}$$

$$\Gamma_{1,3} = \dot{h}_2 + \alpha_1 M_{1,3} \text{sign}\left(\Gamma_{0,3}\right)$$

$$\Gamma_{0,3} = h_2$$

The expressions for $\dot{h}_1$, $\ddot{h}_1$, $\dot{h}_2$, and $\ddot{h}_2$ are given in Sections 3.2.1.1 and 3.2.1.2.

Likewise, the resulting control scheme for PSM2 is shown in Fig. 3.19.

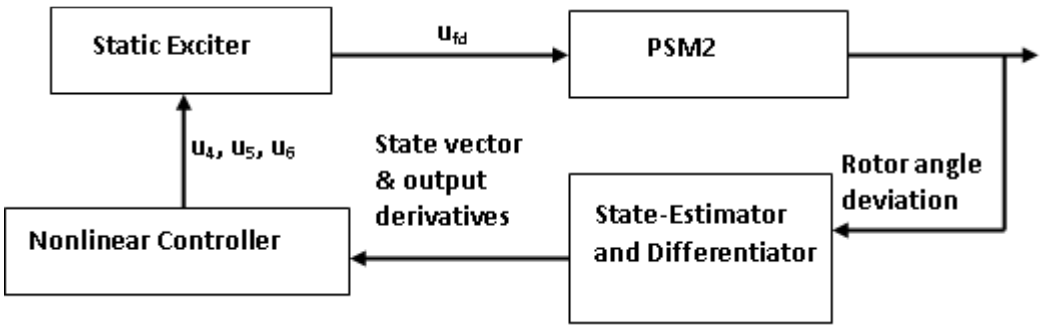

Fig. 3.19: Control scheme for PSM2

3.6 Summary

This chapter discusses several modeling methods of the synchronous generator in stability studies, and a number of nonlinear control schemes. It has been shown that the fourth-and third-order models of SMIB can approximate a sixth-order model correctly, and this supports the underlying system representations used for the construction of the control laws. Moreover, this chapter presented detailed construction of three sets of control signals, including the important concepts of exact and inexact linearization of affine nonlinear systems. It has presented a number of MATLAB tools for verification of the exact and inexact linearizations of nonlinear systems, and for calculating their relative degrees. Besides, to inspire orderly flow of material and enhance intuitive mathematical connection, this chapter has clearly laid out all the control signals as related to each model considered. The next chapter will consider the effect of all the control signals and how the parameters of some of these signals are tuned.

CHAPTER FOUR: CONTROL LAWS' TESTING AND PERFORMANCE EVALUATION

4.0 Introduction

The main purpose of any control system design is to achieve a desirable dynamic characteristic of the system being controlled. For some nonlinear dynamic systems such as power systems, a good performance entails that a number of important system variables must settle quickly (within 2-3s) with minimal oscillations. To maintain synchronism of power system, rotor angles and speeds of all synchronous machines must be stable following perturbation. Besides determination of equilibrium points for PSM1 and PSM2, this chapter focuses on the performance assessment of each of the control laws presented in Chapter 3 when synchronous machines were modeled using PSM1 and PSM2. Moreover, an approximate tuning method for CL1 and CL3 is provided.

4.1 Equilibrium Points for PSM1 and PSM2

Determination of equilibrium or singular points for nonlinear control system is very important for analysis and design purpose because it allows a small-signal operation of nonlinear systems to be studied and understood using linear control theory methods. On the other hand, feedback controllers for general performance improvement can be designed based on the deviations of the state variables from their steady-state values.

Let (x_{10}, x_{20}, x_{30}) and $(x_{10}, x_{20}, x_{30}, x_{40})$ represent the equilibrium points of PSM1 and PSM2, respectively. These are described by equations (4.1) and (4.2) as follows:

$$\begin{pmatrix}\dot{x}_1\\ \dot{x}_2\\ \dot{x}_3\end{pmatrix} =$$

$$\begin{pmatrix} x_2 - \omega_s \\ A_1 + \frac{1}{2}F_2V^2\sin 2x_1 - A_4Vx_3\sin x_1 - \frac{T'_{qo}F_3F_1}{M}v^2(x_2-\omega_s)\cos^2 x_1 \\ -B_1x_3 + B_2V\cos x_1 \end{pmatrix} + \begin{pmatrix} 0 \\ 0 \\ \frac{1}{T'_{do}} \end{pmatrix} u \quad (4.1)$$

$$\begin{pmatrix}\dot{x}_1\\ \dot{x}_2\\ \dot{x}_3\\ \dot{x}_4\end{pmatrix} = \begin{pmatrix} x_2 - \omega_s \\ A_1 - \frac{1}{2}A_2V^2\sin 2x_1 - A_4Vx_3\sin x_1 + A_3Vx_4\cos x_1 \\ -B_1x_3 + B_2V\cos x_1 \\ -\frac{E_1}{T'_{qo}}x_4 + \frac{E_2}{T'_{qo}}V\sin x_1 \end{pmatrix} + \begin{pmatrix} 0 \\ 0 \\ \frac{1}{T'_{do}} \\ 0 \end{pmatrix} u \quad (4.2)$$

At equilibrium, all derivative terms in equation (4.1) are set to zero, i.e.,

- $x_{20} - \omega_s = 0$

$$\Rightarrow x_{20} = \omega_s. \quad (4.3)$$

- $A_1 + \frac{1}{2}F_2V^2\sin 2x_{10} - A_4Vx_{30}\sin x_{10} = 0$

$$\Rightarrow x_{30} = \frac{A_1 + \frac{1}{2}F_2V^2\sin 2x_{10}}{A_4V\sin x_{10}}. \quad (4.4)$$

- $-B_1x_{30} + B_2V\cos x_{10} + \frac{1}{T'_{do}}u_0 = 0$

$$\Rightarrow x_{30} = \frac{B_2V\cos x_{10} + \frac{1}{T'_{do}}u_0}{B_1}. \quad (4.5)$$

Combining equations (4.4) and (4.5), and using the identity $\sin x_{10}\cos x_{10} \equiv \frac{1}{2}\sin 2x_{10}$, gives

$$\left(\frac{1}{2}B_2V^2A_4 - \frac{1}{2}B_1V^2F_2\right)\sin 2x_{10} + \frac{1}{T'_{do}}A_4Vu_0\sin x_{10} = A_1B_1. \quad (4.6)$$

Equation (4.6) is solved numerically to obtain x_{10} (see Appendix D), and from either equation (4.4) or (4.5), x_{30} can be found. Hence,

$$(x_{10}, x_{20}, x_{30}) = \left(\delta_0, \omega_0, E'_{q0}\right) = (0.6768, 314.29, 1.1300).$$

Similarly, the equilibrium point of equation (4.2) is determined as follows:

- $x_{20} - \omega_s = 0$

$$\Rightarrow x_{20} = \omega_s. \tag{4.7}$$

- $$A_1 - \frac{1}{2}A_2V^2\sin 2x_{10} - A_4Vx_{30}\sin x_{10} + A_3Vx_{40}\cos x_{10} = 0 \tag{4.8}$$

- $$-B_1x_{30} + B_2V\cos x_{10} + \frac{1}{T'_{do}}u_0 = 0$$

$$\Rightarrow x_{30} = \frac{B_2V\cos x_{10} + \frac{1}{T'_{do}}u_0}{B_1}. \tag{4.9}$$

- $$-\frac{E_1}{T'_{qo}}x_{40} + \frac{E_2}{T'_{qo}}V\sin x_{10} = 0$$

$$\Rightarrow x_{40} = \frac{E_2V\sin x_{10}}{E_1}. \tag{4.10}$$

Substituting equations (4.9) and (4.10) into equation (4.8) leads to (4.11), which can be solved for x_{10} as before to give

$$\left(\frac{1}{2}B_2V^2A_4 + \frac{1}{2}B_1V^2A_2 - \frac{B_1E_2V^2A_3}{2E_1}\right)\sin 2x_{10} + \frac{1}{T'_{do}}A_4Vu_0\sin x_{10} = A_1B_1, \tag{4.11}$$

Thus, the equilibrium set for PSM2 is

$$(x_{10}, x_{20}, x_{30}, x_{40}) = \left(\delta_0, \omega_0, E'_{q0}, E'_{d0}\right) = (0.6768, 314.29, 1.1300, 0.2927).$$

These two equilibrium sets are stable in the sense of Lyapunov (see Appendix D for further details on how to compute the Jacobian matrix for equations (4.1) and (4.2) and their corresponding eigenvalues).

4.2 System Simulations and Results

This section examines the performances of the three control laws (CL1, CL2, and CL3) proposed in Chapter three when employed to control a single machine connected to an infinite bus. To highlight the improvements that can be achieved with the proposed control laws, closed loop results are compared against the open-loop equivalents

(constant excitation). In this comparison, system operating conditions remain the same; both 3rd- and 4th-order synchronous machine models were employed. A solid symmetrical three-phase fault, which is simulated by a sudden reduction of the infinite bus voltage to zero, was applied to create a temporary mismatch between electromagnetic torque (T_e) and input mechanical torque (T_m); and post-fault and pre-fault conditions were assumed to be the same. Two fault locations were examined: one at the infinite bus ($V_\infty = 0$ and $X_E = 0.24$pu), and the other at the generator terminals ($V_\infty = 0$ and $X_E = 0$). Also, the fault clearance time was varied to show the effectiveness of the proposed control laws in retaining system stability and improving damping; especially as some of these control laws include speed deviation terms. All the system simulations were carried out using MATLAB R2012a on an Intel Celeron CPU530 @ 1.73GHz speed with 1.00GB RAM and 32-bit Windows 7 Ultimate operating system.

4.2.1 Responses of PSM1 under the Action of the Control Laws

A) Fault at infinite bus: V = 0; X_E = 0.24; and fault clearance time tc = 5, 7, and 9 cycles: Fig. 4.1 to Fig. 4.3 show the sets of waveforms of the rotor angle, rotor speed and quadrature axis induced EMF of a synchronous generator for this case. It was observed that, when tc was 5 cycles, power oscillations in load angles and rotor speeds were damped quickly (within 2seconds), with CL1 yielding highest first peaks. Oscillations due to constant excitation were large. For the 7-cycle clearance time, although the load angles and rotor speeds produced from CL1, CL2, and open loop have similar first peak, CL1 and CL2 exhibit better damping of power oscillations. Likewise, in the case of 9-cycle clearance time, oscillations in load angles and rotor speeds for CL1 and CL2 are well damped, but CL1 exhibits better performance as it has lower first peak in the load

angle than that of CL2 and open loop (which means that CL1 improves transient stability margin more than CL2). In all the cases of clearance time considered, it is important to note that E'_q due to CL1 and CL2 reflects the adjustment required to realize the desirable damping in load angles and rotor speeds.

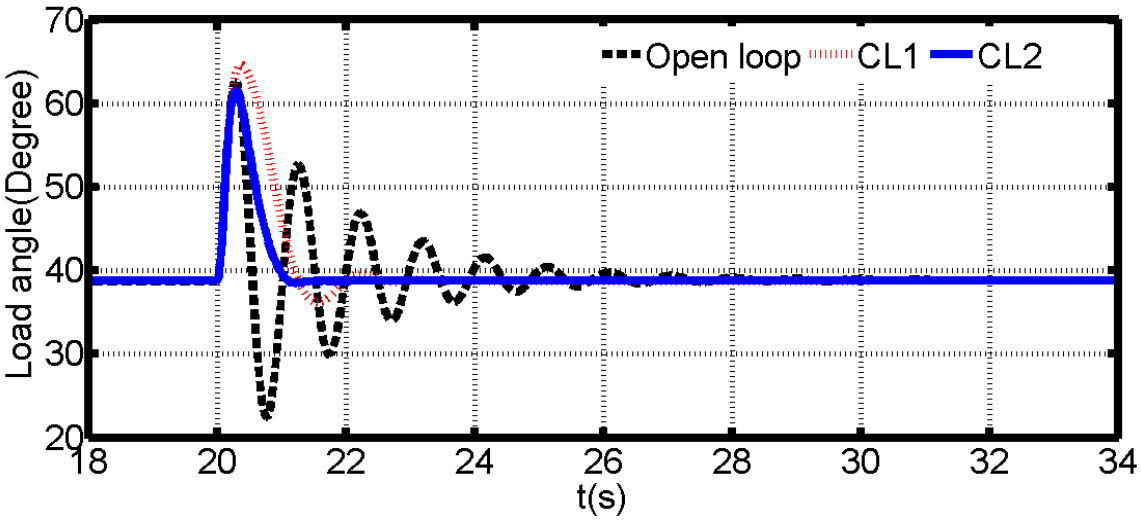

(a)PSM1 rotor angle waveforms for a fault at the infinite bus when closed-loop results for CL1 and CL2 are superimposed on their corresponding open-loop (constant excitation) result

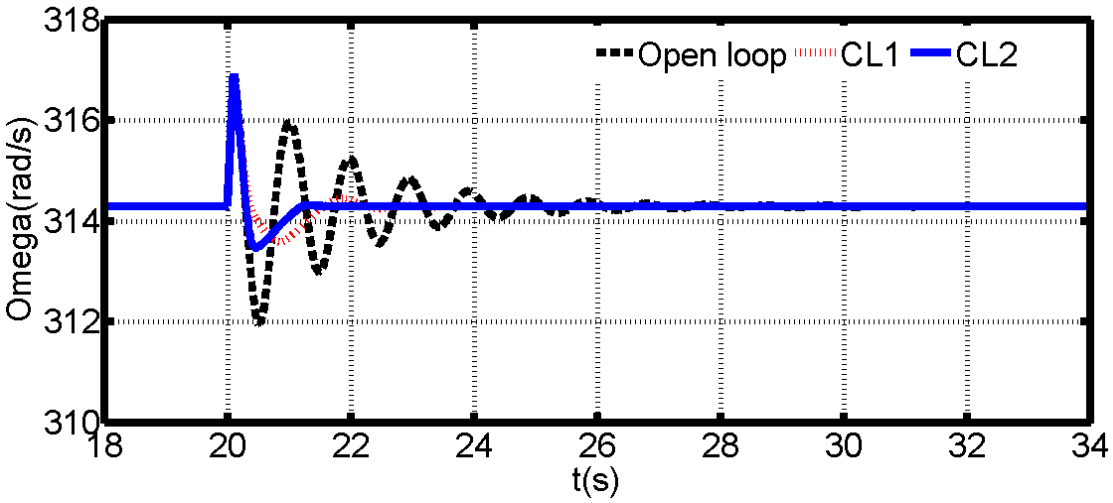

(b)PSM1 rotor speed waveforms for a fault at the infinite bus when closed-loop results obtained with CL1 and CL2 are superimposed on their corresponding open-loop (constant excitation) result

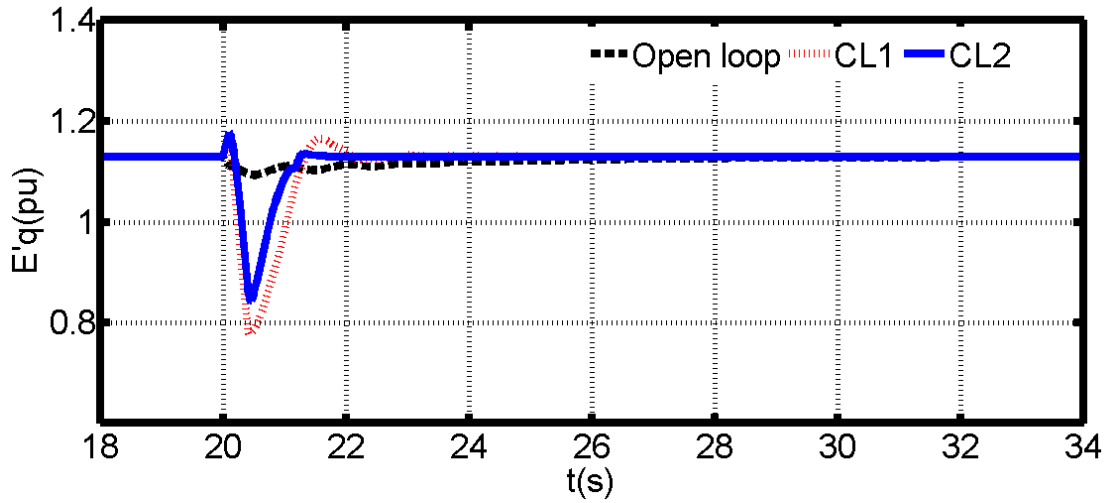

(c)PSM1 Quadrature EMF (E'q) waveforms for a fault at the infinite bus when closed-loop results obtained with CL1 and CL2 are superimposed on their corresponding open-loop (constant excitation) result

Fig. 4.1: PSM1 waveforms comparing the performances of the control laws CL1 and CL2 with the open-loop case when fault ($X_E = 0.24$ and $V = 0$) is cleared after 5 cycles

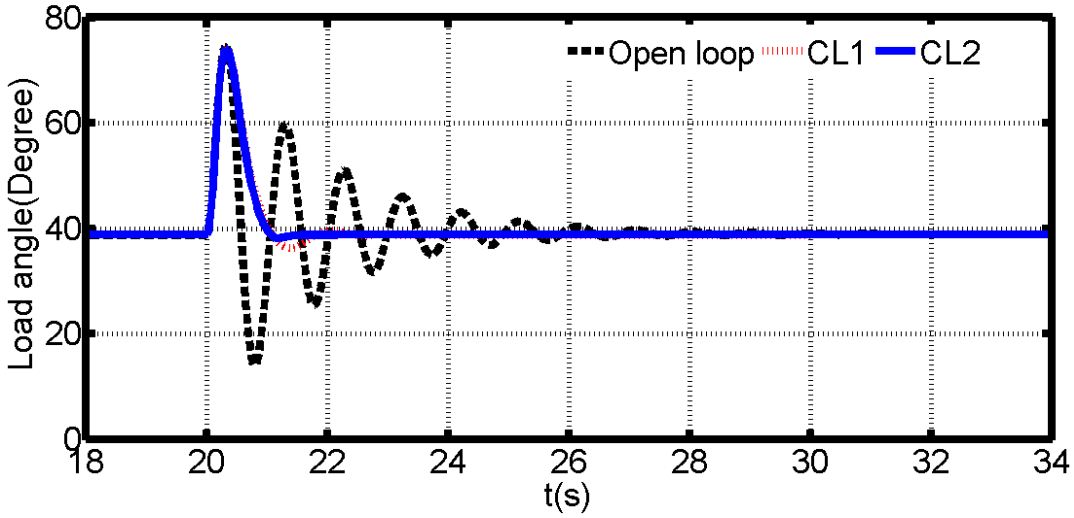

(a) PSM1 rotor angle waveforms for a fault at the infinite bus when closed-loop results for CL1 and CL2 are superimposed on the open-loop (constant excitation) result

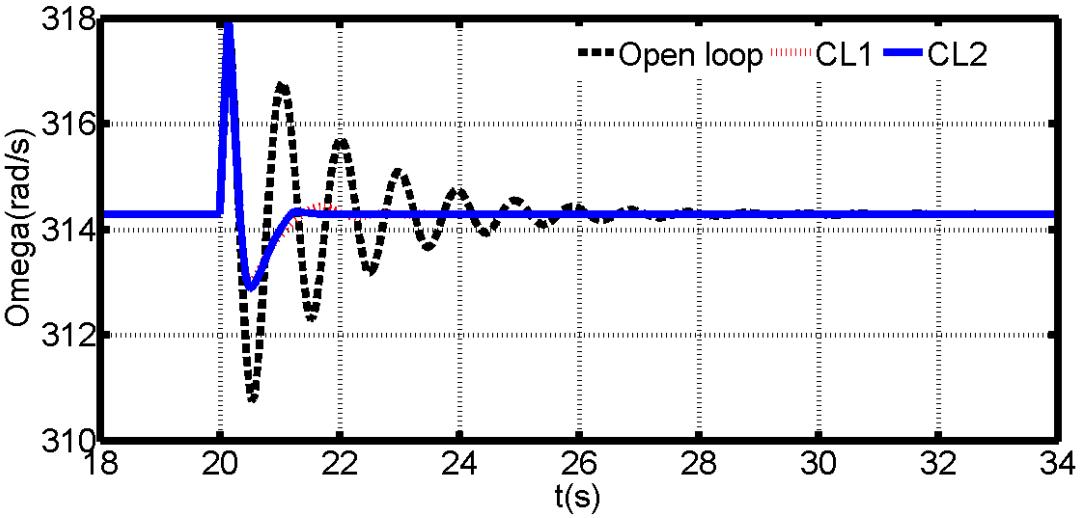

(b) PSM1 rotor speed waveforms for a fault at the infinite bus when closed-loop results obtained with CL1 and CL2 are superimposed on their corresponding open-loop (constant excitation) result

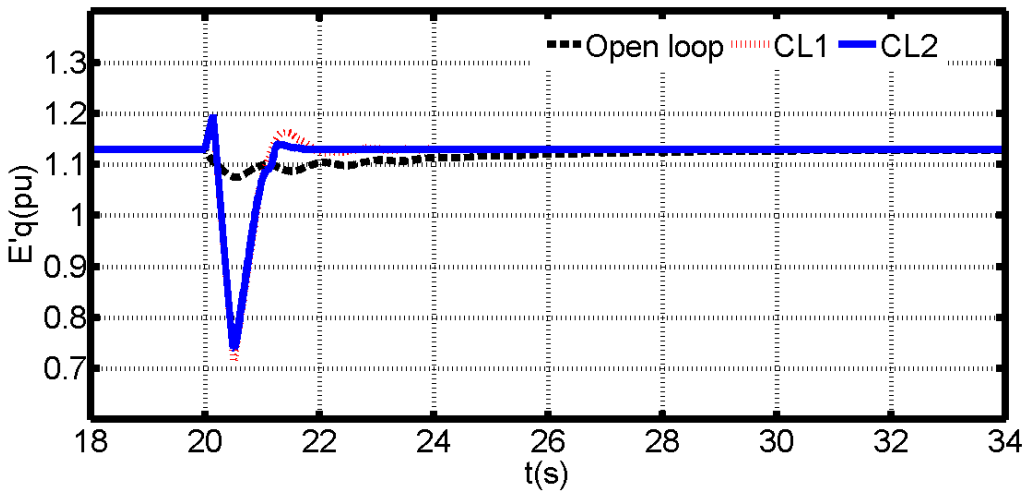

(c) PSM1 Quadrature EMF (E'q) waveforms for a fault at the infinite bus when closed-loop results obtained with CL1 and CL2 are superimposed on their corresponding open-loop (constant excitation) result

Fig. 4.2: PSM1 waveforms comparing the performances of the control laws CL1 and CL2 with the open-loop case when fault ($X_E = 0.24$ and $V = 0$) is cleared after 7 cycles

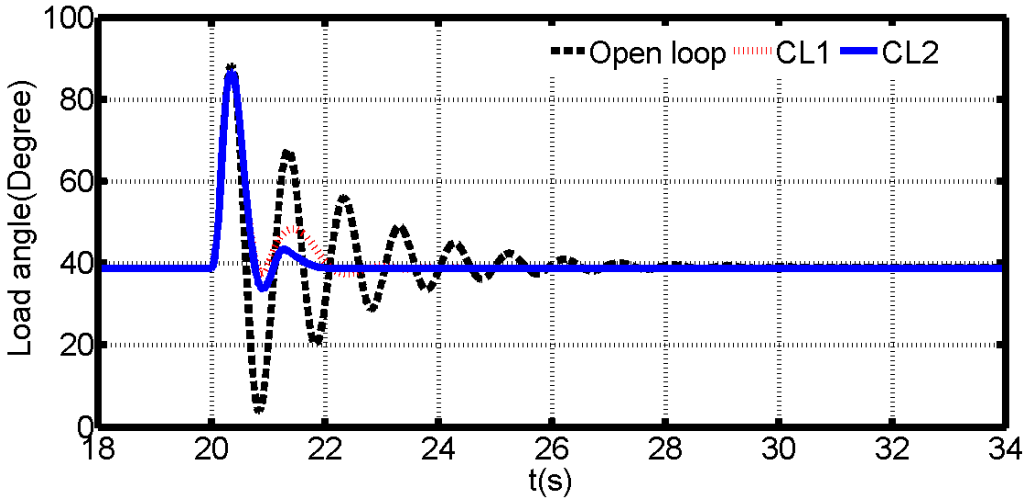

(a) PSM1 rotor angle waveforms for a fault at the infinite bus when closed-loop results for CL1 and CL2 are superimposed on the open-loop (constant excitation) result

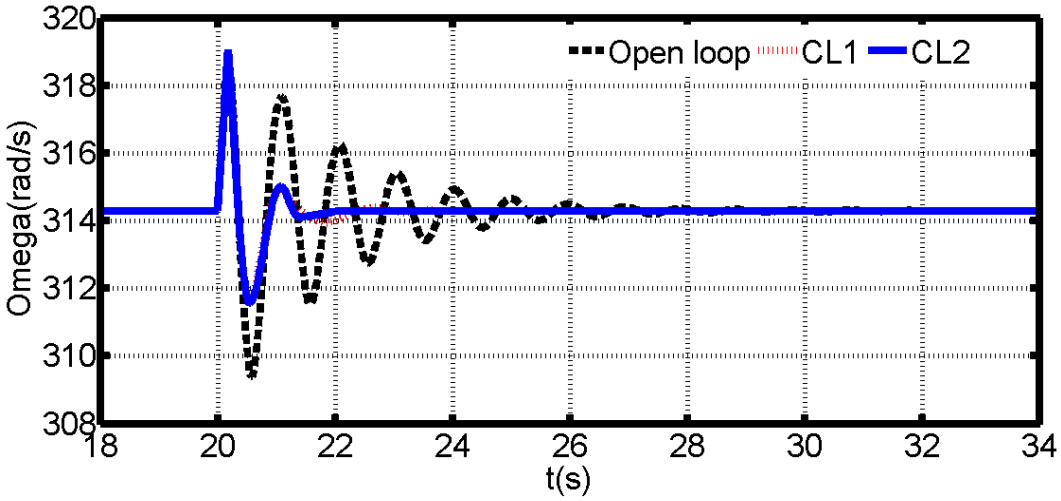

(b) PSM1 rotor speed waveforms for a fault at the infinite bus when closed-loop results obtained with CL1 and CL2 are superimposed on their corresponding open-loop (constant excitation) result

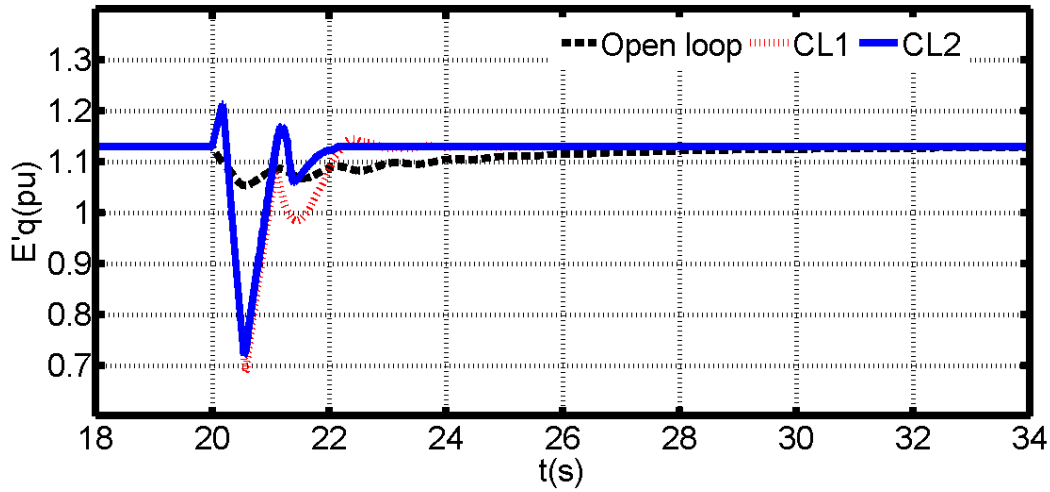

(c) PSM1 Quadrature EMF (E'q) waveforms for a fault at the infinite bus when closed-loop results obtained with CL1 and CL2 are superimposed on their corresponding open-loop (constant excitation) result

Fig. 4.3: PSM1 waveforms comparing the performances of the control laws CL1 and CL2 with the open-loop case when fault ($X_E = 0.24$ and $V = 0$) is cleared after 9 cycles

B) Fault at generator terminals: V =0; X_E=0 and fault clearance time tc=5, 7, and 9 cycles: The waveforms of the system responses are shown in Fig. 4.4 to Fig. 4.6. The observations here are similar to the ones previously presented.

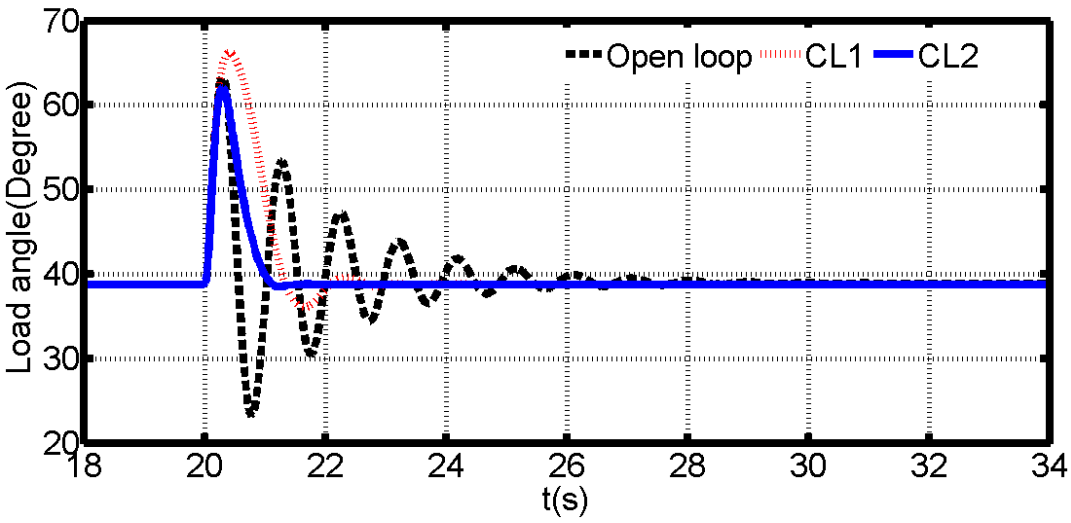

(a) PSM1 rotor angle waveforms for a fault placed at the machine terminals

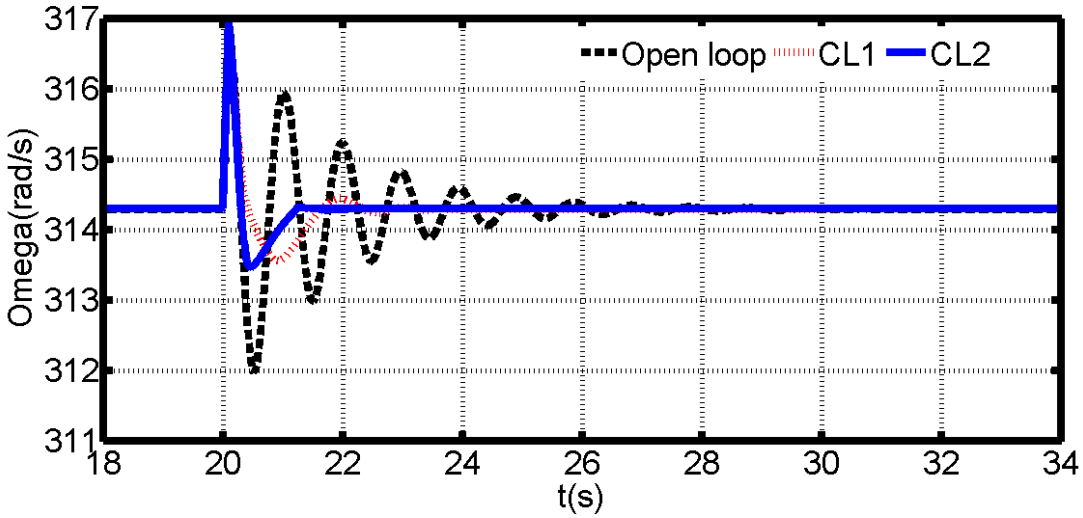

(b) PSM1 rotor speed waveforms for a fault placed at the machine terminals

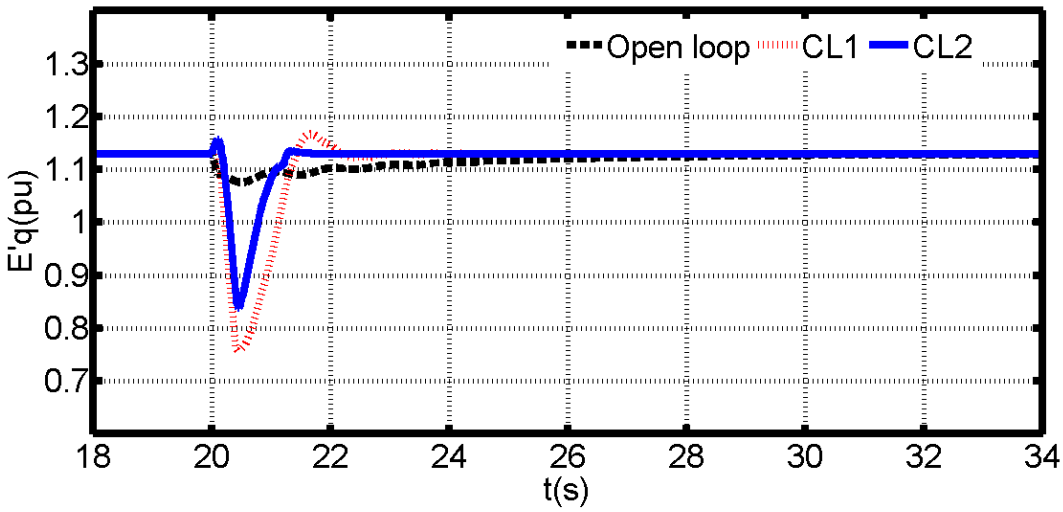

(c) PSM1 Quadrature EMF (E'q) waveforms for a fault placed at the machine terminals

Fig. 4.4: PSM1 waveforms comparing the performances of the control laws CL1 and CL2 with the open-loop case when fault ($X_E = 0$ and $V = 0$) is cleared after 5 cycles

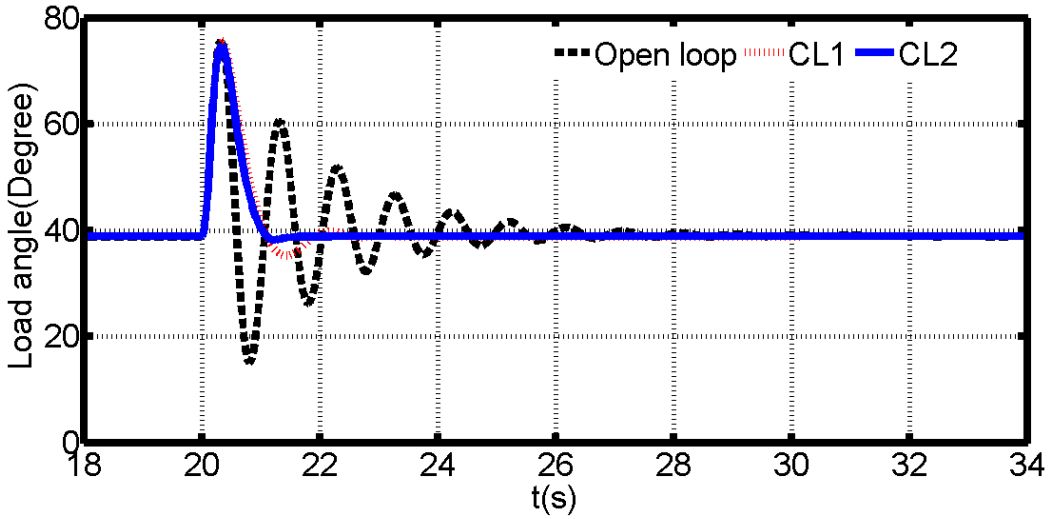

(a) PSM1 rotor angle waveforms for a fault placed at the machine terminals

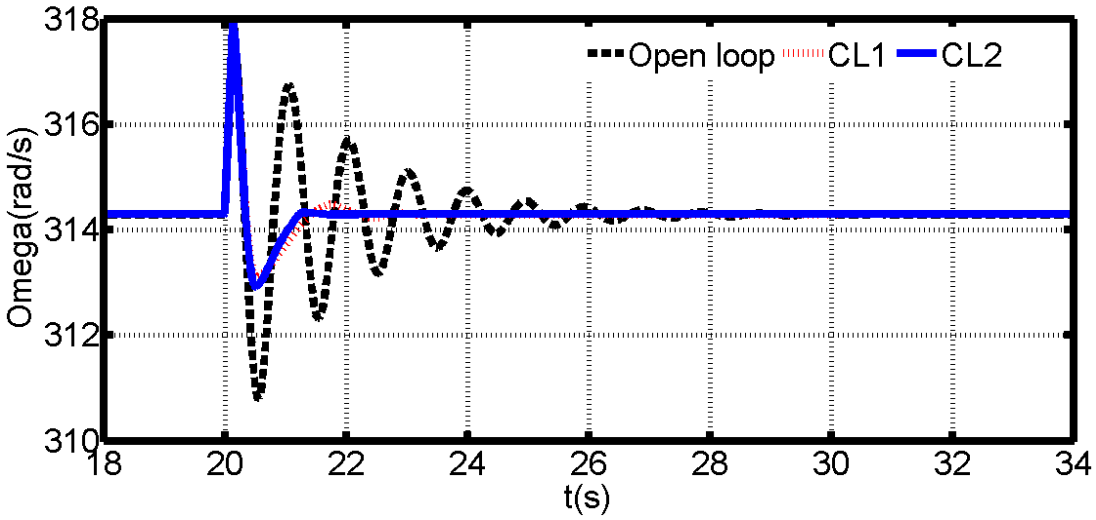

(b) PSM1 rotor speed waveforms for a fault placed at the machine terminals

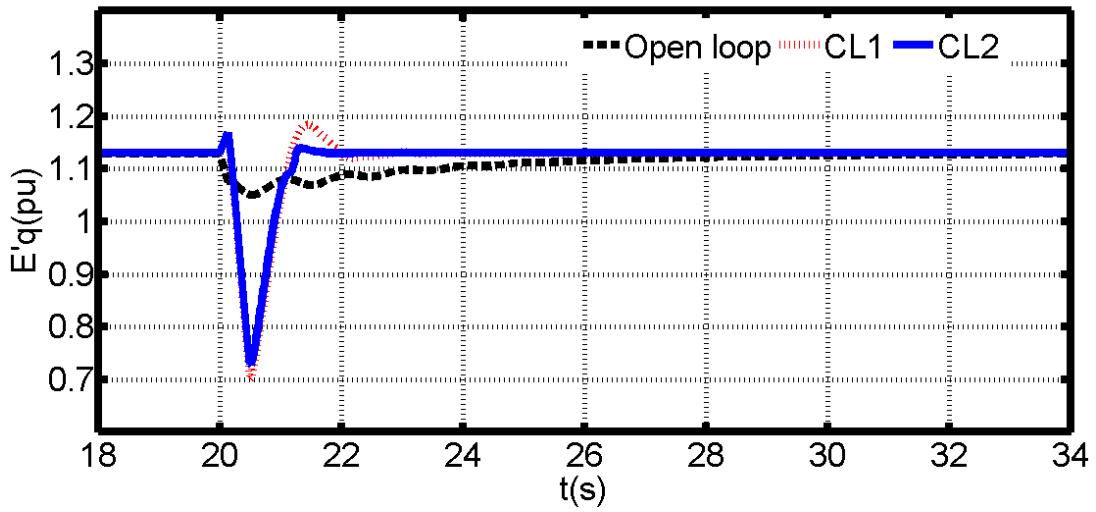

(c) PSM1 Quadrature EMF (E'q) waveforms for a fault placed at the machine terminals

Fig. 4.5: PSM1 waveforms comparing the performances of the control laws CL1 and CL2 with the open-loop case when fault ($X_E = 0$ and $V = 0$) is cleared after 7 cycles

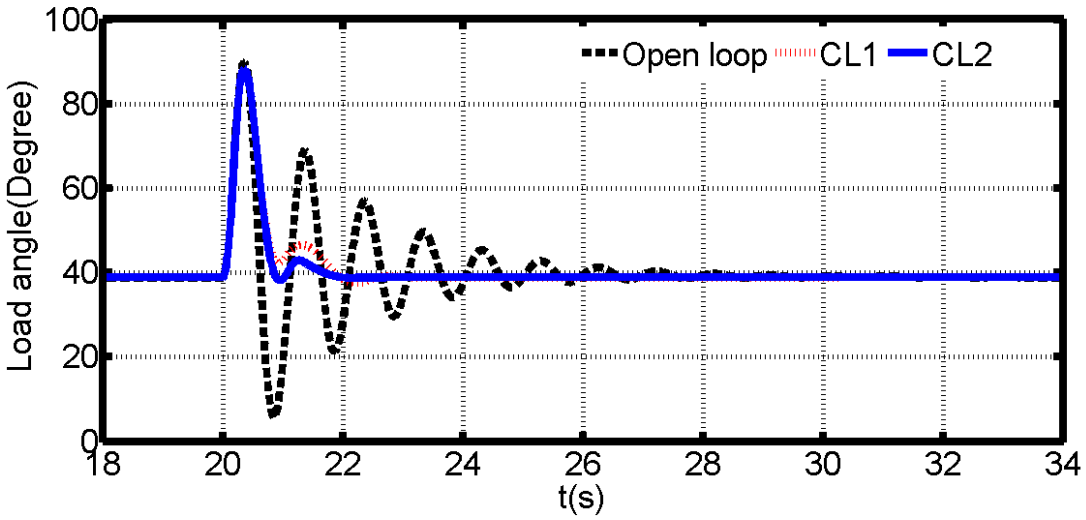

(a) PSM1 rotor angle waveforms for a fault placed at the machine terminals

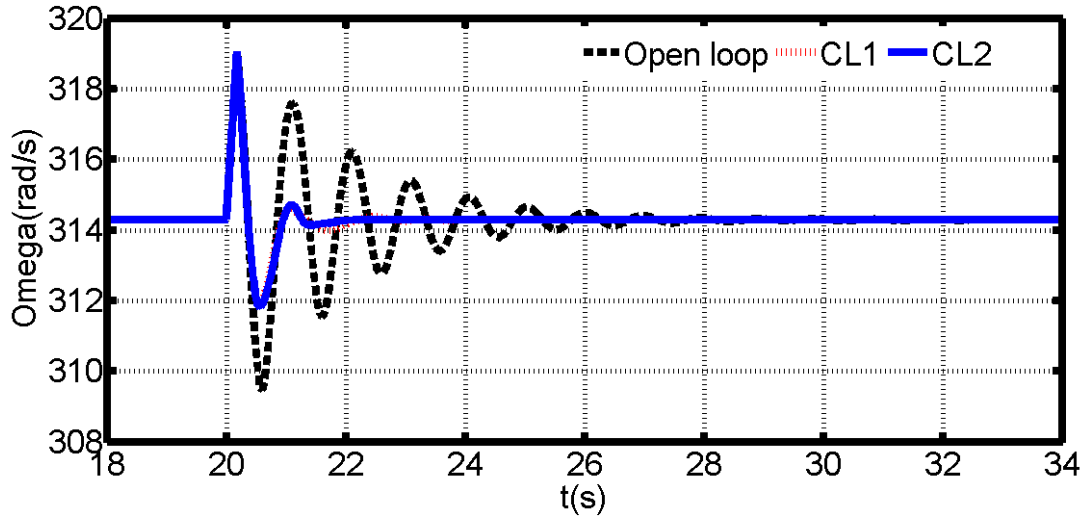

(b) PSM1 rotor speed waveforms for a fault placed at the machine terminals

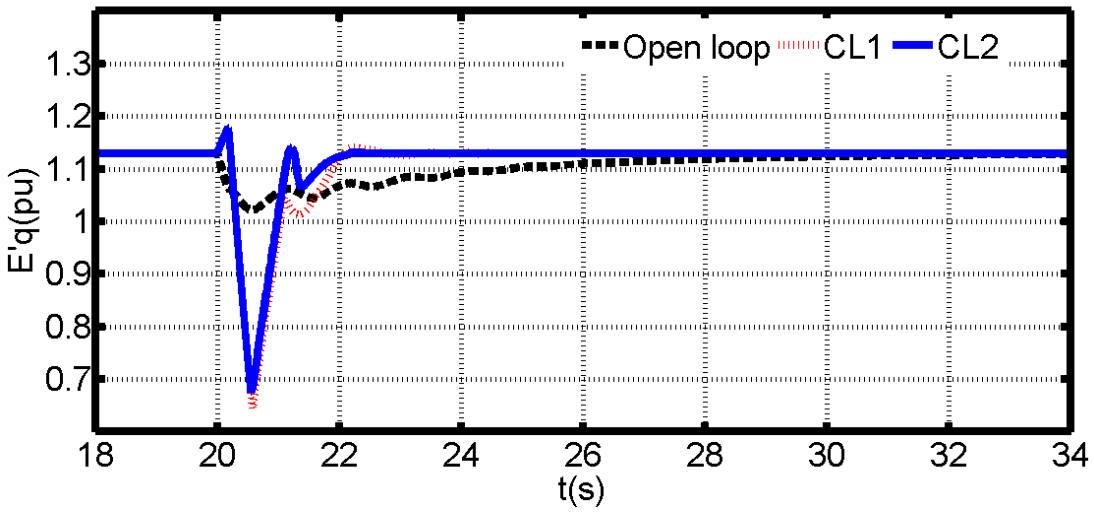

(c) PSM1 Quadrature EMF (E'q) waveforms for a fault placed at the machine terminals

Fig. 4.6: PSM1 waveforms comparing the performances of the control laws CL1 and CL2 with the open-loop case when fault ($X_E = 0$ and $V = 0$) is cleared after 9 cycles

4.2.2 Responses of PSM2 under the Action of the Control Laws

The responses of PSM2 are principally to assess the performance of the control laws when the relative degree of the system with respect to the output function changes. This means assessing the performance of the system when its dynamic behavior changes from a third-order representation to a fourth-order representation. In this case, the fourth-order model (PSM2) was subjected to the same fault considered in Section 4.2.1 under the influence of the control laws. The waveforms of system responses are displayed in this subsection.

Fault at infinite bus: V = 0; X_E = 0.24 and fault clearance time tc = 5, 7, and 9 cycles:

The corresponding system responses are depicted in the waveforms of Fig. 4.7 to Fig. 4.9. The results obtained here are similar to those obtained for PSM1. The only difference is in minor variations in first peaks and settling times of rotor angles and speeds.

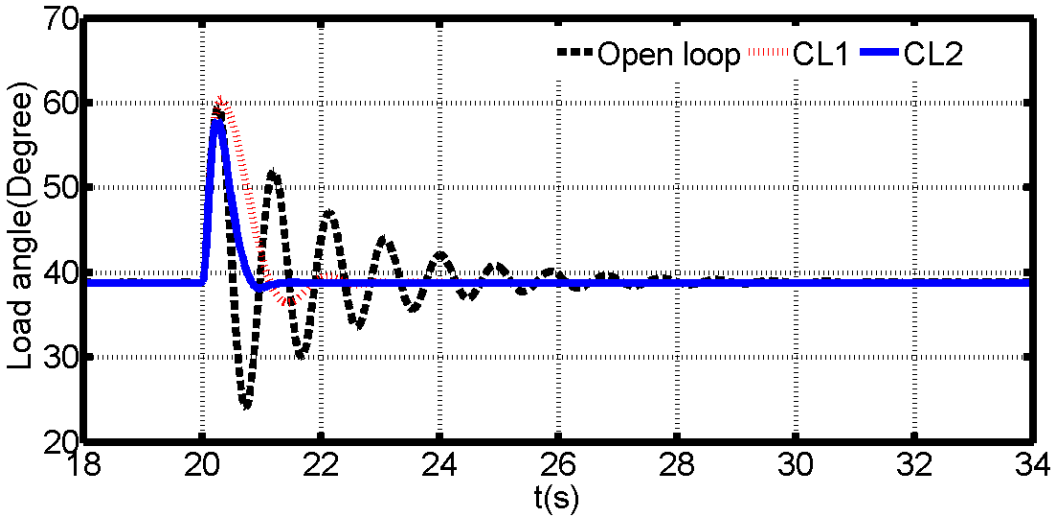

(a) PSM2 rotor angle waveforms for a fault at the infinite bus

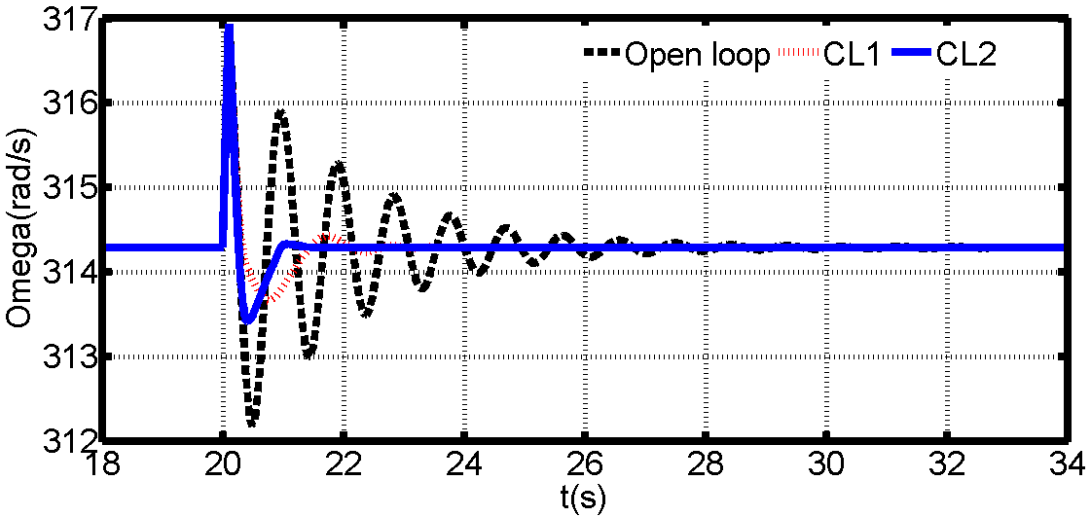

(b) PSM2 rotor speed waveforms for a fault at the infinite bus

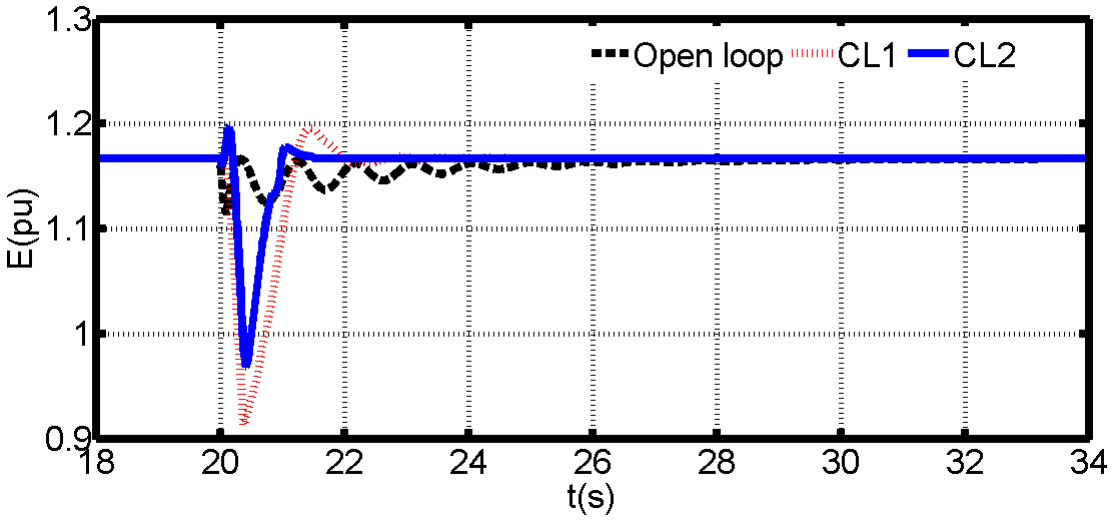

(c) PSM2 internal EMF ($E=\sqrt{(E_d^{'})^2+(E_q^{'})^2}$) waveforms for a fault at the infinite bus

Fig. 4.7: PSM2 waveforms comparing the performances of the control laws CL1 and CL2 with the open-loop case when fault (XE=0.24 and V=0) is cleared after 5 cycles

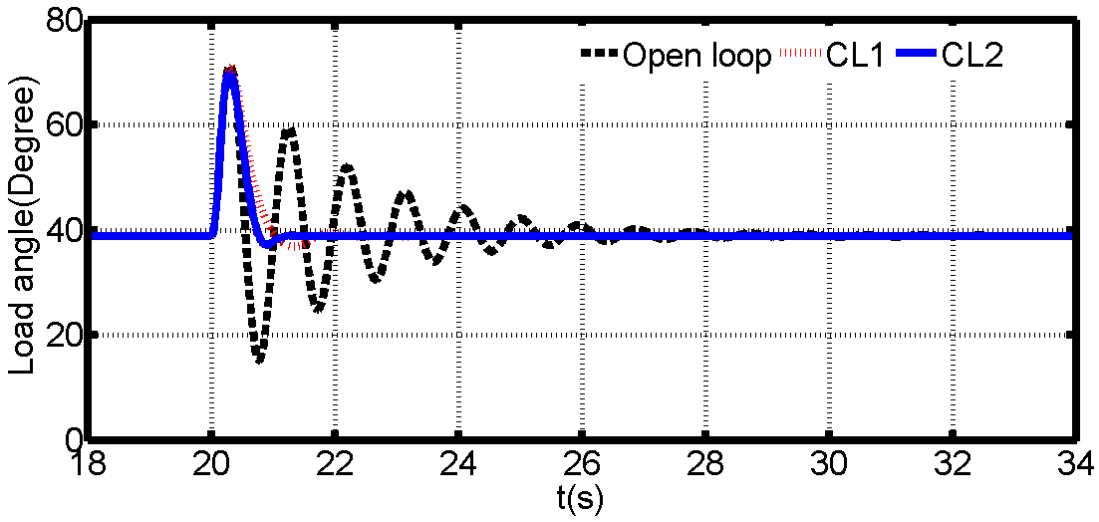

(a) PSM2 rotor angle waveforms for a fault at the infinite bus

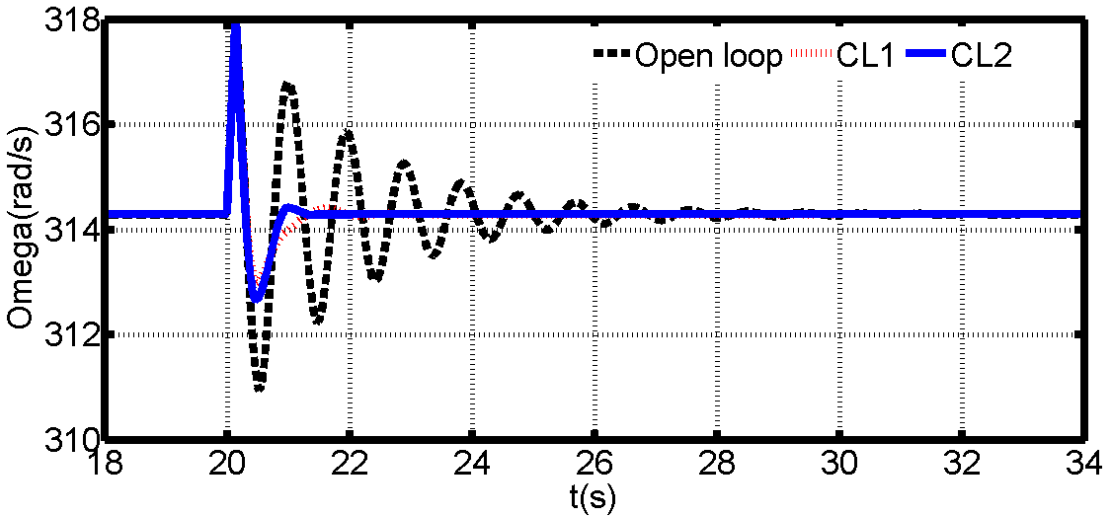

(b) PSM2 rotor speed waveforms for a fault at the infinite bus

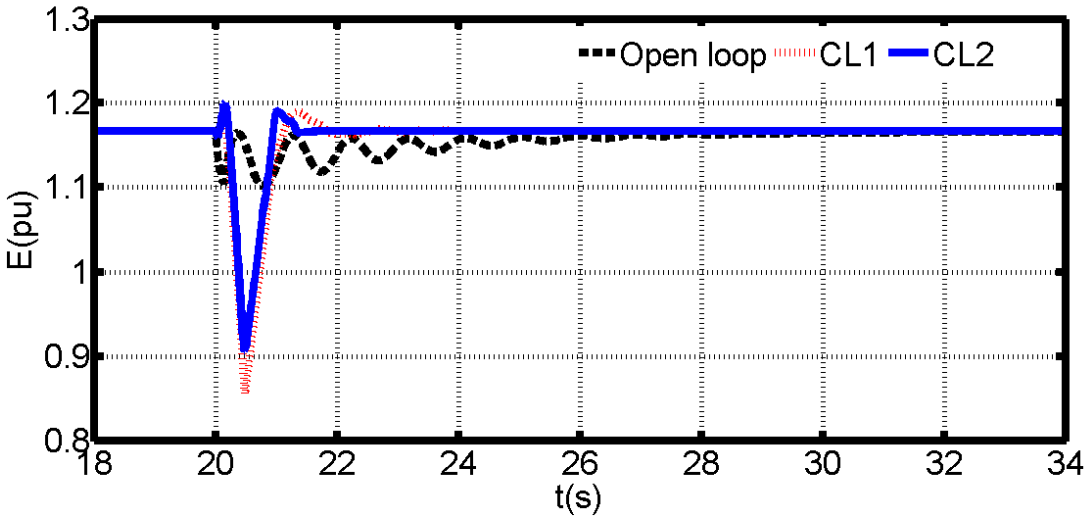

(c) PSM2 internal EMF ($E=\sqrt{(E_d^{'})^2+(E_q^{'})^2}$) waveforms for a fault at the infinite bus

Fig. 4.8: PSM2 waveforms comparing the performances of the control laws CL1 and CL2 with the open-loop case when fault (XE=0.24 and V=0) is cleared after 7 cycles

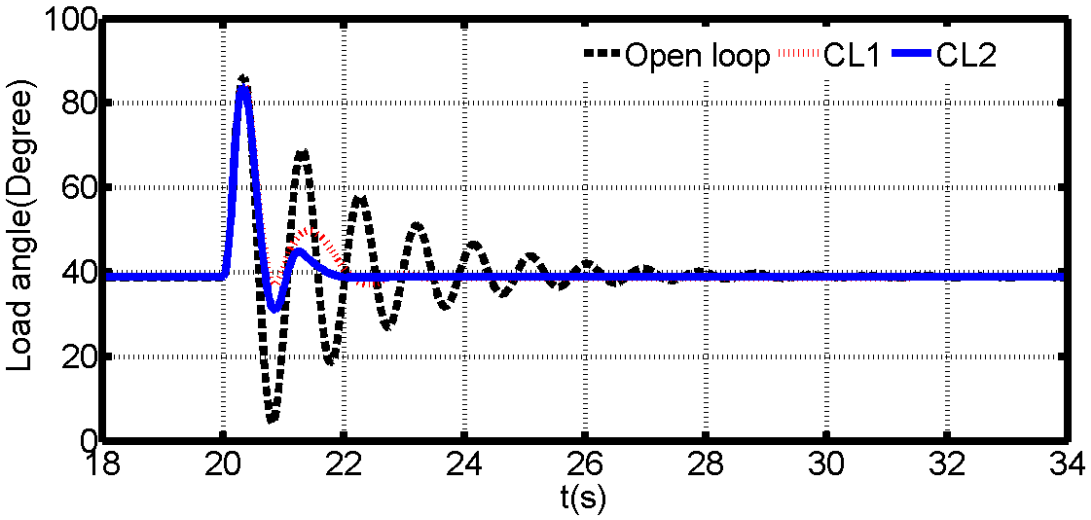

(a) PSM2 rotor angle waveforms for a fault at the infinite bus

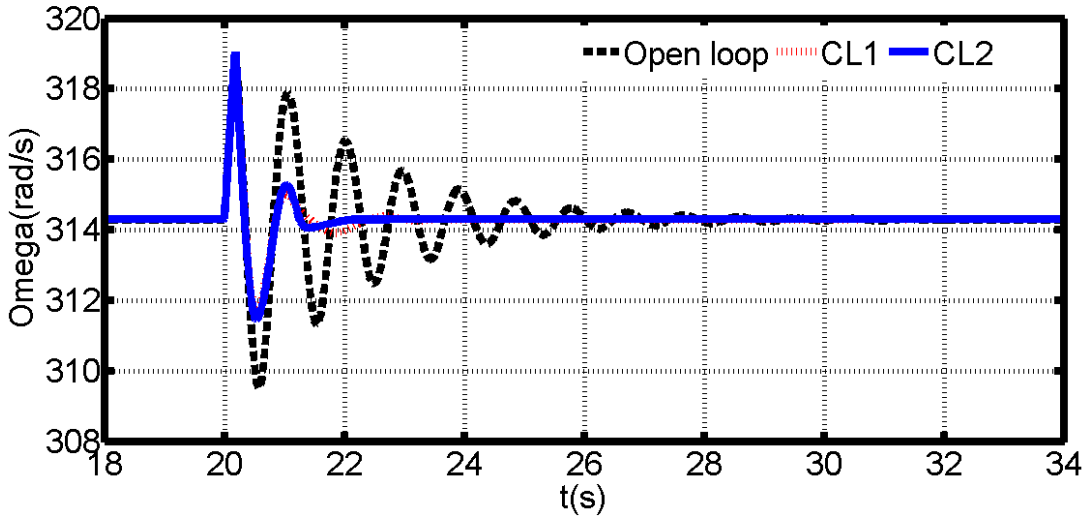

(b) PSM2 rotor speed waveforms for a fault at the infinite bus

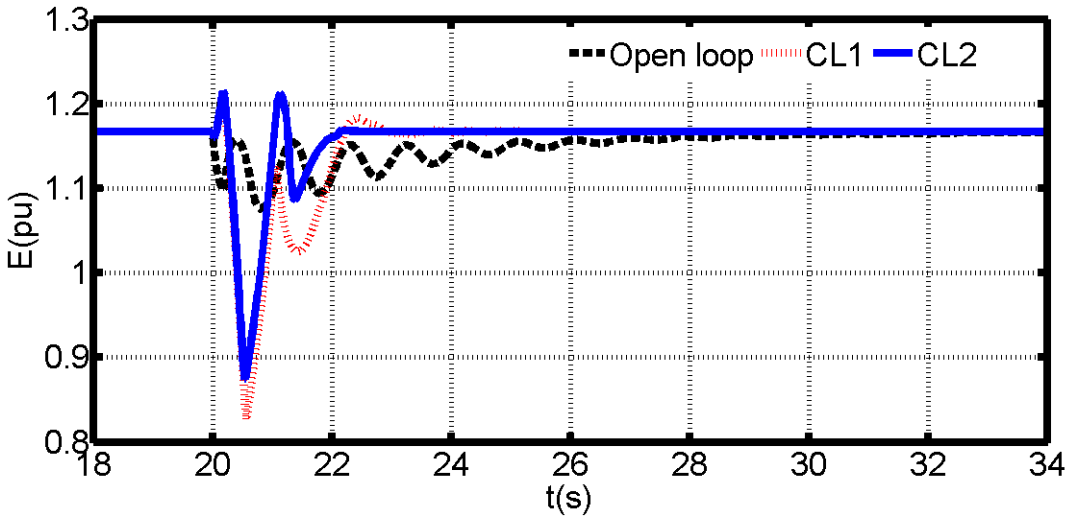

(c) PSM2 internal EMF ($E=\sqrt{(E_d^{'})^2+(E_q^{'})^2}$) waveforms for a fault at the infinite bus

Fig. 4.9: PSM2 waveforms comparing the performances of the control laws CL1 and CL2 with open-loop case when fault (XE=0.24 and V=0) is cleared after 9 cycles

Fault at generator terminals: V = 0; X_E = 0; and fault clearance time tc = 5, 7, and 9 cycles: In this case, the waveforms of the system responses are shown in Fig. 4.10 to Fig. 4.12. Likewise, the results obtained here are similar to those obtained for PSM1.

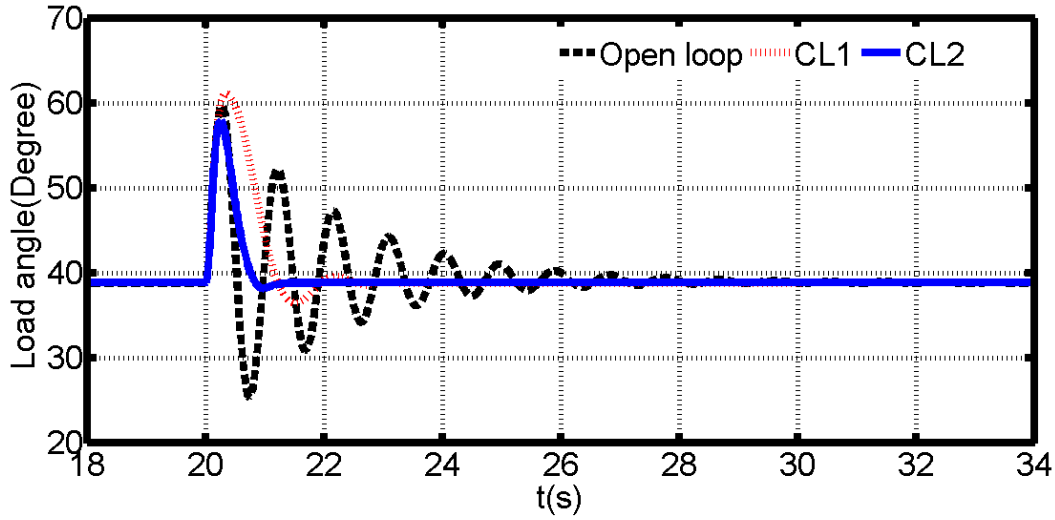

(a) PSM2 rotor angle waveforms for a fault at the generator terminals

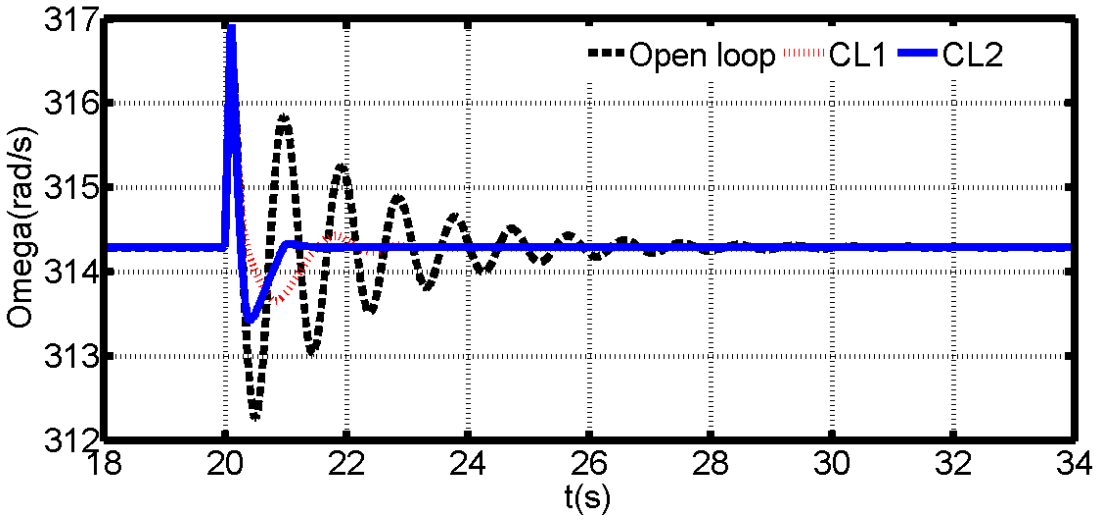

(b) PSM2 rotor speed waveforms for a fault at the generator terminals

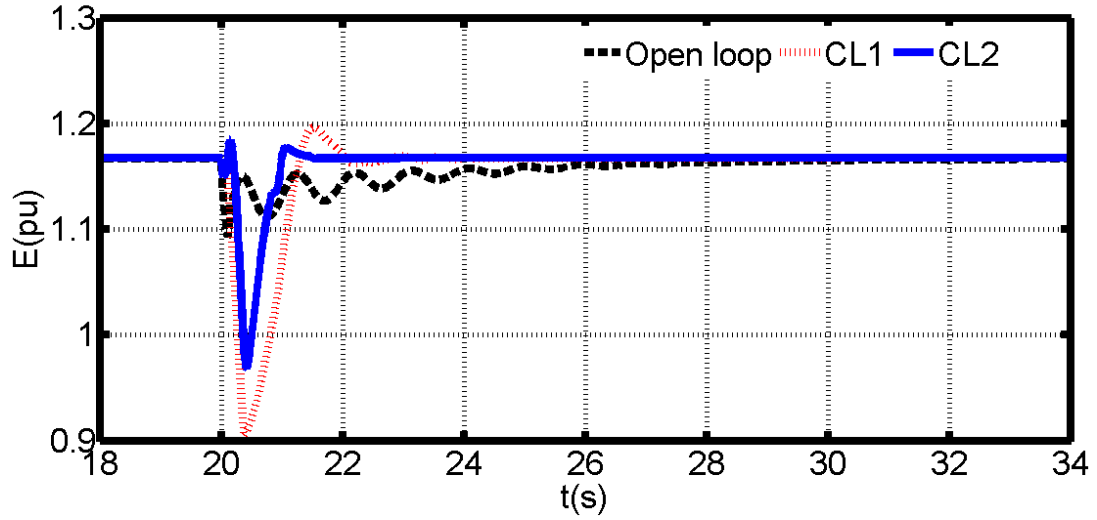

(c) PSM2 internal EMF ($E=\sqrt{(E_d^{'})^2+(E_q^{'})^2}$) waveforms for a fault at the generator terminals

Fig. 4.10: PSM2 waveforms comparing the performances of the control laws CL1 and CL2 with the open-loop case when fault (XE=0 and V=0) is cleared after 5 cycles

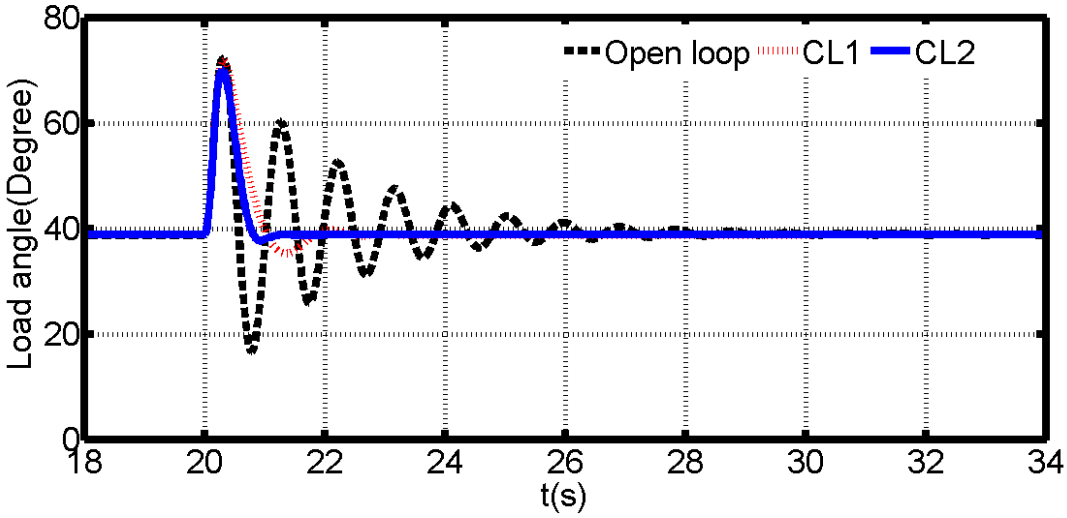

(a) PSM2 rotor angle waveforms for a fault at the generator terminals

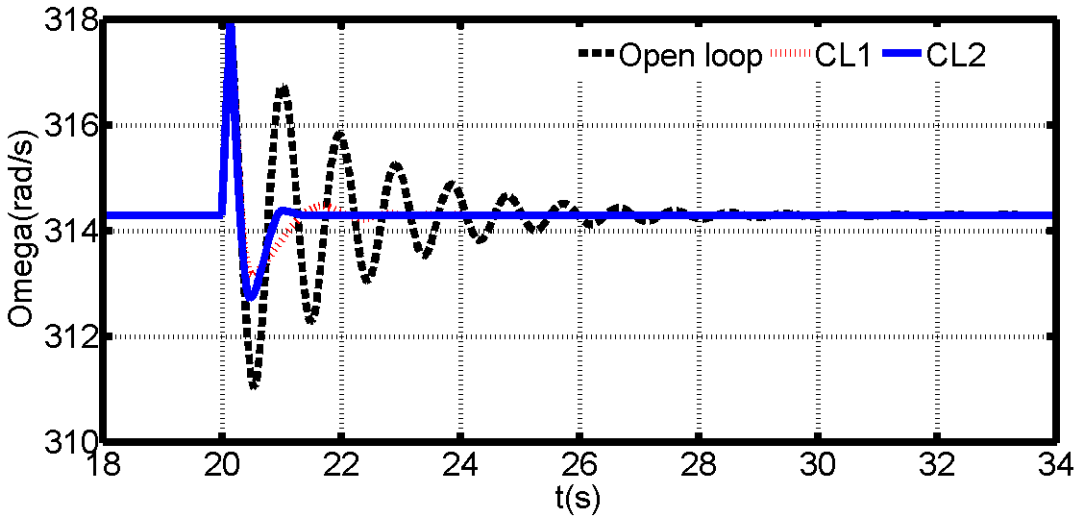

(b) PSM2 rotor speed waveforms for a fault at the generator terminals

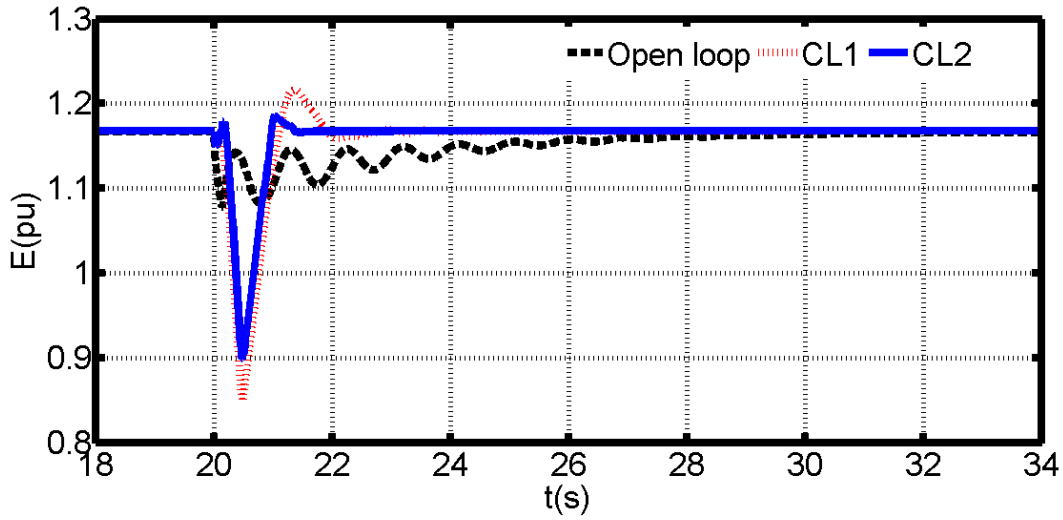

(c) PSM2 internal EMF ($E=\sqrt{(E_d^{'})^2+(E_q^{'})^2}$) waveforms for a fault at the generator terminals

Fig. 4.11: PSM2 waveforms comparing the performances of the control laws CL1 and CL2 with the open-loop case when fault (XE=0 and V=0) is cleared after 7 cycles

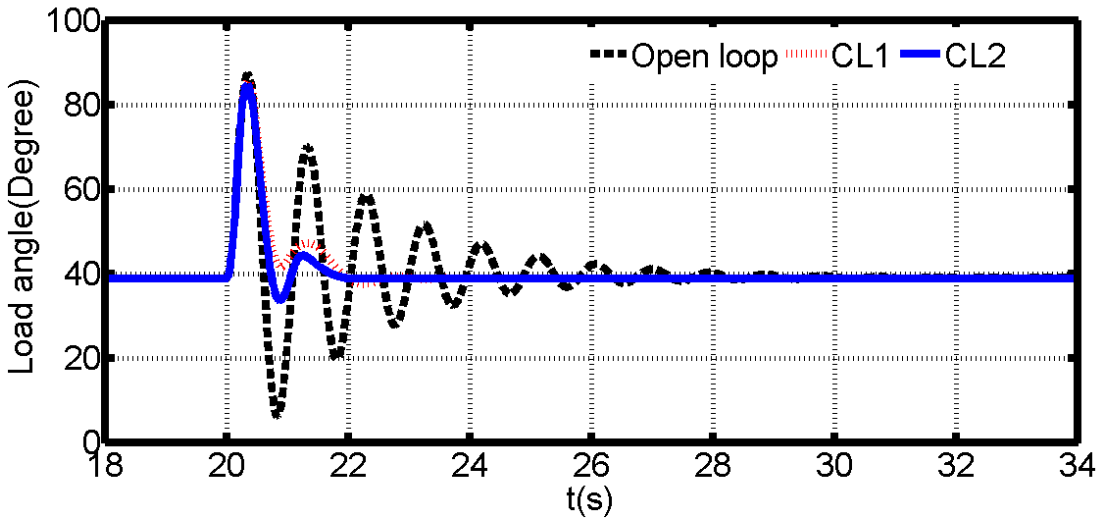

(a) PSM2 rotor angle waveforms for a fault at the generator terminals

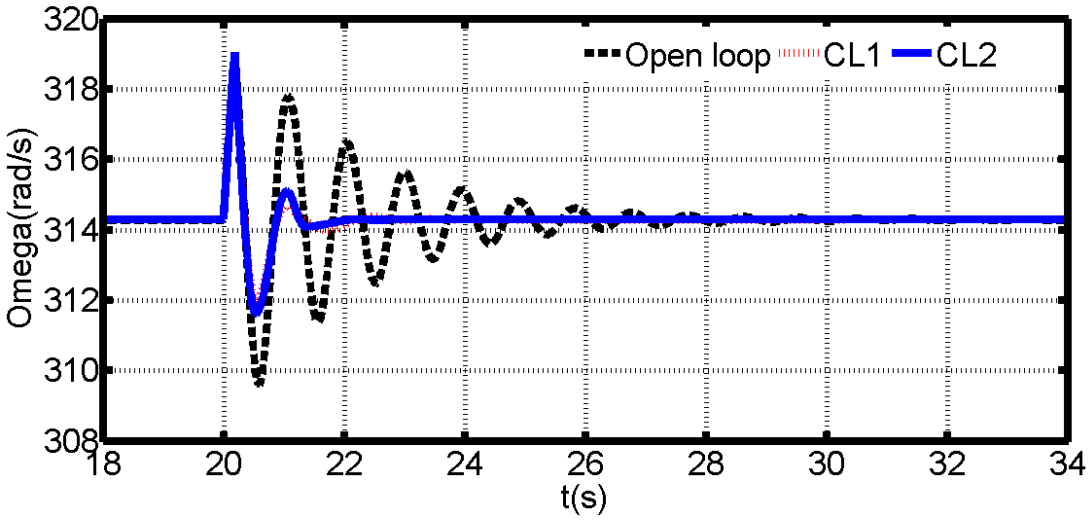

(b) PSM2 rotor speed waveforms for a fault at the generator terminals

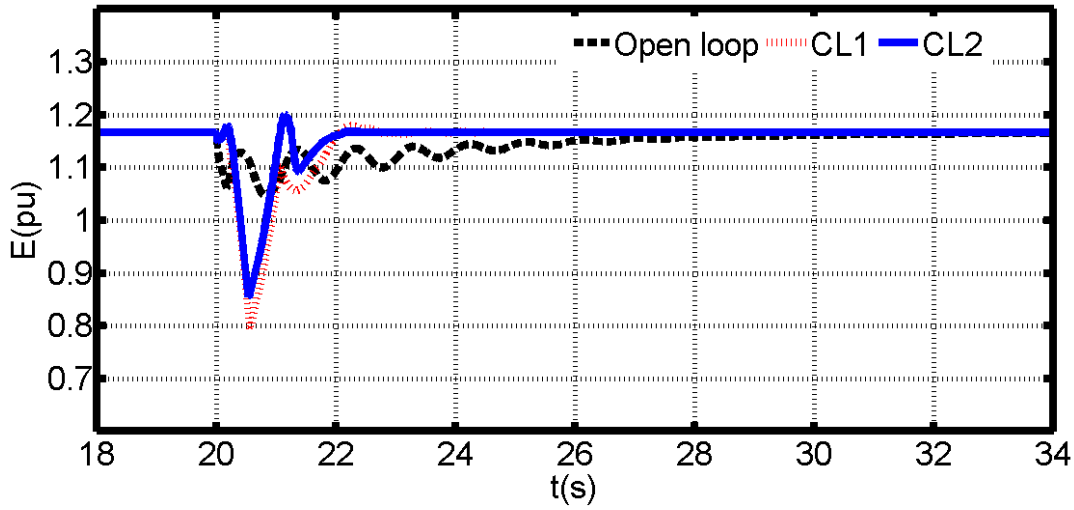

(c) PSM2 internal EMF ($E=\sqrt{(E_d^{'})^2+(E_q^{'})^2}$) waveforms for a fault at the generator terminals

Fig. 4.12: PSM2 waveforms comparing the performances of the control laws CL1 and CL2 with open-loop case when fault (XE=0 and V=0) is cleared after 9 cycles

4.2.3 Evaluation of Control Law 3

Because control law 3 (CL3) is an improvement of the control law 1 (CL1), which was discussed earlier, the studies conducted with CL1 and CL2 will not be repeated with CL3.

Instead, this subsection will assess the performance of CL3 with reference to open loop (constant excitation), CL1 and CL2, with emphasis on the following aspects: extension of critical clearance time, and reduction of first swing and subsequent power oscillations. In an attempt to reduce the number of plots that will be presented in this section, a limited number of selected waveforms obtained using PSM1 and PSM2 will be presented.

A) Fault at infinite bus: V = 0; X_E = 0.24; and fault clearance time tc=9 cycles: Fig. 4.13 (a), Fig. 4.13 (b), and Fig. 4.13 (c) present respectively the synchronous generator rotor angle, rotor speed and quadrature axis induced EMF obtained when the system being studied was subjected to a three-phase fault at an infinite bus, with fault duration of 9 cycles. In this case, a third-order model (PSM1) was used, and open-loop results were compared with those obtained using CL1, CL2 and CL3. It was observed that the load angles and rotor speeds produced from these three control laws and open loop have similar first peak, with CL2 exhibiting better performance from power oscillation point of view, followed by CL3. Fig. 4.13 (c) shows that the improved performance of CL2 is achieved with minimum adjustment of E'_q (adjustment needed in the generator EMF through manipulation of the excitation system to counter the demagnetization effect of the armature reaction during fault)

.

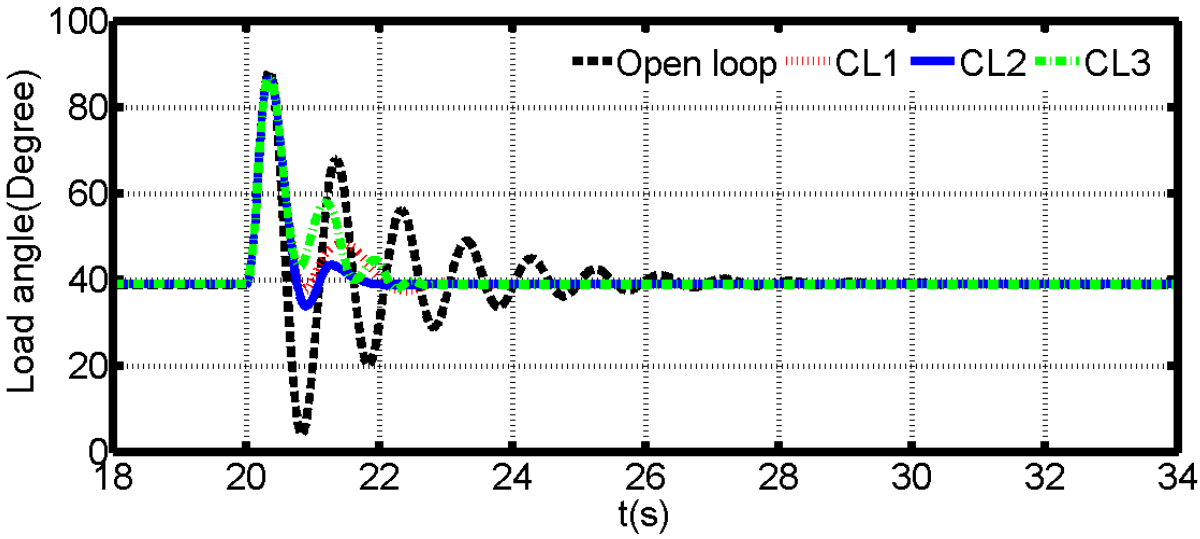

(a) Load angle

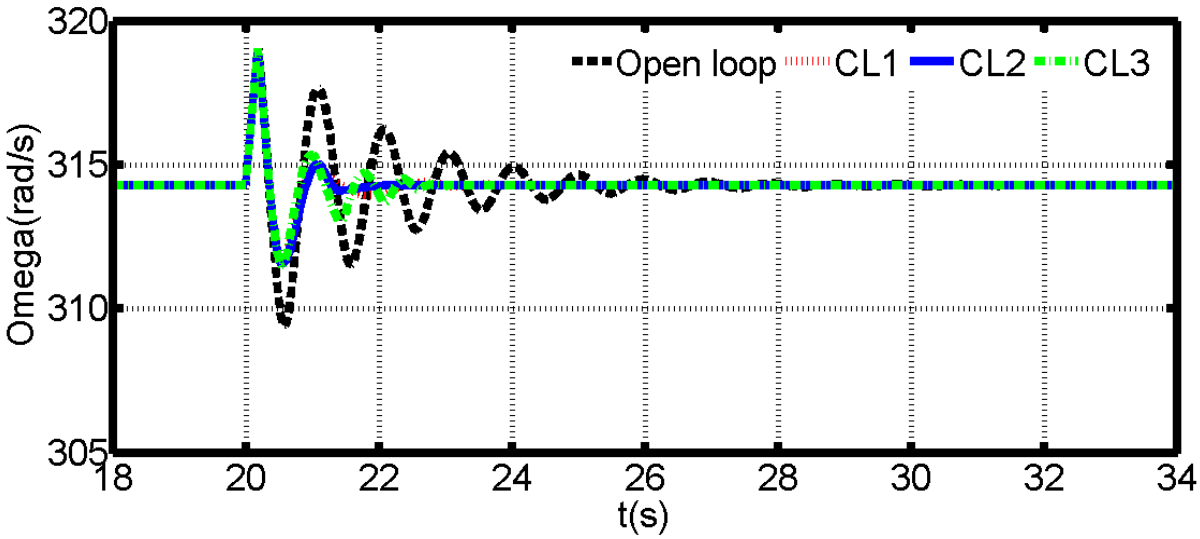

(b) Rotor speed

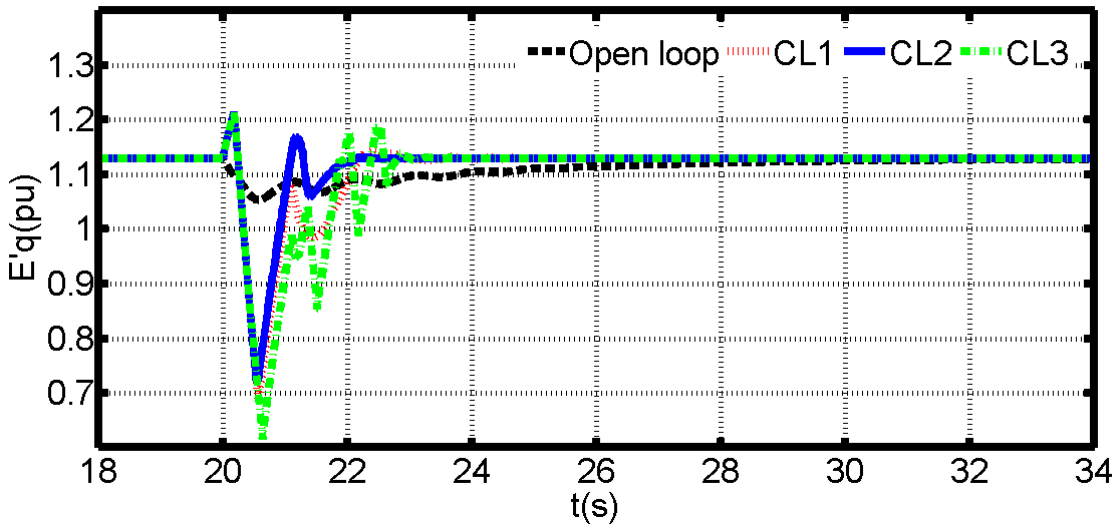

(c) Quadrature EMF (E'q)

Fig. 4.13: PSM1 waveforms comparing the performances of control laws (CL1, CL2 and CL3) with the open-loop case when fault (XE=0.24 and V = 0) is cleared after 9 cycles

B) Fault at infinite bus: V = 0; X_E = 0.24; and fault clearance time tc=14.5 cycles:

This case repeats case A), but for fault clearance time of 14.5 cycles. Observe that the open-loop case has lost synchronism, while the system that is being controlled using CL1, CL2 and CL3 remains operational, with CL3 exhibiting better damping in load angle, but higher first peak than CL2 (see Fig. 4.14 (a)). Fig. 4.14 (b) shows that the rotor speeds for the open-loop and those for CL1, CL2 and CL3 have similar peaks, despite that the open-loop case has fallen out of slip. Fig. 4.14 (c) indicates that the quadrature axis EMF for the open-loop case has collapsed, while those for CL1, CL2 and CL3 regain their previous steady state equilibrium points. Clearing times were increased progressively till 14.5 cycles and 14.7cycles which represent the limits for CL1 and CL3, respectively.

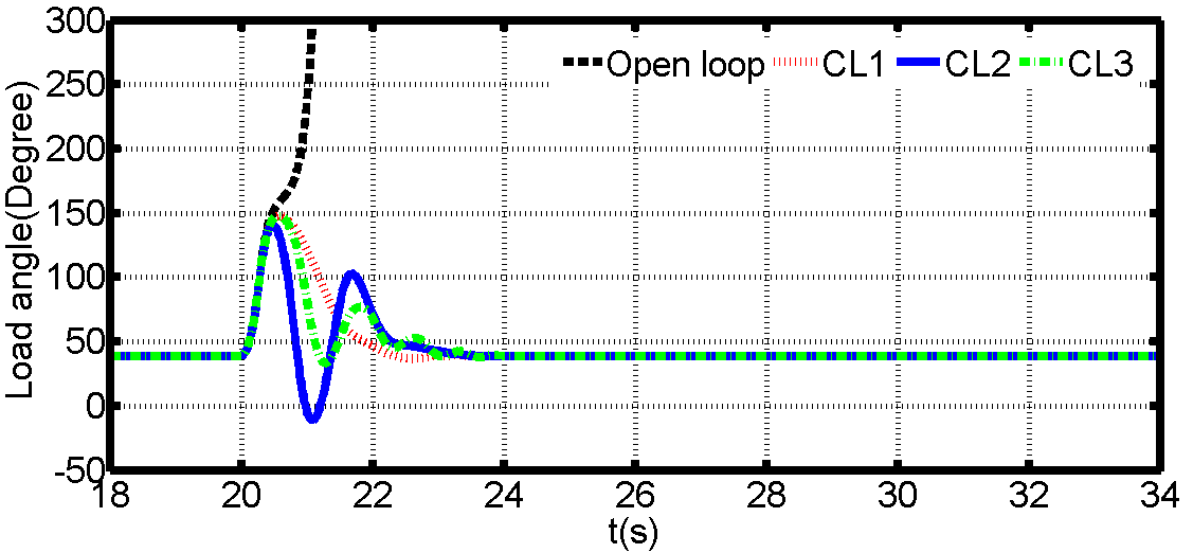

(a) Load angle

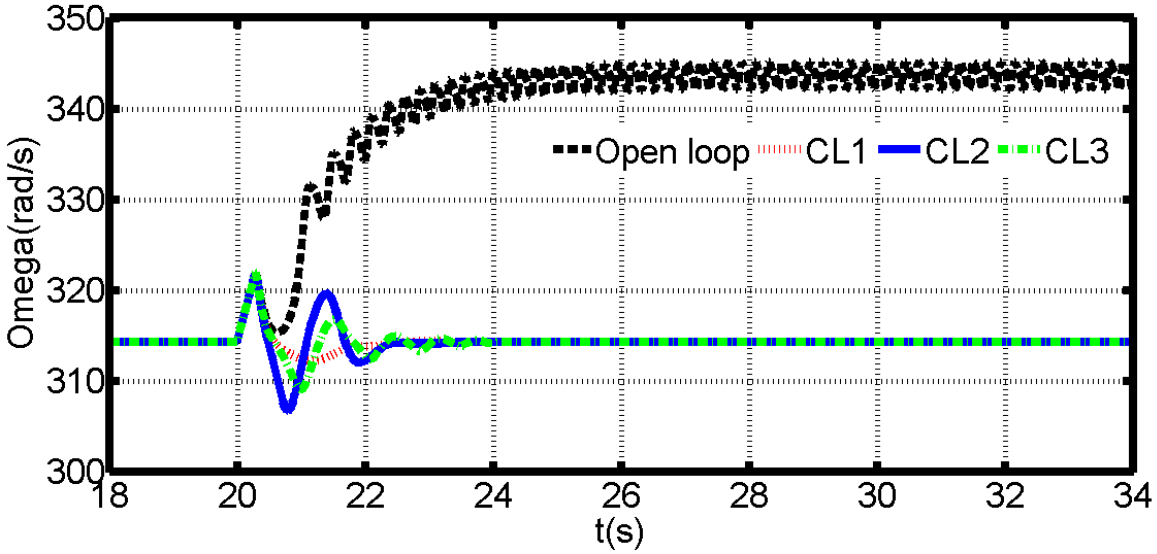

(b) Rotor speed

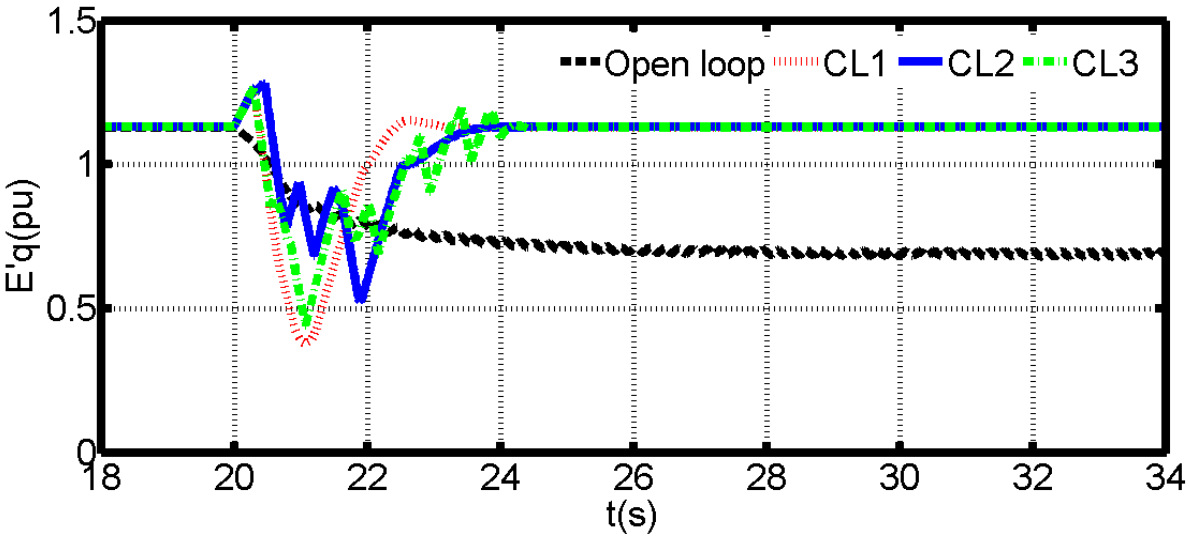

(c) Quadrature EMF (E'_q)

Fig. 4.14: PSM1 waveforms comparing the performances of control laws (CL1, CL2 and CL3) with the open-loop case when fault (XE=0.24 and V = 0) is cleared after 14.5 cycles

C) Fault at infinite bus: V = 0; X_E = 0.24; and fault clearance time tc=14.7 cycles: In an attempt to establish which control law can maintain system stability for an extended period of time, the cases A) and B) are repeated, but this time for fault clearance time of 14.7 cycles. Observe that the cases for the open loop and CL1 have lost their synchronisms, while the system that is being controlled using CL2 and CL3 remains operational, with CL2 exhibiting lower first peak and faster deceleration compared to CL3 (see Fig. 4.15 (a)). The plots for the rotor speeds in Fig. 4.15 (b) support the observations drawn from the results in Fig. 4.15 (a). Fig. 4.15 (c) indicates that the quadrature axis EMF for the open-loop and CL1 cases have collapsed, while those for CL2 and CL3 regain their previous steady state equilibrium points.

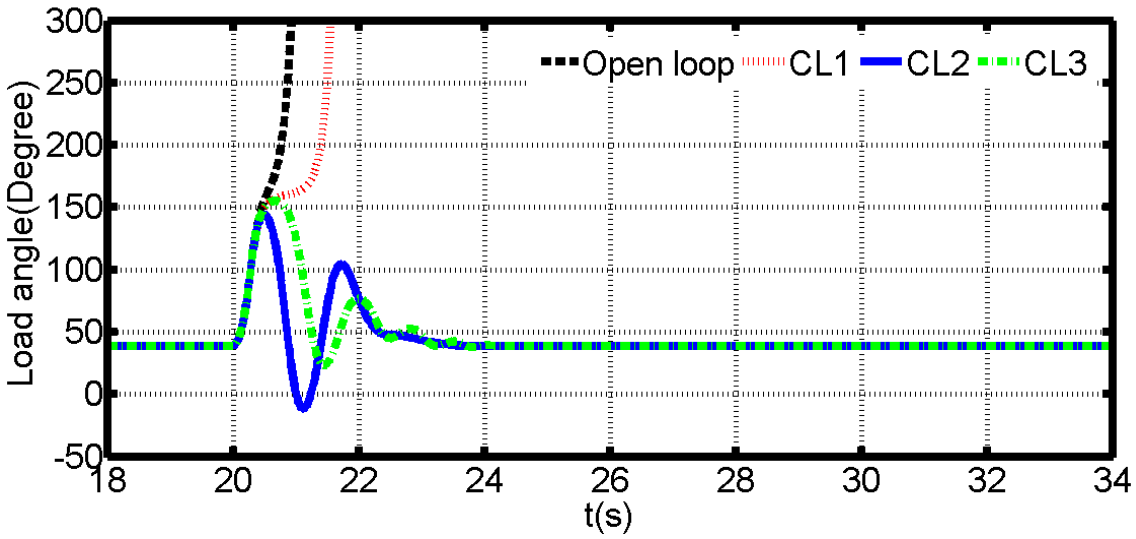

(a) Load angle

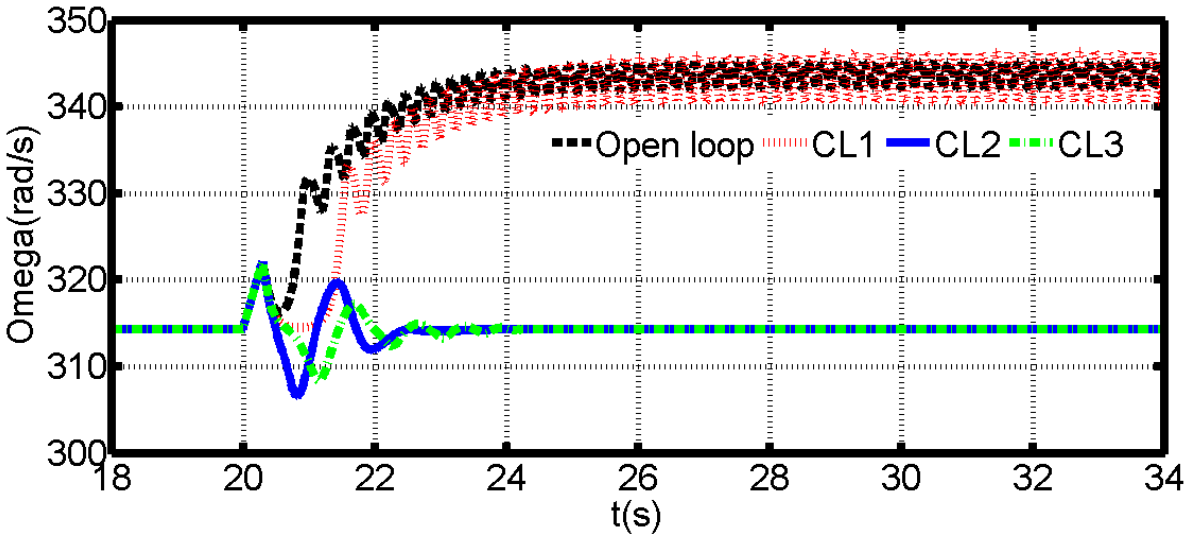

(b) Rotor speed

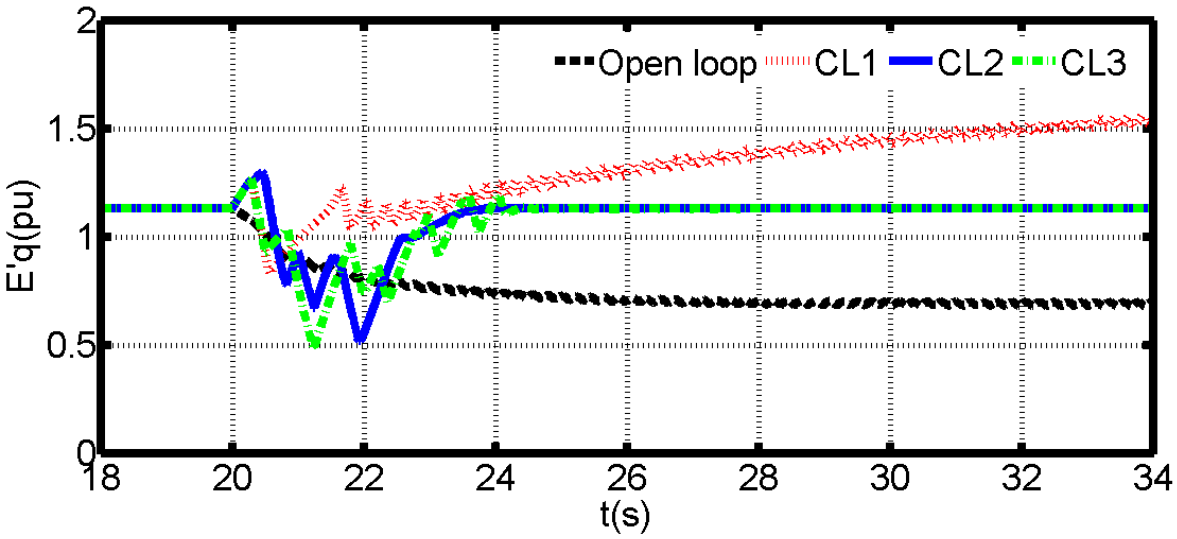

(c) Quadrature EMF (E'_q)

Fig. 4.15: PSM1 waveforms comparing the performances of control laws (CL1, CL2 and CL3) with the open-loop case when fault (XE=0.24 and V = 0) is cleared after 14.7 cycles

D) Fault at infinite bus: V = 0; X_E = 0.24; and fault clearance time tc=15 cycles: To further establish which of the control laws CL2 and CL3 can maintain system stability for a more extended period of time beyond that established in cases A), B) and C), an additional case that increases the fault clearance time to 15 cycles is presented. It is clear from Fig. 4.16 that the cases for the open loop, CL1, and CL3 have lost their synchronisms, while the system that is being controlled using CL2 remains operational. Based on this result and those presented in A) through C), it can be concluded that the control law CL2 performs better than CL1 and CL3 in extending the critical clearance time of a single machine connected to an infinite bus system being studied. Although this conclusion is drawn when the system is modelled using reduced order model PSM1, the use of PSM2 will not affect the validity of this conclusion. To corroborate this point of

view, additional results obtained when PSM1 is replaced by PSM2 are presented in Fig. 4.17 and Fig. 4.18 for fault clearance time of 9 cycles and 14.8 cycles. Fig. 4.18 confirms the superiority of the control law CL2 in ensuring system stability beyond that achievable with CL1 and CL2 as previously suggested above. Fig. 4.19 and Fig. 4.20 are given to reveal the extent to which CL2 can retain fault. As shown in Fig. 4.20, CL2 can withstand fault for a maximum duration of 15.30 cycles.

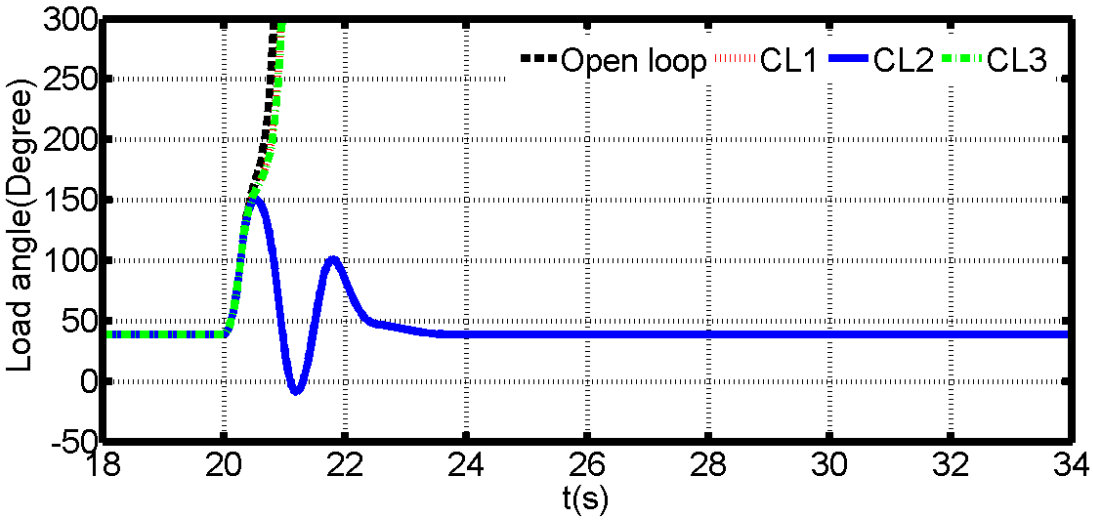

(a) Load angle

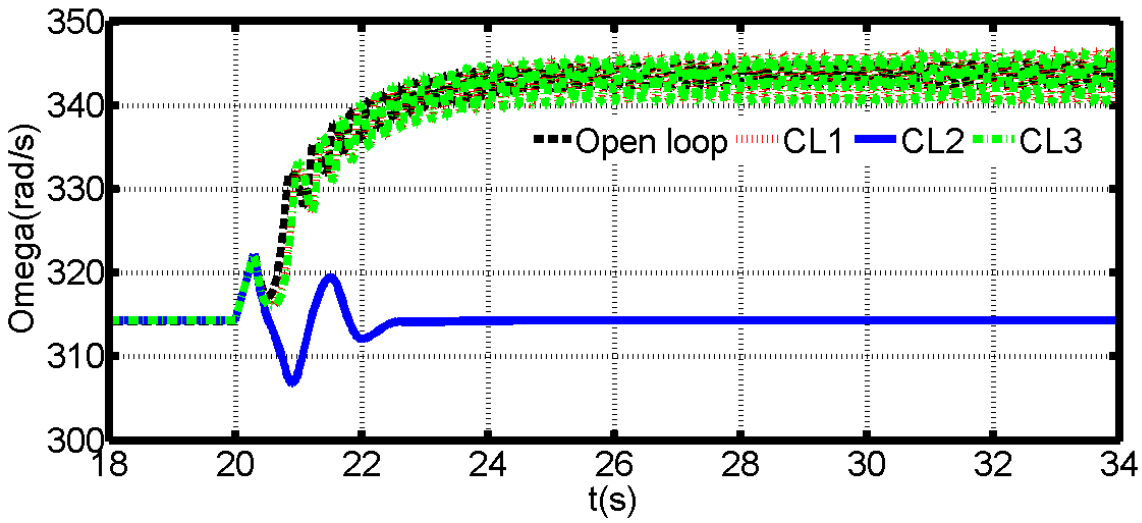

(b) Rotor speed

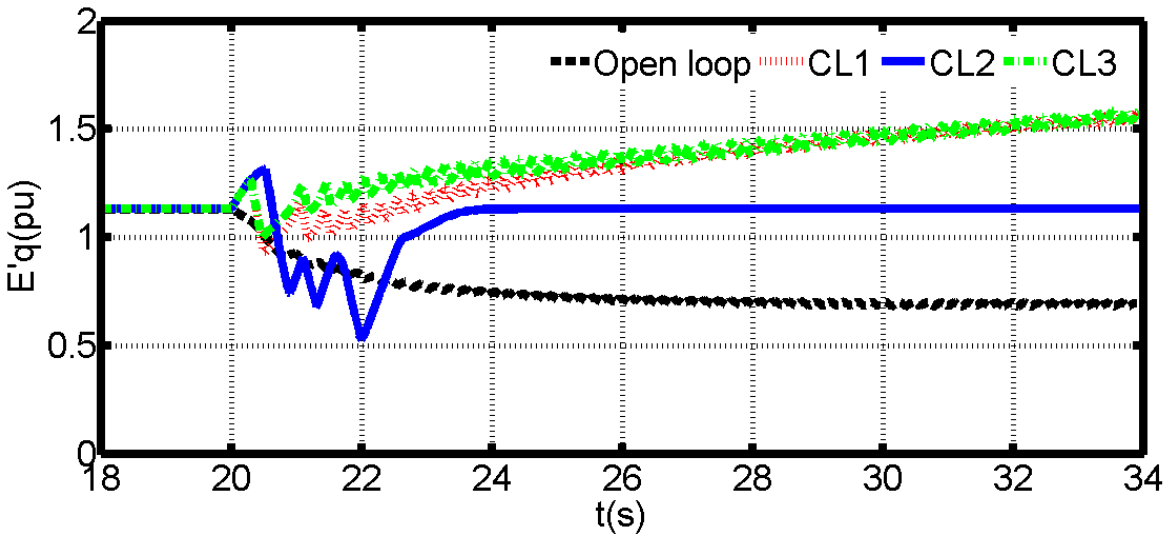

(c) Quadrature EMF (E'_q)

Fig. 4.16: PSM1 waveforms comparing the performances of control laws (CL1, CL2 and CL3) with the open-loop case when fault (XE=0.24 and V = 0) is cleared after 15 cycles

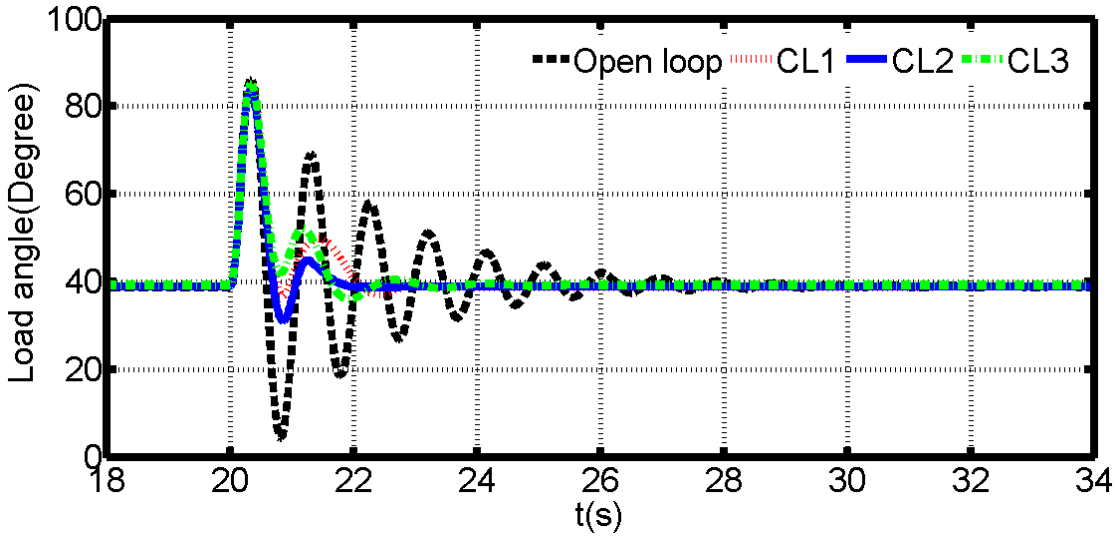

(a) Load angle

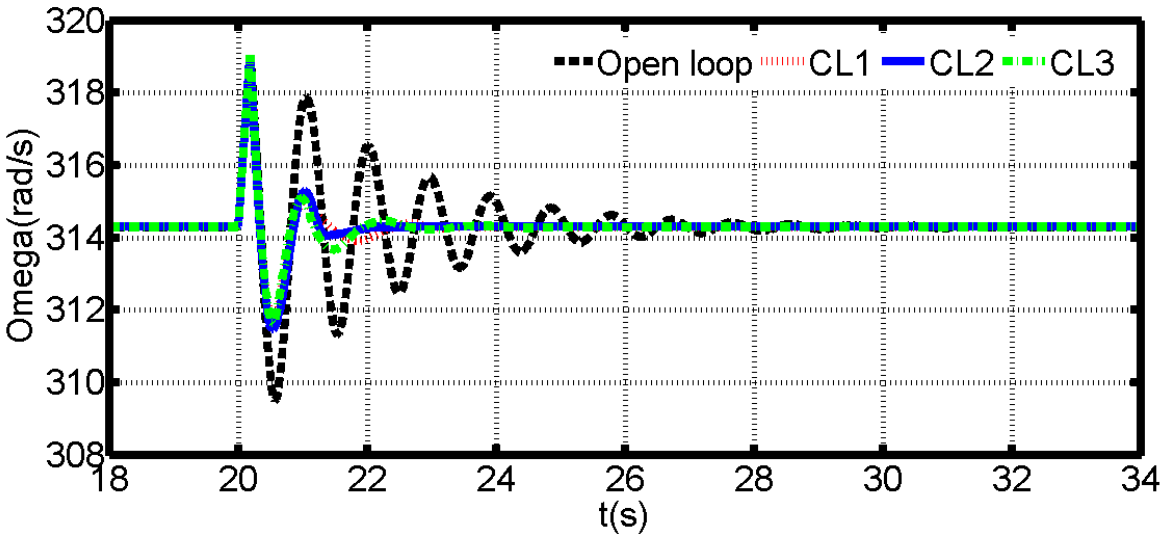

(b) Rotor speed

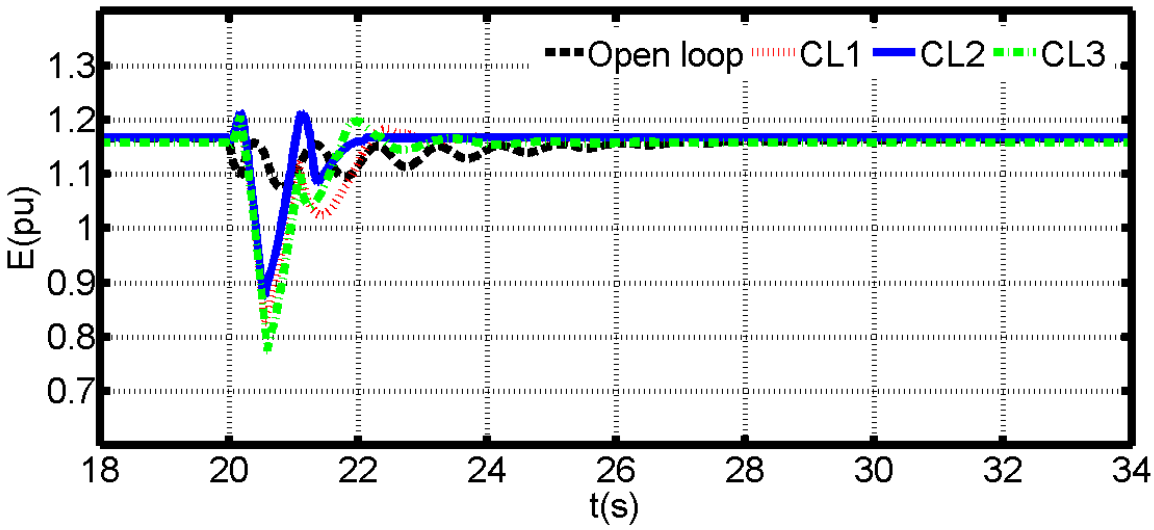

(c) Internal EMF ($E=\sqrt{(E_d^{'})^2+(E_q^{'})^2}$)

Fig. 4.17: PSM2 waveforms comparing the performances of control laws (CL1, CL2 and CL3) with the open-loop case when fault (XE=0.24 and V = 0) is cleared after 9 cycles

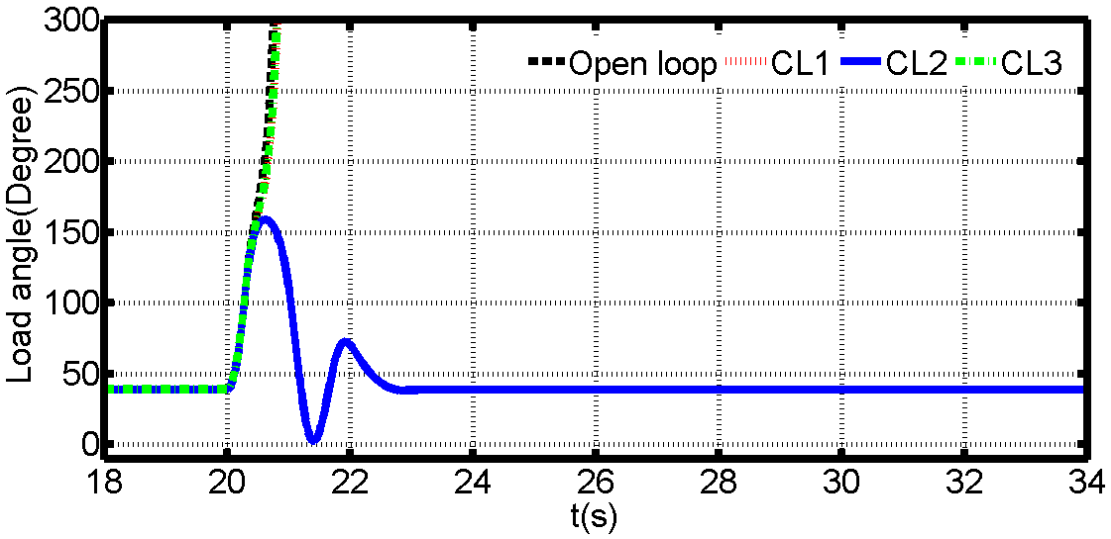

(a) Load angle

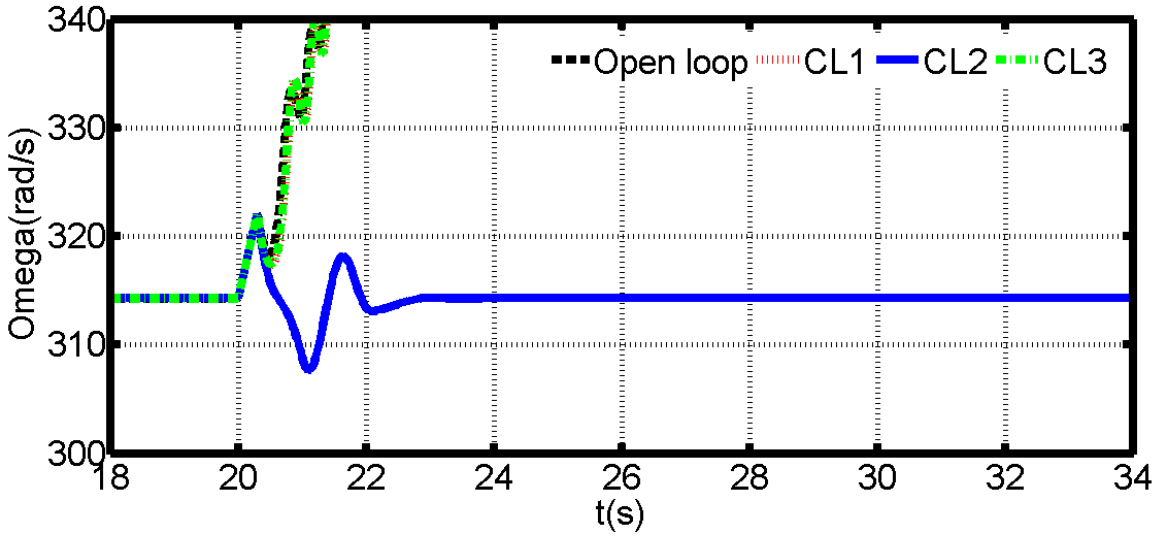

(b) Rotor speed

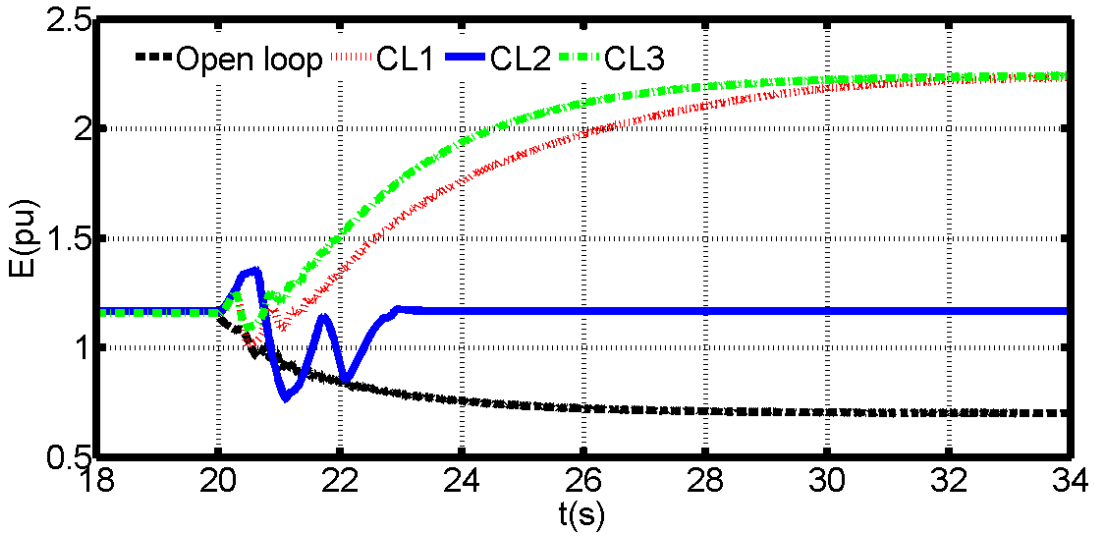

(c) Internal EMF ($E=\sqrt{(E_d^{'})^2+(E_q^{'})^2}$)

Fig. 4.18: PSM2 waveforms comparing the performances of control laws (CL1, CL2 and CL3) with the open-loop case when fault (XE=0.24 and V = 0) is cleared after 14.8 cycles

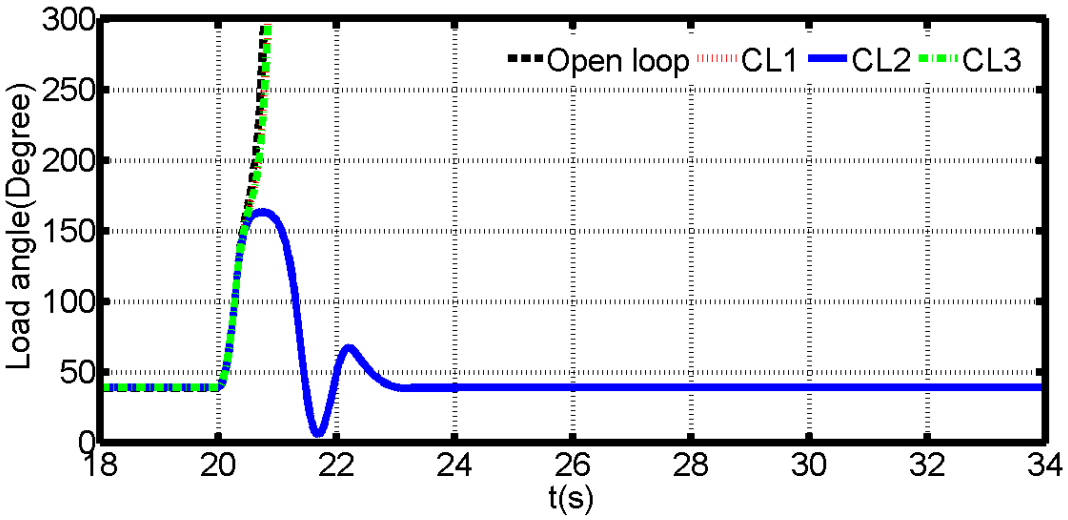

Fig. 4.19: PSM1 load angle waveform comparing the performances of control laws (CL1, CL2 and CL3) with the open-loop case when fault (XE=0.24 and V = 0) is cleared after 15.3 cycles

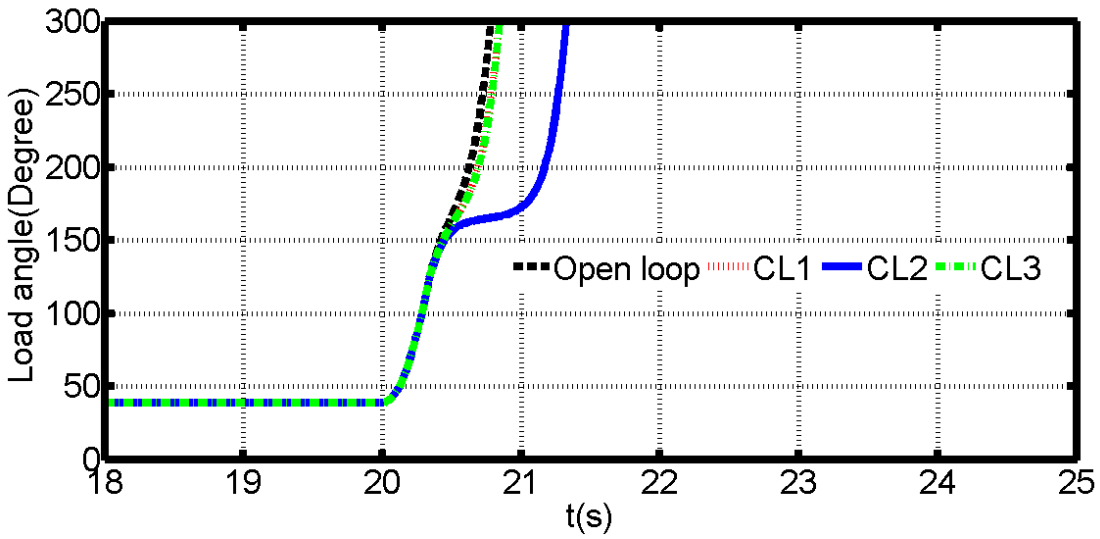

Fig. 4.20: PSM1 load angle waveform comparing the performances of control laws (CL1, CL2 and CL3) with the open-loop case when fault (XE=0.24 and V = 0) is cleared after 15.31 cycles

Sample waveforms that depict the general nature of the control efforts exerted by control laws CL1, CL2, and CL3, respectively (selected from the cases where overall system dynamic characteristics are stabilized) are given in Fig. 4.21 to Fig. 4.23. In these cases and throughout the study, control effort $u(t) = E_F$ is limited to ±5pu.

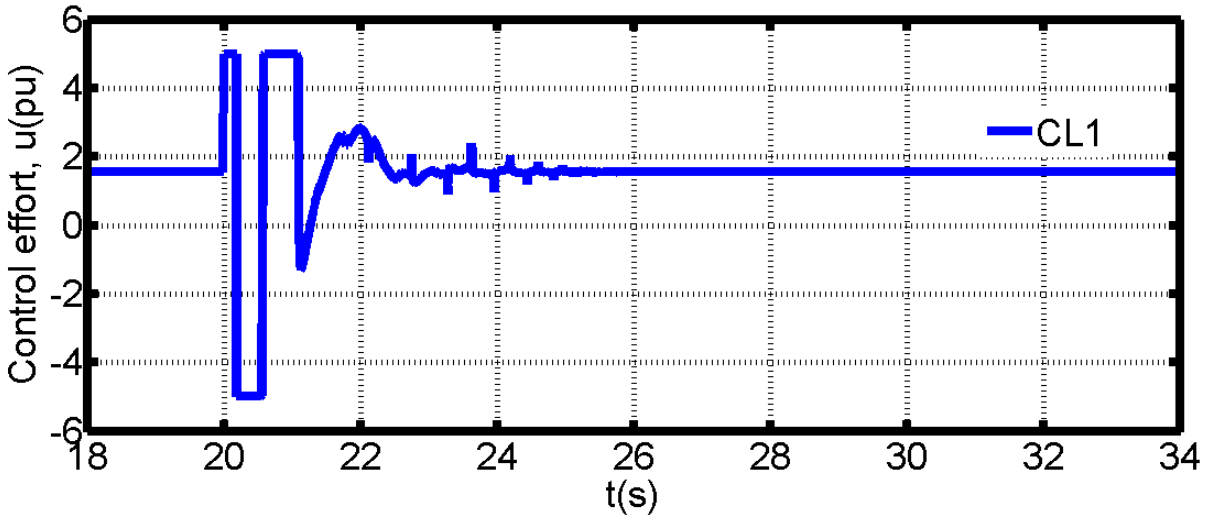

Fig. 4.21: Control effort waveform (CL1)

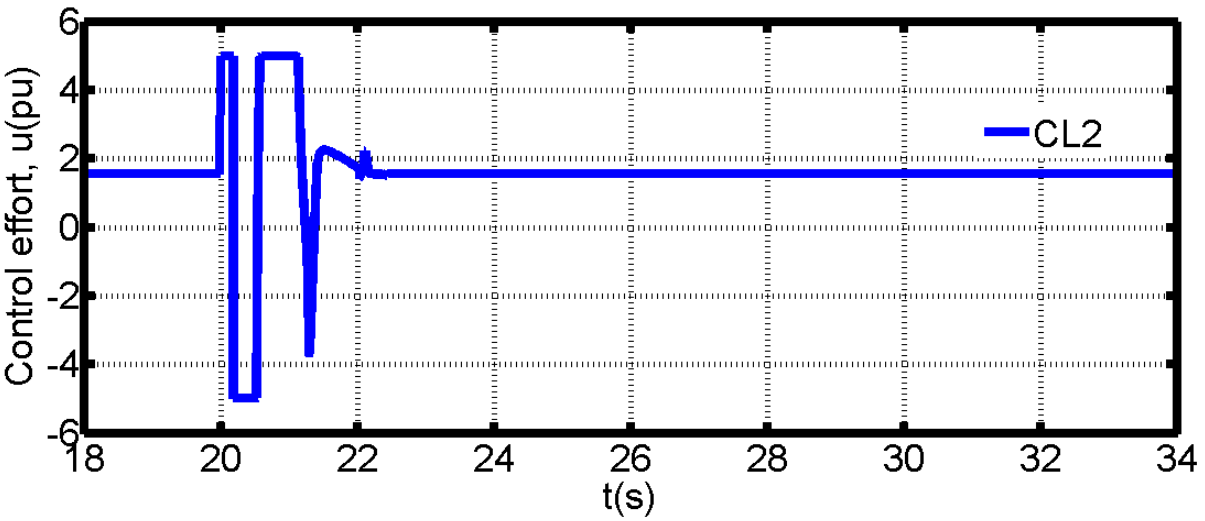

Fig. 4.22: Control effort waveform (CL2)

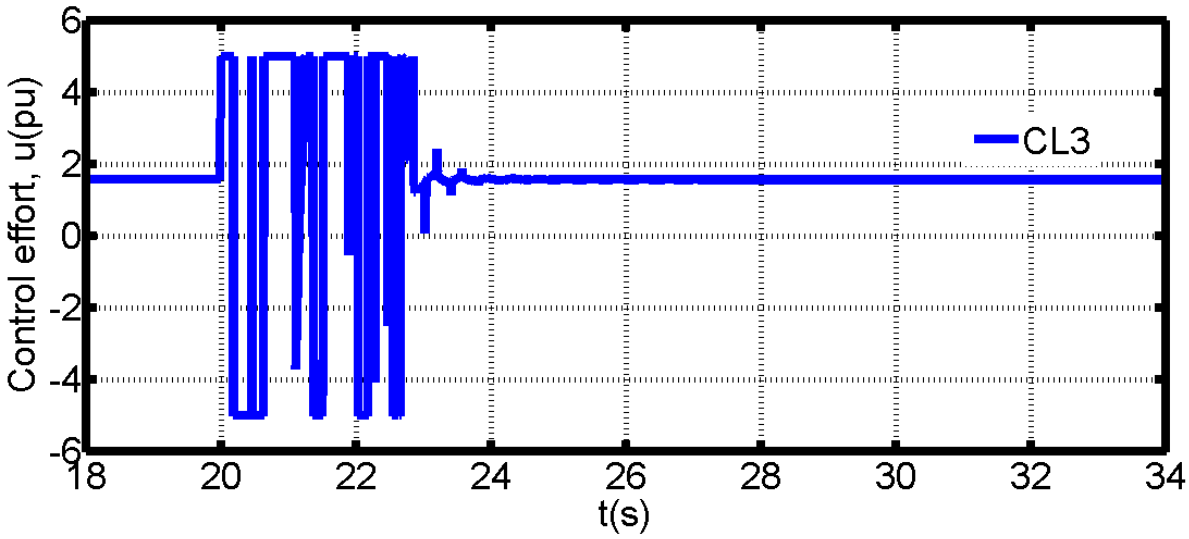

Fig. 4.23: Control effort waveform (CL3)

4.3 General Discussion

The system simulations were performed by considering various degrees of perturbation as highlighted previously. To be able to evaluate the control laws effectively, the system was assumed to be operating close to its initial steady-state operating point before it was disturbed. For both fault locations considered, the oscillations in the load angle following fault clearance under constant excitation (open loop) subsided slowly and took up to 8s for the system to regain its steady state, with high first peak when the fault was at the generator terminal. Furthermore, for most effective performance of the control laws, all the disturbance scenarios were employed to tune their parameters. First, an approximate method of tuning the parameters of CL1 and CL3, which are α_1, α_2, and K, was determined after several simulation runs (see Deduction 4.1 below).

Deduction 4.1: Consider a third-order affine power system model given in equation (4.1). The parameters K, α_1 and α_2 of the sliding mode control law (equations (3.80) and (3.88)) for stabilizing the system are assumed to form the structure of a second-order

linear time-invariant (LTI) system model as depicted in Fig. 4.24. For $\alpha_2 = 3\alpha_1$, where α_1 is a value chosen from a range of 3 and 5, employing the root-locus strategy (Awelewa *et al.*, 2013) to determine K (that will give a closed-loop response with a damping factor of about 0.8) yields K = 16, $\alpha_1 = 3$, and $\alpha_2 = 9$ for CL1 and CL3.

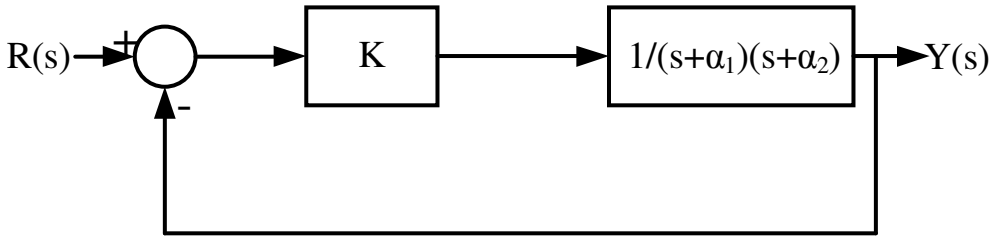

Fig. 4.24: Unity feedback system for finding parameter K

Secondly, the parameters k_1, k_2, and k_3 of CL2 given in equation (3.87) were found using the pole-placement method from

$$p^3 + k_3p^2 + k_2p + k_1 = (p + a_1)(p + a_2)(p + a_3) = 0$$

where $a_1 = 9$, $a_2 = 5$, $a_3 = 2$. Thus, $k_1 = 90$, $k_2 = 73$, and $k_3 = 16$. The value of parameter v_3, from which $v_1 = 1/2$, and $v_2 = 3/5$ were obtained (see Section 3.2.3), is 3/4. The value of the dilation constant v is 2.

Generally, it can be inferred that the responses of PSM1 and PSM2 under all control actions closely correspond, signifying that any uncertainty in the dynamics of the system does not have any appreciable effect on the dynamic characteristics of the system. The only difference is in the small variations of the overshoots of the transient periods and of the settling times. And generally, the longer the fault duration, the higher the peak overshoots of the transients (see Table 4.1 to Table 4.4), and, under this condition, the system is more stressed due to the protracted effect of the fault disturbance.

The control laws, however, have their merits and demerits. As is clear from the waveforms of the system response characteristics, the system rotor angle and speed settle to steady-state values in less than 2.2s or much less under all control laws. CL2 performs better than CL1 and CL3 in terms of damping system oscillations. Under CL2, the rotor angle and speed oscillations died out quickly in less than 1.8s, although their initial peak values are slightly higher. Likewise, the performance of CL3 is better than that of CL1, because it facilitates quicker damping of oscillations. Besides, the performance waveforms of the control laws show CL2 to be faster in reaching a steady constant value (the value under constant excitation) than CL1 and CL3—it settles in about 1.92s, while CL1 and CL3 settle in about 4.32s and 3.32s respectively.

Table 4.1: Peak values and settling times of PSM1 rotor angle and speed closed-loop waveforms for V = 0; X_E = 0.24

Fault cycle	**CL1**				**CL2**			
	δ		**ω**		**δ**		**ω**	
	Peak value(^{o})	Settling time(s)	Peak value(^{o})	Settling time(s)	Peak value(^{o})	Settling time(s)	Peak value(^{o})	Settling time(s)
5	64	1.9	316.8	1.9	62	0.9	317	0.9
7	74	1.76	318	1.76	75	0.86	318	0.86
9	87	1.92	318.9	1.82	88	1.72	319	1.12

Table 4.2: Peak values and settling times of PSM2 rotor angle and speed closed-loop waveforms for V= 0; X_E = 0.24

Fault cycle	**CL1**				**CL2**			
	δ		**ω**		**δ**		**ω**	
	Peak value(^{o})	Settling time(s)	Peak value(^{o})	Settling time(s)	Peak value(^{o})	Settling time(s)	Peak value(^{o})	Settling time(s)
5	60	1.7	316.8	1.1	57	0.9	316.9	0.7
7	69	1.36	317.8	1.06	68	0.86	318	0.86
9	81	1.82	318	1.92	82	1.72	319	1.72

Table 4.3: Peak values and settling times of PSM1 rotor angle and speed closed-loop waveforms for V= 0; $X_E = 0$

Fault cycle	CL1				CL2			
	δ		ω		δ		ω	
	Peak value(^{o})	Settling time(s)	Peak value(^{o})	Settling time(s)	Peak value(^{o})	Settling time(s)	Peak value(^{o})	Settling time(s)
5	65	2.1	317	2.1	62	1	317	1.1
7	76	1.86	318	1.86	75	1.06	318	1.06
9	88	2.06	319	1.82	89	1.76	319	1.12

Table 4.4: Peak values and settling times of PSM2 rotor angle and speed closed-loop waveforms for V= 0; $X_E = 0$

Fault cycle	CL1				CL2			
	δ		ω		δ		ω	
	Peak value(^{o})	Settling time(s)	Peak value(^{o})	Settling time(s)	Peak value(^{o})	Settling time(s)	Peak value(^{o})	Settling time(s)
5	61	1.8	316.8	1.9	57	0.9	316.9	0.9
7	71	1.76	317.9	1.86	69	0.86	318	0.86
9	81	1.82	318	1.82	82	1.72	319	1.72

4.4 Summary

The dynamic simulation of PSM1 and PSM2 as representative models of a SMIB system under the action of three different control laws (as presented in Chapter three) has been considered in this chapter. Various rotor angle, rotor speed, and quadrature-axis EMF waveforms are presented when system was subjected to various durations of a short-circuit fault at the infinite bus and the generator terminal. Also, the methods of computing the parameters of the control laws are given. And under the disturbance scenarios provided in the chapter, all the control laws have been shown to perform well, except for fault durations of 14.7 cycles, 15 cycles, and 15.31 cycles in which CL1, CL3, and CL2, respectively, failed to stabilize the system.

CHAPTER FIVE: CONCLUSION

5.0 Summary

Development of three nonlinear control laws for synchronous generator excitation has been carried out in this work, considering illustrative models of a single machine connected to an infinite bus system. Two of these laws are higher-order sliding mode control laws and the third one is a homogeneous finite-time stabilizing control law.

All the three control laws studied in this Thesis show clear improvement in the transient stability of the system being considered, including in damping of oscillations following fault clearance.

The three proposed controllers employ rotor angle and rotor speed deviations obtained from the plant models as manipulative variables to construct a number of control signals, which are tested using dynamic simulations, considering major perturbation (fault) with different durations (fault clearance times).

Furthermore, under these control signals, the low-frequency oscillations in load angle and rotor speed are damped quickly, with all state variables converging to stable steady-state operating points within approximately 1 to 2.2s. The exception here is where control laws CL1 and CL3 fail to stabilize the system as from the fault durations of 14.7 and 15 cycles, respectively.

The studies conducted in this Thesis show that the proposed controllers extend fault critical time of the system being studied, with CL2 offering the longest extension of this time.

5.1 Achievements and Contributions to Knowledge

This section summarizes the main contributions of this study as follows:

i. Improvement of the existing general higher-order sliding mode control structure for synchronous excitation control.

ii. Development of an approximate method of tuning a general higher-order sliding mode control law for synchronous generator excitation control.

iii. Introduction of a new gain parameter, called dilation constant, to the existing homogeneity-based control structure for synchronous generator excitation control.

iv. Establishment of the property that an affine nonlinear excitation control-based power system model exhibits inherent internal dynamics stability—at least marginally.

v. Development of MATLAB tools for calculating the relative degree of any affine nonlinear system and also for testing its exact linearization condition.

vi. Extension of the third-order SMIB model to include an additional term in the rotor speed dynamics. This could offer more accurate representation for power system stability analysis.

5.2 Recommendations for Future Work

i. For practical implementation of the control signals constructed in this Thesis, it is important to adopt a good and stable state-estimating algorithm for obtaining the output function.

ii. Calculation of output function time derivatives required for the complete computation of the control signals should be carried out online using an accurate and very effective differentiator.

iii. Dynamic interactions between the controls developed in this Thesis and other generation unit controls should be investigated.

iv. Investigation of transient stability of larger power systems, especially the Nigerian Power Network, using the control schemes developed in this Thesis should be carried out. For the Nigerian Power Network, this investigation can be conducted if complete manufacturers' data of all generating units are available.

References

Abdel-Magid, Y. L., Abido, M. A., Al-Baiyat, S., & Mantawy, A. H. (Nov. 1999). Simultaneous Stabilization of Multi-machine Power Systems via Genetic Algorithms. *IEEE Trans. Power Systems, 14*(4), 1428-1439.

Albertos, P., & Mareels, I. (2010). *Feedback and Control for Everyone*: Springer-Verlag, Berlin Heidelberg.

Anderson, J. H. (1971). The control of a synchronous machine using optimal control theory. *Proceedings of the IEEE, 59*(1), 25-35. doi: 10.1109/PROC.1971.8086

Arjona, M. A., Escarela-Perez, R., Espinosa-Perez, G., & Alvarez-Ramirez, J. (2009). Validity testing of third-order nonlinear models for synchronous generators. *Electric Power Systems Research*, 79, 953-958.

Anderson, J. H. (1971). The control of a synchronous machine using optimal control theory. *Proceedings of the IEEE, 59*(1), 25-35. doi: 10.1109/PROC.1971.8086

Astrom, K.J., & Wittenmark, B. (1995). *Adaptive Control* (Second ed.): Addison-Wesley.

Atabak, K., & Saeed, S. (2012). Application of Sliding Mode Control in Single Machine Infinite Bus System (SMIB). *Australian Journal of Basic and Applied Sciences, 6*(5), 165-174.

Atherton, D.P. (1981). *Stability of Nonlinear Systems*: John Wiley, New York.

Awelewa, A. A., Samuel, I. A., Abdulkareem, A., & Iyiola, S. O. (Feb. 2013). An Undergraduate Control Tutorial on Root Locus-Based Magnetic Levitation System Stabilization. *International Journal of Engineering & Computer Science IJECS-IJENS, 13*(1), 22-30.

Bhat, S., & Bernstein, D. (2005). Geometric Homogeneity with Applications to Finite Time Stability. *Math. Control, Signals Systems, 17*, 101-127.

Burns, Roland S. (2001). *Advanced Control Engineering*: Butterworth-Heinemann Edition, Woburn.

Chapman, J. W., Ilic, M. D., & King, C. A. (1993). Stabilizing a Multi-machine Power Systems via Decentralized Feedback Linearizing Excitation Control. *IEEE Trans. Power Systems, 8*, 830-838.

Chaturvedi, D. K., & Malik, O. P. (Feb. 2005). Generalized Neuron-Based Adaptive PSS for Multi-machine Environment. *IEEE Trans. P S, 20*(1), 358-366.

Chiang, Hsiao-Dong. (2011). *Direct Methods for Stability Analysis of Electric Power Systems: Theoretical Foundation, BCU Methodologies, and Applications*: John Wiley & Sons, Inc.

Chow, J. H., Wu, F. F., & Momoh, J. A. (2005). *Applied Mathematics for Restructured Electric Power Systems*: Springer.

Colbia-Vega, A., de Leon-Morales, J., Fridman, L., Solas-Pena, O., & Mata-Jimenez, M.T. (2008). Robust excitation control design using sliding-mode technique for multimachine power systems. *Electric Power Systems Research*, 78, 1627-1634.

Concordia, C. (1951). *Synchronous Machines*: John Wiley & Sons.

Dandeno, P. L., Karas, A. N., McClymont, K. R., & Watson, W. (1987). Effect of high-speed rectifier excitation systems on generator stability limits. *IEEE Trans., PAS, 87*, 190-196.

Demello, F. P., & Concordia, Charles. (1969). Concepts of Synchronous Machine Stability as Affected by Excitation Control. *Power Apparatus and Systems, IEEE Transactions on, PAS-88*(4), 316-329. doi: 10.1109/TPAS.1969.292452

Demello, F. P., Hannet, L. N., & Undrill, J. M. (1978). Practical approach to supplementary stabilizing from accelerating power. *IEEE Trans., PAS, 97*, 1515-1522.

Emel'yanov, S.V. (1959). Use of nonlinear correcting devices of switching type to improve the quality of second-order automatic control systems. *Avtomati Telemekh, 20*(7).

Enrico, D. T., Silvio, M. I., & Francesco, T. (2008). Feedback-linearization and feedback-feedforward decentralized control for multimhacine power system. Electric Power System Research, *78*, 382-391.

Espinosa-Perez, G., Alcantar, M. G., & Ramirez, G. G. (1997). Passivity-Based Speed Control of Synchronous Generators. *IEEE International Symposium on Industrial Electronics, 1*, 101-106.

Falkner, C. M., & Hech, B. S. (June 1995). *A Comparison of Nonlinear Controllers on a Single Generator-Infinite Bus Power System.* Paper presented at the Proceedings of the American Control Conference, Seattle, Washington, 1550-1555.

Falkner, C. M., & Heck, B. S. (Dec. 2000). *Design of Passivity-Based Output Feedback Controller for Power System Stabilization*. Paper presented at the Proceeedings of 39th IEEE Conference on Decision and Control, 3063-3068.

Filippov, A.F. (1960). Differential equations with discontinuous right-hand side. *Mathematicheskii Sbornik, 51*(1).

Fitzgerald, A. E., Kingsley, C., & Umans, S. D. (1983). *Electric Machinery* (Fourth ed.): McGraw-Hill, New York, NY.

Furuta, K., & Pan, Y. (1999). Variable structure control of continuous-time system with sliding sector. *Proc. IFAC, World Congress, Beijing*.

Fusco, G., & Russo, M. (July 2012). *Controller Design for Voltage Regulation and Stabilization in Multimachine Power Systems*. Paper presented at the 2012 20th Mediterranean Conference on Control and Automation, Barcelona, Spain.

Gan, D., Qu, Z., & Cai, H. (2000). Multi-machine Power System Excitation Control Design via Theories of Feedback Linearization Control and Nonlinear Robust Control. *International Journal of Systems Science, 31*(4), 519-527.

Garima, A., Lini, M., & Chatterji S. (2014). MATLAB/SIMULINK BASED SIMULATION OF AN HYBRID POWER FLOW CONTROLLER. Proceedings of 2014 Fourth International Conference on Advanced Computing & Communication Technologies, 523-531.

Ghandakly, A. A., & Farhoud, A. M. (1992). A parametric optimized self-tuning regulator for power system stabilizer. *IEEE Trans. PS, 7*(3), 1245-1250.

Ghandakly, A., & Dai, J. J. (Aug. 1992). An Adaptive Synchronous Generator Stabilizer Design by Generalized Multivariable Pole Shifting (GMPS) Technique. *IEEE Trans. Power Systems, 7*(3), 1239-1244.

Ghandakly, A., & P. Kronegger. (Nov. 1987). An Adaptive Time-Optimal Controller for Generating Units Stabilizer Loops. *IEEE Trans. PS, 2*(4), 1085-1090.

Gu, W., & Bollinger, K. E. (Aug. 1989). A Self-tuning Power System Stabilizer for Wide-Range Synchronous Generator Operation. *IEEE Trans. Power Systems, 4*(3), 1191-1198.

Hahn, W. (1963). *Theory and Application of Lyapunov's Direct Method*: Prentice-Hall, Englewood Cliffs, NJ.

Hajagos, L. (July 2003). *An update on power system stabilization via excitation control.* Paper presented at the Power Engineering Society General Meeting, 2003, IEEE.

Handschin, E., Hoffmann, W., Reyer, F., Stephanblome, T., Schlucking, U., Westermann, D., & Ahmed, S. S. (1994). A new method of excitation control based on fuzzy set theory. *Power Systems, IEEE Transactions on, 9*(1), 533-539. doi: 10.1109/59.317569

Huerta, H., Alexander, G. L., & Jose, M.C. (2010). Decentralized sliding mode block control of multimachine power systems. *International Journal of Electrical Power and Energy Systems, 32*, 1-11.

Huerta, H., Alexander, G. L., & Jose, M.C. (2011). Robust multimachine power systems control via high order sliding modes. *Electric Power Systems Research, 81*, 1602-1609.

Hung, J.Y., Gao, W., & Hung, J.C. (Feb. 1993). Variable structure control: a survey. *IEEE Transactions on Industrial Electronics, 40*(1), 2-22.

IEEE PES Working Group Report. (1995). Power System Oscillations, IEEE Special Publication 95-TP-101.

IEEE Standard 1110 (11th November, 2003). IEEE Guide for Synchronous Generator Modeling Practices and Applications in Power System Stability Analyses. IEEE Power Engineering Society, IEEE.

Irvin, E., Barret, J. P., Charcossey, C., & Monville, J. P. (1979). Improving Power Network Stability and Unit Stress with Adaptive Generator Control. *Automatica, 15*, 31-46.

Isidori, A. (1995). *Nonlinear Control Systems: An Introduction* (Third ed.): Springer-Verlag, New York.

Itkis, U. (1976). *Control Systems with Variable Structure*: John Wiley & Sons, New York.

Juan, F.-V., & Gerald, L. (2010). Variable structure control for power systems stabilization. *International Journal of Electrical and Energy Systems, 32*, 101-107.

Kanniah, J., Malik, O. P., & Hope, G. S. (May 1984). Excitation Control of Synchronous Generators using Adaptive Regulators Part I— Theory and Simulation Results. *IEEE Trans. Power Apparatus and Systems, 103*(5), 897-903.

Kasturi, R., & Doraraju, P. (May/June 1970). Relative Dynamic Stability Regions of Power Systems. *IEEE Trans., PAS, 89*, 966-974.

Katende, J., & Awelewa, A. A. (Oct. 2007). *A Sliding Mode Controller for Synchronous Generator Excitation*. Paper presented at the International

Conference and Exhibition on Power and Telecommunications (ICEPT): Deployment of Innovative Energy and Telecommunications Infrastructures for Regional Integration, Lagos, Nigeria, 68-72.

Khalil, H.K. (1996). *Nonlinear Systems* (Second ed.): Prentice-Hall, Englewood Cliffs, NJ.

Khalil, H.K. (2015). *Nonlinear Control* (Global ed.): Pearson Education Ltd., England.

Kimbark, E. W. (1956). *Power System Stability*: Wiley, New York.

Kokotovic, P. V., & Sauer, P. W. (March 1989). Integral Manifold as Tool for Reduced-Order Modeling of Nonlinear Systems: A Synchronous Machine Case Study. *IEEE Trans. Circuits and Systems, 36*(3), 403-410.

Kumar, P. P., Babu, M. R., & Saraswathi (2012). Dynamic Analysis of Single Machine Infinite Bus System using Single Input and Dual Input PSS. *International Electrical Engineering Journal, 3*(2), 632-641.

Kundur, P. (1994). *Power System Stability and Control*: New York: McGraw-Hill.

Kundur, P., & Dandeno, P. L. (July 1983). Implementation of Advanced Generator Models into Power System Stability Programs. *IEEE Trans., PAS, 102*(7), 2047-2054.

Kundur, P., Klein, M., Rogers, G. R., & Zywno, M. S. (May 1989). Application of Power System Stabilizers for Enhancement of Overall System Stability. *IEEE Trans., Power Systems, 4*(2), 614-626.

Kundur, P., Paserba, J., Ajjarapu, V., Andersson, G., Bose, A., Canizares, C., Vittal, V. (2004). Definition and classification of power system stability

IEEE/CIGRE joint task force on stability terms and definitions. *Power Systems, IEEE Transactions on, 19*(3), 1387-1401. doi: 10.1109/TPWRS.2004.825981

Larsen, E. V., & Swann, D. A. (1981). Applying Power System Stabilizers. *IEEE Trans., PAS, 100*(6), 3017-3046.

Levant, A. (2001). Universal SISO Sliding Mode Controllers with Finite-Time Convergence. *IEEE Trans. Automatic Control, 46*(9), 1447-1451.

Levant, A. (2005). Homogeneity approach to high-order sliding mode design. *Automatica, 41*, 823-830.

Li-Jun, C., & Erlich, I. (Feb. 2005). Simultaneous Coordinated Tuning of PSS and FACTS Damping Controllers in Large Power Systems. *IEEE Trans. Power Systems, 20*(1).

Li, X., & Caizares, C. A. (June 28-July 2 2009). *Chaotic behavior observations in a power system model.* Paper presented at the PowerTech, 2009 IEEE Bucharest.

Lim, C. M., & Elangovan, S. (May 1985). Design of Stabilizers in Multi-machine Power Systems. *Proc. IEE, 132*(3), 146-153.

Lin, C.F. (1964). *Advanced Control Systems Design*: Prentice-Hall, Englewood Cliffs, NJ.

Lu, Q., Mei, S., Hu, W., Song, Y. H., Goto, M., & Konishi, H. (2000a). Decentralised nonlinear H∞ excitation control based on regulation linearisation. *Generation, Transmission and Distribution, IEE Proceedings-, 147*(4), 245-251. doi: 10.1049/ip-gtd:20000441

Lu, Q., Mei, S., Shen, T., & Hu, W. (2000b). Recursive Design of Nonlinear H∞ Excitation Controller. *Science in China, 43*(1), 23-31.

Lu, Q., Sun, Y., & Mei, S. (2001). *Nonlinear Control Systems and Power System Dynamics*: Kluwer Academic Publisher.

Lu, Q., & Xu, Z. (Nov. 1996). Decentralized Nonlinear Optimal Excitation Control. *IEEE Trans. Power Systems, 11*(4), 1957-1962.

Lu, Q., Sun, Y., & Lee, G. K. F. (1989). Nonlinear Optimal Excitation Control For Multimachine Systems. In A. J. Calvaer (Ed.), *Power Systems: Modelling and Control Applications* (pp. 27-32). Oxford: Pergamon.

Mahmud, M. A., Hossain, M. J., Pota, H. R., & Ali, M. S. (Sep. 2011). *Generalized Lyapunov Function for Stability Analysis of Interconnected Power Systems*. Paper presented at the Universities Power Engineering Conference (AUPEC), 2011 21st Australasian.

Mahmud, M. A., Hossain, M. J., & Pota, H. R. (November 2011). Selection Output Function in Nonlinear Feedback Linearizing Excitation Control for Power Systems. 2011 Ausralian Control Conference, Melboune, Australia.

Mariani, E., & Murthy, S. S. (1997). *Control of Modern Integrated Power Systems: Advances in Industrial Control*: Springer-Verlag London Limited.

McCulloch, W.S., & Pitts, W.H. (1943). A Logical Calculus of Ideas Immanent in Nervous Activity. *Bulletin of Mathematical Biophysics, 5*, 115-133.

Mielczarski, W., & Zajaczkowjki, A. M. (1994). Nonlinear Field Voltage Control of a Synchronous Generator using Feedback Linearization. *Automatica, 30*, 1625-1630.

Mohler, R.R. (1994). *Nonlinear Systems: Dynamics and Control* (Vol. 1): Prentice-Hall, Englewood Cliffs, NJ.

Mukhopadhyay, B. K., & Malik, M. F. (1972). Optimal Control of Synchronous Machine Excitation by Quasilinearization Techniques. *IEEE Proceedings, 119*(1), 91-98.

Nagrath, I. J., & Kothari, D. P. (2003). *Power System Engineering* McGraw-Hill, New Delhi, India.

Nagrath, I.J., & Gopal, M. (2007). *Control Systems Engineering* (Fifth ed.): New Age International Publishers.

Nambu, M., & Ohsawa, Y. (1996). Development of an Advanced Power System Stabilizer using a Strict Linearization Approach. *IEEE Trans. Power Systems, 11*, 813-818.

Nandam, P. K., & Sen, P. C. (1995). Industrial applications of sliding mode control. *Proc. IEEE/IAS International Conference on Industrial Automation and Control*, 275-280.

Nargsarkar, T.K., & Sukhija, M.S. (2007). *Power System Analysis*: Oxford University Press.

Ogata, Katsuhiko. (1997). *Modern Control Engineering* (Third ed.): Prentice Hall, Upper Saddle River, New Jersey.

Ortega, R., Galaz, M., Astolfi, A., Yuanzhang, Sun, & Shen, T. (2005). Transient stabilization of multimachine power systems with nontrivial transfer conductances. *Automatic Control, IEEE Transactions on, 50*(1), 60-75. doi: 10.1109/TAC.2004.840477

Pierre, D. A. (May 1987). A Perspective on Adaptive Control of Power Systems. *IEEE Trans. Power Systems, Power Systems (PWRS)-2*(2), 387-396.

Ping, Z., Jiebin, Z., Zhenxing, L., Wei, Y., Shaorong, W. (2014). Design of a Nonlinear Excitation Controller using Synergetic Control Theory. *IEEE(978-1-4799-7537-2/14)*.

Pogromsky, A., Fradkov, A., & Hill, D. (Dec. 1996). *Passivity-Based Damping of Power System Oscillations*. IEEE Decision & Control Conference, 3876-3881.

Pouyan, P., Kundur, P. S., & Taylor, C. W. (September/October 2006). *The Anatomy of a Power Grid Blackout*. IEEE Power and Energy Magzine, 22-29.

Ravel, G., Alonso, D. M., & Moiola, J. L. (2008). Bifurcation Theory Applied to the Analysis of Power Systems. *Union Mathematical Argentina, 49*(1), 1-14.

Roberts, J., & Ian, A. (1997). Lyapunov Functions for Multi-machine Power Systems with Dynamic Loads. *IEEE Trans. Circuits and Systems, 44*(9), 796-812.

Rui, Y., Zhao, Y. D., Saha, T. K., & Rajat, M. (2010). A power system nonlinear adaptive decentralized controller design. *Automatica, 46*, 330-336.

Samarasinghe, V. G. D. C., & Pahalawatha, N. C. (July 1994). Design of Universal Variable Structure Controller for Dynamic Stabilization of Power Systems. *IEE Proceedings on Generation, Transmission, and Distribution, 141*(4), 363-368.

Sauer, P. W., Ahmed-Zaid, S., & Kokotovic, P. V. (1988). An Integral Manifold Approach to Reduced-Order Dynamic Modeling of Synchronous Machines. *IEEE Trans. Power Systems, 3*(1), 17-23.

Shuji, C., Jiang, L., Yao, W., & Wu, Q. H. (2014). Application of Switched System Theory in Power System Stability. *IEEE (978-1-4799-6557-1/14)*.

Slotine, Jean-Jacques E., & Li, Weiping. (1991). *Applied Nonlinear Control*: Prentice Hall, Eaglewood Cliffs, New Jessey.

Sun, Y., & Lu, Q. (1996). *Decentralized Excitation Control by Feedback Linearization.* Paper presented at the Proceedings of the IEEE Winter Meeting, Baltimas, Maryland, USA.

Takagi, T., & Sugeno, M. (1985). Fuzzy Identification of System and its Applications to Modeling and Control. *IEEE Transaction on Systems, Man, & Cybernetics, 15*, 116-132.

Unsal, C., & Kachroo, P. (March 1999). Sliding mode measurement feedback control for antilock braking systems. *IEEE Transactions on Control Systems Technology, 7*(2), 271-281.

Utkin, V. I. (1993). Sliding mode control design principles and applications to electric drives. *IEEE Transactions on Industrial Electronics, 40*(1), 23-36.

Utkin, V.I. (1992). *Sliding Modes in Control Optimization*: Springer, Berlin Heidelberg.

Venkatesh, G., & Rao, P. K. (October 2012). Improvement of Dynamic Stability of a Single Machine Infinite-Bus Power System using Fuzzy Logic based Power System Stabilizer. *International Journal of Engineering Research and Development, 4*(5), 60-70.

Wu, C. J., & Hsu, Y. Y. (Aug. 1988). Design of Self-tuning PID Power System Stabilizer for Multi-machine Power Systems. *IEEE Trans. Power Systems, 3*(3), 1059-1064.

Yee, S. K., & Milanovic, J. V. (Aug. 2008). Fuzzy Logic Controller for Decentralized Stabilization of Multi-machine Power Systems. *IEEE Trans. Fuzzy Systems, 16*(4), 971-981.

Ying, H. (2000). *Fuzzy Control and Modeling: Analytical Foundations and Applications*: IEEE Press.

Yoerger, D.R., Newman, J.B., & Slotine, J.-J. E. (1986). Supervisory control system for the JASON ROV. *IEEE J. Oceanic Eng, 11*(3), 392-400.

Yu, Y. N., & Moussa, H. A. M. (May/June 1972). Optimal Stabilization of a Multi-machine System. *IEEE Trans., PAS*, 1114-1182.

Yu, Yao-nan, Vongsuriya, K., & Wedman, L. N. (1970). Application of an Optimal Control Theory to a Power System. *Power Apparatus and Systems, IEEE Transactions on, PAS-89*(1), 55-62. doi: 10.1109/TPAS.1970.292668.

Yun, L., Kiam, H. A., & Gregory, C. Y. C. (February 2006). Patents, Software, and Hardware for PID Control: An Overview and Analysis of the Current Art. *IEEE Control Systems Magzine*, 42-54.

Zadeh, L.A. (1973). Outline of a New Approach of Complex Systems and Decision Processes. *IEEE Transaction on Systems, Man, & Cybernetics, 3*, 28-44.

Zhang, Y., Chen, G. P., Malik, O. P., & Hope, G. S. (1995). Artificial Neural Network Power System Stabilizer in Multi-machine Power System Environment. *IEEE Trans. Energy Conversion, 10*(1), 147-155.

Zhang, Y., Chen, G. P., Malik, O. P., & Hope, G. S. (March 1993). An Artificial Neural Network-Based Adaptive Power System Stabilizer. *IEEE Trans. Energy Conversion, 8*(1), 71-77.

Zhang, Y., Chen, G. P., Malik, O. P., & Hope, G. S. (May 1993). *A multi-input Power System Stabilizer Based on Artificial Neural Networks*. Paper presented at the Proceedings IEEE WESCANEX93, Saskatoon, SK, Canada.

Appendix A: Damper Winding Manifold Approximation

A.1 α^2 Approximation

To find G_0 and G_1 in equations (3.32) and (3.33), equation (3.31) is modified as

$$\alpha\frac{\partial(G_0+G_1\alpha)}{\partial\delta}\frac{d\delta}{dt}+\alpha\frac{\partial(G_0+G_1\alpha)}{\partial\omega}\frac{d\omega}{dt}+\alpha\frac{\partial(G_0+G_1\alpha)}{\partial E'_q}\frac{dE'_q}{dt}$$

$$=-E_1(G_0+G_1\alpha)+E_2V\sin\delta. \qquad (A.1)$$

The corresponding coefficients of α^0 and α^1on both sides of equation (A.1) are equated respectively as follows:

$$\alpha^0:\quad 0=-E_1G_0+E_2V\sin\delta \qquad (A.2)$$

$$\therefore G_0=\frac{E_2}{E_1}V\sin\delta.$$

$$\alpha^1:\quad \frac{\partial(G_0)}{\partial\delta}\frac{d\delta}{dt}+\frac{\partial(G_0)}{\partial\omega}\frac{d\omega}{dt}+\frac{\partial(G_0)}{\partial E'_q}\frac{dE'_q}{dt}=-E_1G_1 \qquad (A.3)$$

$$\left(\frac{E_2}{E_1}V\cos\delta\right)(\omega-\omega_s)+(0)\frac{d\omega}{dt}+(0)\frac{dE'_q}{dt}=-E_1G_1$$

$$\therefore G_1=-\left(\frac{E_2}{E_1^2}V\cos\delta\right)(\omega-\omega_s)$$

A.2 α^3 Approximation

To find H_2, equation (A.1) is rewritten as

$$\alpha\frac{\partial(G_0+G_1\alpha+G_2\alpha^2)}{\partial\delta}\frac{d\delta}{dt}+\alpha\frac{\partial(G_0+G_1\alpha+G_2\alpha^2)}{\partial\omega}\frac{d\omega}{dt}+\alpha\frac{\partial(G_0+G_1\alpha+G_2\alpha^2)}{\partial E'_q}\frac{dE'_q}{dt}$$

$$=-E_1(G_0+G_1\alpha+G_2\alpha^2)+E_2V\sin\delta \qquad (A.4)$$

or

$$\frac{\partial(\alpha G_0+G_1\alpha^2+G_2\alpha^3)}{\partial\delta}\frac{d\delta}{dt}+\frac{\partial(G_1\alpha^2+G_2\alpha^3)}{\partial\omega}\frac{d\omega}{dt}+\frac{\partial(G_2\alpha^3)}{\partial E'_q}\frac{dE'_q}{dt}$$

$$=-E_1G_0+E_2V\sin\delta-E_1G_1\alpha-E_1G_2\alpha^2 \qquad (A.5)$$

since $\frac{\partial(G_0)}{\partial\omega}=\frac{\partial(G_0)}{\partial E'_q}=\frac{\partial(G_1)}{\partial E'_q}=0.$

The second term in equation (A.5) can be expanded to give

$$\frac{\partial(G_1\alpha^2+G_2\alpha^3)}{\partial\omega}\frac{d\omega}{dt}=\frac{\partial(G_1\alpha^2+G_2\alpha^3)}{\partial\omega}(A_1-\frac{1}{2}A_2V^2\sin2\delta+A_3VE'_d\cos\delta-$$

$$A_4VE'_q\sin\delta)$$

or

$$\frac{\partial(G_1\alpha^2+G_2\alpha^3)}{\partial\omega}\frac{d\omega}{dt}=\frac{\partial(G_1\alpha^2+G_2\alpha^3)}{\partial\omega}\Big(A_1-\frac{1}{2}A_2V^2\sin2\delta+A_3V\cos\delta(G_0+$$

$$G_1\alpha+G_2\alpha^2)-A_4VE'_q\sin\delta\Big) \qquad (A.6)$$

Substituting equation (A.6) into equation (A.5) and comparing coefficients of α^2on both sides of the resulting equation leads to

$$\frac{\partial(G_1)}{\partial\delta}(\omega-\omega_2)+\frac{\partial(G_1)}{\partial\omega}\Big(A_1-\frac{1}{2}A_2V^2\sin2\delta-A_4VE'_q\sin\delta+G_0A_3V\cos\delta\Big)=$$

$$-E_1G_2. \qquad (A.7)$$

Hence,

$$G_2=-\frac{1}{E_1}\frac{\partial(G_1)}{\partial\delta}(\omega-\omega_2)-\frac{1}{E_1}\frac{\partial(G_1)}{\partial\omega}\Big(A_1-\frac{1}{2}A_2V^2\sin2\delta-A_4VE'_q\sin\delta+$$

$$G_0A_3V\cos\delta\Big)=G_2^1+G_2^2. \qquad (A.8)$$

where

$$G_2^1=-\frac{1}{E_1}\Big(\frac{E_2}{E_1^2}V\sin\delta\Big)(\omega-\omega_s)^2$$

$$G_2^2=\frac{1}{E_1}\frac{E_2}{E_1^2}V\cos\delta\Big(A_1-\frac{1}{2}A_2V^2\sin2\delta-A_4VE'_q\sin\delta+A_3F_1V^2\sin\delta\cos\delta\Big)$$

The expression for E'_d is now obtained from equation (A.9), and is given in equation (3.36).

$$E'_d=G_0+G_1\alpha+G_2\alpha^2 \qquad (A.9)$$

Also, the expression in equation (3.43) can be obtained by substituting equation (3.36) into equation (3.17) as follows:

$$\frac{d\omega}{dt} = A_1 - \frac{1}{2}A_2V^2\sin 2\delta - A_4VE'_q\sin\delta + A_3V\cos\delta\left\{F_1V\sin\delta - \alpha\frac{F_1}{E_1}V(\omega - \omega_s)\cos\delta - \alpha^2\frac{F_1}{E_1^2}(\omega - \omega_s)^2V\sin\delta + \alpha^2\frac{F_1}{E_1^2}V\cos\delta\left[T_1 + A_3F_1V^2\sin\delta\cos\delta - A_4VE'_q\sin\delta\right]\right\} \quad (A.10)$$

By ignoring all terms in α^2 except those that are proportional to $(\omega - \omega_s)^2$, equation (A.10) can be rearranged to give equation (3.43).

Appendix B: Algorithm for Output Function Derivation

The algorithm for deriving the output function that guarantees r = n for a SISO nonlinear system is as follows:

Consider a general nonlinear SISO system defined as

$$\dot{x} = \mathrm{f}(x) + \mathrm{g}(x)\mathrm{u}. \tag{B.1}$$

The following are the steps for finding an output function that makes r equal to n.

Step 1:Create the set

$$\mathrm{S} = \left\{\mathrm{g}(x), \mathrm{ad_f g}(x), \mathrm{ad_f^2 g}(x), \cdots, \mathrm{ad_f^{n-1} g}(x)\right\}, \tag{B.2}$$

and establish the subsets S_1, S_2, …, S_n, where S_i is composed of the first i elements of S. That is,

$$\mathrm{S_1} = \{\mathrm{g}(x)\},$$

$$\mathrm{S_2} = \{\mathrm{g}(x), \mathrm{ad_f g}(x)\},$$

$$\mathrm{S_3} = \left\{\mathrm{g}(x), \mathrm{ad_f g}(x), \mathrm{ad_f^2 g}(x)\right\},$$

$$\vdots$$

$$\mathrm{S_n} = \left\{\mathrm{g}(x), \mathrm{ad_f g}(x), \mathrm{ad_f^2 g}(x), \cdots, \mathrm{ad_f^{n-1} g}(x)\right\}. \tag{B.3}$$

The elements of S in equation (B.2) are determined appropriately.

Step 2:Find the vectors $\bar{\mathrm{S}}_1, \bar{\mathrm{S}}_2, \cdots, \bar{\mathrm{S}}_n$. $\bar{\mathrm{S}}_i$ and all the elements of S_i are linearly dependent. In other words, $\bar{\mathrm{S}}_i$ represents a linear combination of the elements of S_i. This can be mathematically expressed as

$$\bar{\mathrm{S}}_1 + \alpha_{11}(x)\mathrm{g}(x) = 0,$$

$$\bar{\mathrm{S}}_2 + \alpha_{21}\mathrm{g}(x) + \alpha_{22}\mathrm{ad_f g}(x) = 0,$$

$$\bar{\mathrm{S}}_3 + \alpha_{31}\mathrm{g}(x) + \alpha_{32}\mathrm{ad_f g}(x) + \alpha_{33}\mathrm{ad_f^2 g}(x) = 0,$$

$$\vdots$$

$$\bar{S}_n + \alpha_{n1} g(x) + \alpha_{n2} ad_f g(x) + \cdots + \alpha_{nn} ad_f^{n-1} g(x) = 0. \quad (B.4)$$

Step 3: Obtain the transformation function X = P(V) by finding the integral curve

$$P(v_1, v_2, \cdots, v_n) = \Phi_{v_1}^{\bar{S}_1} \circ \Phi_{v_2}^{\bar{S}_2} \circ \cdots \circ \Phi_{v_n}^{\bar{S}_n}(X_0). \quad (B.5)$$

This is done by computing sequentially

$$\Phi_{v_n}^{\bar{S}_n}(X_0) \Rightarrow \frac{d}{dv_n}\begin{pmatrix} x_1 \\ x_2 \\ \vdots \\ x_n \end{pmatrix} = \bar{S}_n: \quad \begin{pmatrix} x_1(0) \\ x_2(0) \\ \vdots \\ x_n(0) \end{pmatrix} = X_0,$$

$$\Phi_{v_{n-1}}^{\bar{S}_{n-1}} \circ \Phi_{v_n}^{\bar{S}_n}(X_0) \Rightarrow \frac{d}{dv_{n-1}}\begin{pmatrix} x_1 \\ x_2 \\ \vdots \\ x_n \end{pmatrix} = \bar{S}_{n-1}: \quad \begin{pmatrix} x_1(0) \\ x_2(0) \\ \vdots \\ x_n(0) \end{pmatrix} = \Phi_{v_n}^{\bar{S}_n}(X_0),$$

$$\vdots$$

$$\Phi_{v_1}^{\bar{S}_1} \circ \Phi_{v_2}^{\bar{S}_2} \circ \cdots \circ \Phi_{v_n}^{\bar{S}_n}(X_0) \Rightarrow \frac{d}{dv_1}\begin{pmatrix} x_1 \\ x_2 \\ \vdots \\ x_n \end{pmatrix} = \bar{S}_1: \begin{pmatrix} x_1(0) \\ x_2(0) \\ \vdots \\ x_n(0) \end{pmatrix} = \Phi_{v_2}^{\bar{S}_2} \circ \cdots \circ \Phi_{v_n}^{\bar{S}_n}(X_0).$$

The result of Step 3 gives

$$\begin{pmatrix} x_1 \\ x_2 \\ \vdots \\ x_n \end{pmatrix} = \begin{pmatrix} P_1(v_1, v_2, \cdots, v_n) \\ P_2(v_1, v_2, \cdots, v_n) \\ \vdots \\ P_n(v_1, v_2, \cdots, v_n) \end{pmatrix},$$

from which the inverse function

$$\begin{pmatrix} v_1 \\ v_2 \\ \vdots \\ v_n \end{pmatrix} = \begin{pmatrix} P_1^{-1}(x_1, x_2, \cdots, x_n) \\ P_2^{-1}(x_1, x_2, \cdots, x_n) \\ \vdots \\ P_n^{-1}(x_1, x_2, \cdots, x_n) \end{pmatrix}$$

could be found. v_n is actually the function being sought for. The procedure in Step 4 validates this function.

Step 4: Determine new function vectors $\hat{f}(x)$ and $\hat{g}(x)$:

$$\hat{f}(x) = J_{T_{n-1}} f(x) = \begin{pmatrix} \hat{f}_1(x) \\ \hat{f}_2(x) \\ \vdots \\ \hat{f}_n(x) \end{pmatrix} \tag{B.6}$$

$$\hat{g}(x) = J_{T_{n-1}} g(x) = \begin{pmatrix} \hat{g}_1(x) \\ 0 \\ \vdots \\ 0 \end{pmatrix} = \tag{B.7}$$

where T_{n-1} denotes the transformation

$$z_1^{(n-1)} = f_2^{(n-2)}\Big|_{V=P^{-1}(X)}$$

$$z_2^{(n-1)} = f_3^{(n-2)}\Big|_{V=P^{-1}(X)}$$

$$\vdots$$

$$z_n^{(n-1)} = v_n|_{V=P^{-1}(X)}$$

and

$$f^{(n-1)}(v) = J_{T_{n-2}} f^{(n-1)}(v).$$

$T_1, T_2, \ldots, T_{n-2}$ and $f^0, f^1, \ldots, f^{n-2}$ are required to obtain the transformation T_{n-1}. The starting point is the calculation of the pair (f^0, T_1) given by

$$f^{(0)}(v) = J_{P^{-1}} f(x)|_{X=P(V)} = \begin{pmatrix} f_1^{(0)}(v) \\ f_2^{(0)}(v) \\ \vdots \\ f_n^{(0)}(v) \end{pmatrix};$$

T_1:

$$z_1^{(1)} = f_2^{(0)}(v)$$

$$z_2^{(1)} = f_3^{(0)}(v)$$

$$\vdots$$

$$z_n^{(1)} = v_n$$

The form of equation (B.7) is very important, as it determines whether these steps indeed produce exact linearization results—or whether this algorithm has 'converged' (so to speak).

Application of this algorithm to the fourth-order model, rewritten as equation (B.8), is given below.

$$\underbrace{\begin{pmatrix}\dot{x}_1\\ \dot{x}_2\\ \dot{x}_3\\ \dot{x}_4\end{pmatrix}}_{\dot{x}} = \underbrace{\begin{pmatrix} -\frac{\mathrm{E}_1}{\mathrm{T}'_{\mathrm{qo}}}x_1 + \frac{\mathrm{E}_2}{\mathrm{T}'_{\mathrm{qo}}}\mathrm{V}\sin x_4 \\ -\mathrm{B}_1 x_2 + \mathrm{B}_2 \mathrm{V}\cos x_4 \\ \mathrm{A}_1 - \frac{1}{2}\mathrm{A}_2\mathrm{V}^2\sin 2x_4 - \mathrm{A}_4\mathrm{V}x_2\sin x_4 + \mathrm{A}_3\mathrm{V}x_1\cos x_4 \\ x_3 - \omega_{\mathrm{s}}\end{pmatrix}}_{f(x)} + \underbrace{\begin{pmatrix}0\\ \frac{1}{T'_{do}}\\ 0\\ 0\end{pmatrix}}_{g(x)} \qquad (\mathrm{B}.8)$$

Step 1:

$\mathrm{S} = \{\mathrm{g}(x), \mathrm{ad_f g}(x), \mathrm{ad_f^2 g}(x), \mathrm{ad_f^3 g}(x)\}$.

Therefore,

$\mathrm{S}_1 = \{\mathrm{g}(x)\}$;

$\mathrm{S}_2 = \{\mathrm{g}(x), \mathrm{ad_f g}(x)\}$;

$\mathrm{S}_3 = \{\mathrm{g}(x), \mathrm{ad_f g}(x), \mathrm{ad_f^2 g}(x)\}$;

$\mathrm{S}_4 = \{\mathrm{g}(x), \mathrm{ad_f g}(x), \mathrm{ad_f^2 g}(x), \mathrm{ad_f^3 g}(x)\}$.

All elements of S are found in the following.

$$\mathrm{g}(x) = \begin{pmatrix}0\\ \frac{1}{T'_{do}}\\ 0\\ 0\end{pmatrix};$$

$$\mathrm{ad_f g}(x) = \begin{pmatrix} 0 \\ \frac{\mathrm{B_1}}{T'_{do}} \\ \frac{\mathrm{A_4 V}}{T'_{do}} \sin x_4 \\ 0 \end{pmatrix};$$

$$\mathrm{ad_f^2 g}(x) = \begin{pmatrix} 0 \\ \frac{B_1^2}{T'_{do}} \\ \frac{\mathrm{A_4 V}}{T'_{do}} \cos x_4 (x_3 - \omega_s) + \frac{\mathrm{B_1}}{T'_{do}} \mathrm{A_4 V} \sin x_4 \\ -\frac{\mathrm{A_4 V}}{T'_{do}} \sin x_4 \end{pmatrix};$$

$$\mathrm{ad_f^3 g}(x) = \begin{pmatrix} \frac{\mathrm{E_2 A_4 V^2}}{2T'_{qo}T'_{do}} \sin 2x_4 \\ \frac{B_1^3}{T'_{do}} - \frac{\mathrm{B_2 A_4 V^2}}{T'_{do}} \sin^2 x_4 \\ \mathrm{S(3,4)} \\ -2\frac{\mathrm{A_4 V}}{T'_{do}} \cos x_4 (x_3 - \omega_s) - \frac{\mathrm{B_1 A_4 V}}{T'_{do}} \sin x_4 \end{pmatrix};$$

where

$$\mathrm{S(3,4)} = \frac{\mathrm{A_4 V}}{T'_{do}} [\mathrm{A_1} \cos x_4 + B_1^2 \sin x_4 + \mathrm{A_3 V} x_1 \cos 2x_4 - \mathrm{A_4 V} x_2 \sin 2x_4 -$$

$$\frac{\mathrm{A_2 V^2}}{4} \sin 2x_4 - \mathrm{A_2 V^2} \cos 2x_4 \sin x_4 - \sin x_4 (x_3 - \omega_s)^2 +$$

$$\mathrm{B_1} \cos x_4 (x_3 - \omega_s)].$$

Step 2:

$$\bar{\mathrm{S}}_1 + \alpha_{11} \begin{pmatrix} 0 \\ \frac{1}{T'_{do}} \\ 0 \\ 0 \end{pmatrix} = \begin{pmatrix} 0 \\ 0 \\ 0 \\ 0 \end{pmatrix},$$

$$\bar{\mathrm{S}}_2 + \alpha_{21} \begin{pmatrix} 0 \\ \frac{1}{T'_{do}} \\ 0 \\ 0 \end{pmatrix} + \alpha_{22} \begin{pmatrix} 0 \\ \frac{\mathrm{B_1}}{T'_{do}} \\ \frac{\mathrm{A_4 V}}{T'_{do}} \sin x_4 \\ 0 \end{pmatrix} = \begin{pmatrix} 0 \\ 0 \\ 0 \\ 0 \end{pmatrix},$$

$$\bar{S}_3 + \alpha_{31}\begin{pmatrix} 0 \\ \frac{1}{T'_{do}} \\ 0 \\ 0 \end{pmatrix} + \alpha_{32}\begin{pmatrix} 0 \\ \frac{B_1}{T'_{do}} \\ \frac{A_4 V}{T'_{do}}\sin x_4 \\ 0 \end{pmatrix} +$$

$$\alpha_{33}\begin{pmatrix} 0 \\ \frac{B_1^2}{T'_{do}} \\ \frac{A_4 V}{T'_{do}}\cos x_4(x_3 - \omega_s) + \frac{B_1}{T'_{do}}A_4 V\sin x_4 \\ -\frac{A_4 V}{T'_{do}}\sin x_4 \end{pmatrix} = \begin{pmatrix} 0 \\ 0 \\ 0 \\ 0 \end{pmatrix},$$

$$\bar{S}_4 + \alpha_{41}\begin{pmatrix} 0 \\ \frac{1}{T'_{do}} \\ 0 \\ 0 \end{pmatrix} + \alpha_{42}\begin{pmatrix} 0 \\ \frac{B_1}{T'_{do}} \\ \frac{A_4 V}{T'_{do}}\sin x_4 \\ 0 \end{pmatrix} +$$

$$\alpha_{43}\begin{pmatrix} 0 \\ \frac{B_1^2}{T'_{do}} \\ \frac{A_4 V}{T'_{do}}\cos x_4(x_3 - \omega_s) + \frac{B_1}{T'_{do}}A_4 V\sin x_4 \\ -\frac{A_4 V}{T'_{do}}\sin x_4 \end{pmatrix} +$$

$$\alpha_{44}\begin{pmatrix} \frac{E_2 A_4 V^2}{2T'_{qo}T'_{do}}\sin 2x_4 \\ \frac{B_1^3}{T'_{do}} - \frac{B_2 A_4 V^2}{T'_{do}}\sin^2 x_4 \\ S(3,4) \\ -2\frac{A_4 V}{T'_{do}}\cos x_4(x_3 - \omega_s) - \frac{B_1 A_4 V}{T'_{do}}\sin x_4 \end{pmatrix} = \begin{pmatrix} 0 \\ 0 \\ 0 \\ 0 \end{pmatrix}$$

The values of vectors $\bar{S}_1, \bar{S}_2, \bar{S}_3, \bar{S}_4$ are found without much difficulty from the above expressions, and are given as

$$\bar{S}_1 = \begin{pmatrix} 0 \\ 1 \\ 0 \\ 0 \end{pmatrix}; \bar{S}_2 = \begin{pmatrix} 0 \\ 0 \\ 1 \\ 0 \end{pmatrix}; \bar{S}_3 = \begin{pmatrix} 0 \\ 0 \\ 0 \\ 1 \end{pmatrix}; \bar{S}_4 = \begin{pmatrix} 1 \\ 0 \\ 0 \\ 0 \end{pmatrix}.$$

Step 4:

$$P(v_1, v_2, \cdots, v_n) = \Phi_{v_1}^{\bar{S}_1} \circ \Phi_{v_2}^{\bar{S}_2} \circ \Phi_{v_3}^{\bar{S}_3} \circ \Phi_{v_4}^{\bar{S}_4}(X_0).$$

$$\Phi_{v_4}^{\bar{S}_4}(X_0) \Rightarrow \frac{d}{dv_4}\begin{pmatrix} x_1 \\ x_2 \\ x_3 \\ x_4 \end{pmatrix} = \begin{pmatrix} 1 \\ 0 \\ 0 \end{pmatrix}: \quad \begin{pmatrix} x_1(0) \\ x_2(0) \\ x_3(0) \\ x_4(0) \end{pmatrix} = \begin{pmatrix} E'_{d0} \\ E'_{q0} \\ \omega_0 \\ \delta_0 \end{pmatrix}$$

$$\therefore \begin{pmatrix} x_1 \\ x_2 \\ x_3 \\ x_4 \end{pmatrix} = \begin{pmatrix} E'_{d0} + v_4 \\ E'_{q0} \\ \omega_0 \\ \delta_0 \end{pmatrix}.$$

$$\Phi_{v_3}^{\bar{S}_3} \circ \Phi_{v_4}^{\bar{S}_4}(X_0) \Rightarrow \frac{d}{dv_3}\begin{pmatrix} x_1 \\ x_2 \\ x_3 \\ x_4 \end{pmatrix} = \begin{pmatrix} 0 \\ 0 \\ 0 \\ 1 \end{pmatrix}: \quad \begin{pmatrix} x_1(0) \\ x_2(0) \\ x_3(0) \\ x_4(0) \end{pmatrix} = \begin{pmatrix} E'_{d0} + v_4 \\ E'_{q0} \\ \omega_0 \\ \delta_0 \end{pmatrix}$$

$$\therefore \begin{pmatrix} x_1 \\ x_2 \\ x_3 \\ x_4 \end{pmatrix} = \begin{pmatrix} E'_{d0} + v_4 \\ E'_{q0} \\ \omega_0 \\ \delta_0 + v_3 \end{pmatrix}.$$

$$\Phi_{v_2}^{\bar{S}_2} \circ \Phi_{v_3}^{\bar{S}_3} \circ \Phi_{v_4}^{\bar{S}_4}(X_0) \Rightarrow \frac{d}{dv_2}\begin{pmatrix} x_1 \\ x_2 \\ x_3 \\ x_4 \end{pmatrix} = \begin{pmatrix} 0 \\ 0 \\ 1 \\ 0 \end{pmatrix}: \begin{pmatrix} x_1(0) \\ x_2(0) \\ x_3(0) \\ x_4(0) \end{pmatrix} = \begin{pmatrix} E'_{d0} + v_4 \\ E'_{q0} \\ \omega_0 \\ \delta_0 + v_3 \end{pmatrix}$$

$$\therefore \begin{pmatrix} x_1 \\ x_2 \\ x_3 \\ x_4 \end{pmatrix} = \begin{pmatrix} E'_{d0} + v_4 \\ E'_{q0} \\ \omega_0 + v_2 \\ \delta_0 + v_3 \end{pmatrix}.$$

$$\Phi_{v_1}^{\bar{S}_1} \circ \Phi_{v_2}^{\bar{S}_2} \circ \Phi_{v_3}^{\bar{S}_3} \circ \Phi_{v_4}^{\bar{S}_4}(X_0) \Rightarrow \frac{d}{dv_1}\begin{pmatrix} x_1 \\ x_2 \\ x_3 \\ x_4 \end{pmatrix} = \begin{pmatrix} 0 \\ 1 \\ 0 \\ 0 \end{pmatrix}: \begin{pmatrix} x_1(0) \\ x_2(0) \\ x_3(0) \\ x_4(0) \end{pmatrix} = \begin{pmatrix} E'_{d0} + v_4 \\ E'_{q0} \\ \omega_0 + v_2 \\ \delta_0 + v_3 \end{pmatrix}$$

$$\therefore \begin{pmatrix} x_1 \\ x_2 \\ x_3 \\ x_4 \end{pmatrix} = \begin{pmatrix} E'_{d0} + v_4 \\ E'_{q0} + v_1 \\ \omega_0 + v_2 \\ \delta_0 + v_3 \end{pmatrix}.$$

Thus,

$$\begin{pmatrix} x_1 \\ x_2 \\ x_3 \\ x_4 \end{pmatrix} = \begin{pmatrix} \mathrm{P}_1(\mathrm{v}_1, \mathrm{v}_2, \mathrm{v}_3, \mathrm{v}_4) \\ \mathrm{P}_2(\mathrm{v}_1, \mathrm{v}_2, \mathrm{v}_3, \mathrm{v}_4) \\ \mathrm{P}_3(\mathrm{v}_1, \mathrm{v}_2, \mathrm{v}_3, \mathrm{v}_4) \\ \mathrm{P}_4(\mathrm{v}_1, \mathrm{v}_2, \mathrm{v}_3, \mathrm{v}_4) \end{pmatrix} = \begin{pmatrix} \mathrm{E}'_{\mathrm{d}0} + \mathrm{v}_4 \\ \mathrm{E}'_{\mathrm{q}0} + \mathrm{v}_1 \\ \omega_0 + \mathrm{v}_2 \\ \delta_0 + \mathrm{v}_3 \end{pmatrix},$$

and

$$\begin{pmatrix} \mathrm{v}_1 \\ \mathrm{v}_2 \\ \mathrm{v}_3 \\ \mathrm{v}_4 \end{pmatrix} = \begin{pmatrix} \mathrm{P}_1^{-1}(x_1, x_2, x_3, x_4) \\ \mathrm{P}_2^{-1}(x_1, x_2, x_3, x_4) \\ \mathrm{P}_3^{-1}(x_1, x_2, x_3, x_4) \\ \mathrm{P}_4^{-1}(x_1, x_2, x_3, x_4) \end{pmatrix} = \begin{pmatrix} x_2 - \mathrm{E}'_{\mathrm{q}0} \\ x_3 - \omega_0 \\ x_4 - \delta_0 \\ x_1 - \mathrm{E}'_{\mathrm{d}0} \end{pmatrix}.$$

The output function is $\mathrm{v}_4 = x_1 - \mathrm{E}'_{\mathrm{d}0} = \mathrm{E}'_{\mathrm{d}} - \mathrm{E}'_{\mathrm{d}0}$.

Appendix C: Novel MATLAB Tools for General Affine Systems

C.1 MATLAB Code for Testing the Exact Linearization Condition for a General Affine Nonlinear System

```
% This function OutputResult=ELCOND(F,G,S)is used to determine the exact
%linearization conditions for any given affine nonlinear SISO system dX/dt=f(X) +
%g(X)u, where X represents the states (x1, x2,...,xn) of the system. F,G, and S are
%symbolic expressions for f(x),g(x), and the states, respectively.OutputResult is a vector
%of string elements stating whether the system can be exactly linearized or not. Note that
%the order of the system must be at least 2.ALSO,NOTE THAT THE STATES IN F
%AND G APPEAR AS x1, x2, x3,..., xn, WITH THESE , OF COURSE, HAVING
%BEEN DEFINED AS SYMBOLIC VARIABLES. For example, the system
%dx(1)/dt=x(1)sin x(2)+20x(1)-2u and dx(2)/dt=cos x(1)+ 10u having steady-state values
%x0(1)=0.5 and x0(2)=2 is created as: syms x1 x2 f g
% f=[x1*sin(x2)+ 20*x1 cos(x1)+10]';g=[-2 10]';x=[x1 x2]';
functionOutputResult=elcond(f,g,x)
sysorder=length(f);d=sysorder-1;
m=zeros(sysorder,sysorder);dd=zeros(sysorder,d);
M= sym(m);D=sym(dd);
f_diff=jacobian(f,x);
M(:,1)=g;
% Compute the elements of M
for k=2:sysorder
   M(:,k)=(jacobian(M(:,k-1),x)*f)-(f_diff*M(:,k-1));
```

```
end
% Compute the elements of D and De
if d==1;
D(:,d)=g;
else
fori=2:d;
D(:,i)=M(:,i);
end
D(:,1)=g;
   De=D;
   De(:,sysorder)=jacobian(D(:,2),x)*D(:,1)-jacobian(D(:,1),x)*D(:,2);
end
% Check for the exact linearization conditions
input('Enter all the n steady-state values as : x1 =  ; x2 = ; x3 =  ; ... ; xn =  ;   ')
input('Enter all the system parameters if any or press the return key       ')
M_comp=subs(M);D_comp=subs(D);De_comp=subs(De);
M_rank=rank(M_comp);D_rank=rank(D_comp);De_rank=rank(De_comp);
if d==1;
ifM_rank==sysorder;
OutputResult='The system can be exactly linearized, i.e., there is an output function
that makes the system relative equal to the system order ';
else
OutputResult='The system cannot be exactly linearized, i.e.,an output function does
```

not exist to make the system relative equal to the system order ';

end

else

ifM_rank==sysorder&&D_rank==De_rank;

OutputResult='The system can be exactly linearized, i.e., there is an output function that makes the system relative degree equal to the system order';

else

OutputResult='The system cannot be exactly linearized, i.e.,an output function does not exist to make the system relative degree equal to the system order';

end

end

C.2 MATLAB Code for Finding the Relative Degree of a General Affine Nonlinear System

% This function RelativeDegree=RELDEG(F,G,H,S) is used to determine the relative %degree of any given affine nonlinear SISO system dX/dt=f(X) + g(X)u, y=h(X), where %X represents the states (x1, x2,...,xn) of the system. F, G, H and S are symbolic %expressions for f(x), g(x), h(x) and the states, respectively; f and g vector functions,

% and h is a scalar function. RelativeDegree is a positive integer between 1 and the order %(i.e., n) of the system. Note that the order of the system must be at least 2.

% ALSO,NOTE THAT THE STATES IN F, G AND H APPEAR AS x1, x2, x3,..., xn, %WITH THESE , OF COURSE, HAVING BEEN DEFINED AS SYMBOLIC %VARIABLES. For example,the system dx(1)/dt=x(1)sin x(2)+20x(1)-2u, dx(2)/dt=cos

```
%x(1)+ 10u and y=x(1) + x(2) having steady-state values x0(1)=0.5 and x0(2)=2 is
%created as: syms x1 x2 f g h
% f=[x1*sin(x2)+ 20*x1 cos(x1)+10]';g=[-2 10]';h=x1+x2;x=[x1 x2]';
functionreldegResult=reldeg(f,g,h,x)
sysorder=length(f);
m=zeros(1,sysorder);d=zeros(1,sysorder);
LfHx= sym(m);LgLfHx=sym(d);
LfHx(1)=h; % the first element of LfHx
% Compute the other elements of LfHx
ifsysorder==2
LfHx(sysorder)=jacobian(LfHx(sysorder-1),x)*f;
else
for k=2:sysorder
LfHx(k)=jacobian(LfHx(k-1),x)*f;
end
end
% Compute the elements of LgLfHx
for k=1:sysorder
LgLfHx(k)=jacobian(LfHx(k),x)*g;
end
% Find the relative degree of the system
input('Enter all the n steady-state values as : x1 =  ; x2 = ; x3 =  ; ... ; xn =  ;   ')
input('Enter the values for all the system parameters if any or press the return key    ')
```

```
LgLfHx_comp=subs(LgLfHx);

p=find(LgLfHx_comp);

RelativeDegree=p(1);

% Output the result

reldegResult=['the relative degree of the system is: ' num2str(RelativeDegree)];
```

Appendix D: Equilibrium Point Computation of PSM1 and PSM2

D.1 Using MATLAB Function 'fsolve' to Solve Equations (4.6) and (4.11)

```
% %This function file creates equation (4.6).
functionaweresult = awefun(x)
system_parameters;
aweresult=((b2*v*v*a4/2)-(b1*f2*v*v/2))*sin(2*x(1))+(a4*v/tdop)*x(2)*sin(x(1))-
x(3)*b1/M;
%This script file solves equation (4.6) by calling function file 'awefun'
options=optimset('Algorithm','Levenberg-Marquardt');
x_steadystate=fsolve(@awefun, X0, options)
```

D.2 Computing the Jacobian Matrix of f(x) of PSM1 and PSM2

```
% This script computes the jacobian matrix of function vector f(x) of PSM1 and can be
%modified for PSM2 as well.
syms x1 x2 x3;
system_parameters;
 j1=x2-ws;
 j2=(0.8413/M)+0.5*f2*v*v*sin(2*x1)-a4*v*x3*sin(x1)-(1/M)*tqop*f3*f1*v*v*(x2-
ws)*cos(x1)*cos(x1);
 j3=-b1*x3+b2*v*cos(x1)+(1/tdop)*1.5603;
syspsm1=jacobian([j1;j2;j3],[x1 x2 x3]);
```